Title
Ab INITIO THEORETICAL METHODS FOR EXCITED STATES APPLICATION TO KETENE AND FORMALDEHYDE

Author
Allen, W.D.

Publication Date
1987-08-01

Lawrence Berkeley Laboratory
UNIVERSITY OF CALIFORNIA

Materials & Chemical Sciences Division

Ab Initio Theoretical Methods for Excited States Application to Ketene and Formaldehyde

W.D. Allen
(Ph.D. Thesis)

August 1987

Prepared for the U.S. Department of Energy under Contract DE-AC03-76SF00098

DISCLAIMER

Ab Initio Theoretical Methods for Excited States Application to Ketene and Formaldehyde

Wesley David Allen
(Ph.D. Thesis)

August 1987

Department of Chemistry
and
Materials & Chemical Sciences Division
Lawrence Berkeley Laboratory
University of California
Berkeley, California 94720

This work was supported by the U.S. Department of Energy
under contract No. DE-AC03-76SF00098

Ab Initio Theoretical Methods for Excited States Application to Ketene and Formaldehyde

Wesley David Allen

Department of Chemistry
University of California
Berkeley, California 94720

ABSTRACT

Extensive *ab initio* studies of the $\tilde{X}^1A_1$, $\tilde{a}^3A_2$ ($^3A''$), $\tilde{A}^1A_2$ ($^1A''$), $\tilde{b}^3A_1$ ($^3A'$), $\tilde{B}^1B_1$, and 2^1A_1 electronic states of ketene have been performed with the goal of providing an essentially complete theoretical description of these low-lying states. Geometrical structures, vertical and adiabatic excitation energies, and vibrational frequencies have been determined for these states, and correlation diagrams and transition states for dissociation to methylene and carbon monoxide have been investigated in detail. Both self-consistent-field (SCF) and configuration interaction singles and doubles (CISD) methods have been employed with double-zeta plus polarization (DZP), DZP + Rydberg (DZP+R), and, in cases, quadruple-zeta plus double-polarization (QZ2P) basis sets. The theoretical results are discussed in the context of ketene as a paradigm of five features exhibited in general by certain electronic states: (1) the correlation of excited states to fragments, (2) gross qualitative differences between singlet and triplet states with the same orbital occupancies, (3) conical intersections of potential energy surfaces, (4) variational collapse of trial wave functions, and (5) Rydberg-valence mixing.

A new, optimally efficient formalism is presented for the analytic evaluation of two-configuration self-consistent-field configuration interaction (TCSCF-CI) energy first derivatives, and this TCSCF-CI gradient procedure is adapted and applied to singlet excited electronic states of the same symmetry as the ground state. The resulting adaptation, the SCFX-CI gradient procedure, is the simplest means by which dynamical electron correlation can be incorporated effectively for such electronic

states, because conventional SCF-CI wave functions are unreliable in these cases due to the possibility of variational collapse. In addition to the 2^1A_1 state of ketene, the SCFX-CI and TCSCF-CI gradient methods are applied to the $\tilde{X}^1A_1$, $(\pi\rightarrow\pi^*)$ 2^1A_1, and $(n\rightarrow 3p_y)$ 2^1A_1 states of formaldehyde. Specifically, geometrical structures, excitation energies, and harmonic vibrational frequencies obtained with DZP and DZP+R basis sets are reported for H_2CO.

ACKNOWLEDGEMENTS

Oh how different it was from what I envisioned. There were no days to sit under the summer sun and contemplate the mysteries of the universe. There were few days for intellectual exploration outside of the field of theoretical chemistry. But fortunately there were seventy-five or more softball games to be played! I would have liked to be able to catch my breath along the way, but perhaps God had different plans. And so it is time to acknowledge those who supported and guided me during my graduate studies at Berkeley.

Professor Henry F. Schaefer III has had an enormous influence on my life, an influence which is probably even greater than either he or I would be willing to admit. The education that Professor Schaefer afforded me was primarily not an education in quantum chemistry, that I received through interaction with his research group. Professor Schaefer taught me about life in and out of the scientific community. He opened many doors for me and at times shoved me through them. I thank him for great patience and a caring spirit.

More importantly, I thank my wife Debbie for maintaining faith in me. She has sacrificed much and loved more. When I was in need of assistance, she was always there. This dissertation is only one of the many fruits of her labors in the preparation of manuscripts. I also thank my parents for much love and support over the past 25 years. I learned perseverance at an early age picking up rocks out of my father's pasture!

There are many individuals to be thanked in the Chemistry Department at Berkeley. Professors William H. Miller and Jeffrey A. Reimer were very supportive and were most helpful recently in my getting an academic position at Stanford. As a teaching assistant for both of these men, I appreciate the confidence they showed in me. Dr. Roger "Sparky" Grev was a willing partner in many debates concerning

theoretical chemistry. I only wish I knew as much about chemistry as he knows about baseball. Dr. Tim Lee and Dr. Yukio Yamaguchi were of enormous help in the practical matter of running calculations, getting computer codes to work, and generally learning the business of quantum chemistry. Andy Scheiner, Richard Remington, and Allen Clabo also deserve credit for enduring four years at Berkeley with me. There are of course many other individuals in the Schaefer group to thank whom I have not named here. Finally, let me thank John Tromp for continually reminding me not to take life too seriously.

Acknowledgements of assistance for specific parts of the work described in this dissertation are contained in Chapters 2, 3, and 4. The research was primarily supported by the Director, Office of Energy Research, Office of Basic Energy Sciences, Chemical Sciences Division of the U.S. Department of Energy under Contract No. DE-AC03-76SF00098.

Whatever you do, work at it with all your heart,

as working for the Lord, not for men.

Colossians 3:23

Table of Contents

Chapter 1 Ketene as a Paradigm of Features Exhibited by Excited Electronic States

A detailed understanding of the photochemistry of polyatomic molecules is predicated upon knowledge of the potential energy surfaces of excited electronic states. *Ab initio* theoretical studies can be especially helpful in this area by providing geometrical structures, vertical and adiabatic excitation energies, and vibrational frequencies of excited electronic states and also by establishing the correlation between the electronic states of a parent molecule and those of its fragments. Despite the fact that the study of excited electronic states using *ab initio* methods has traditionally been a treacherous enterprise, such methods are employed successfully in this dissertation to examine the low-lying electronic states of the ketene and formaldehyde molecules. Many problems have been encountered in this undertaking which are not factors in the study of ground states, but through painstaking efforts these problems have in large part been dealt with effectively.

In Chapter 2 a survey is made of the low-lying $\tilde{X}^1A_1$, $^3A''$, $^1A''$, $^3A'$, $^1B_1$, and 2^1A_1 electronic states of ketene, and the theoretical results described therein provide the foundation for understanding the photochemistry of this important molecule. In Chapter 3 the $\tilde{X}^1A_1$, $^3A''$, $^1A''$, and $^3A'$ states are examined further with the primary purpose of ascertaining the details of the reaction paths for the dissociation $\tilde{a}^3A''$ $CH_2CO \rightarrow \tilde{X}^3B_1$ CH_2 + $\tilde{X}^1\Sigma^+$ CO. Chapter 4 provides a new theoretical formalism for investigating singlet excited electronic states of the same symmetry as the ground state through analytic configuration interaction gradient techniques. Application is made to the 2^1A_1 states of formaldehyde and ketene. The formaldehyde results resolve some long-standing questions concerning the $(\pi\rightarrow\pi^*)^1$ state in addition to demonstrating the viability of the new CI gradient procedure. Moreover, the 2^1A_1

H_2CO results provide for an enlightening comparison with the 2^1A_1 state of ketene. A summary is given in Chapter 5.

The obvious goal of this dissertation is then to provide an essentially complete theoretical description of all of the low-lying electronic states of ketene. However, by chronicling theoretical efforts toward understanding the electronic states of ketene, a model for attacking similar chemical systems is provided, because ketene can be considered a paradigm of features exhibited in general by excited electronic states. This point can be illustrated with at least five examples. (References appear in Chapters 2-4.)

(1) **The correlation of excited states to fragments.** The photodissociation of ketene to methylene and carbon monoxide has been the object of a plethora of experimental and theoretical studies since 1950. The dissociation paths involved in the correlation of the excited states of ketene to $\tilde{X}^1\Sigma^+$ CO plus $\tilde{X}^3B_1$, $\tilde{a}^1A_1$, or $\tilde{b}^1B_1$ CH_2 are of fundamental interest to the understanding of photofragmentation dynamics in general.

(2) **Gross qualitative differences between singlet and triplet states with the same orbital occupancies.** Naively one would expect singlet and triplet states with the same orbital occupancies to have similar geometrical structures, vibrational frequencies, and excitation energies; however, the ability of an excited singlet state to interact with a singlet ground state in certain cases causes gross disparities in the qualitative features displayed by analogous singlet and triplet states. A dramatic demonstration of this phenomenon is seen in the $^3A_1$ and 2^1A_1 states of ketene. The a″ vibrational frequencies of the lower-lying $^3A''$ and $^1A''$ states are also radically different.

(3) **Conical intersections of potential energy surfaces.** For a nonlinear molecule containing N atoms, two intersecting 3N-6 dimensional potential energy hypersurfaces will in general coincide in a region of dimension 3N-8. In other words, if

plotted against two properly selected coordinates, the potential energy surfaces will display intersections consisting of two cones whose apices coincide. Such conical intersections among excited electronic states lead to peculiar phenomena, and the $(^3A_2,^3A_1)$ intersections in the ketene molecule provide one example.

(4) **Variational collapse of trial wave functions.** Trial wave functions optimized in a variational sense for excited electronic states are frequently only poor descriptions of lower states of the same spin and spatial symmetry unless appropriate constraints are imposed. This problem is called variational collapse and has been the downfall of many previous investigations of excited electronic states. The 2^1A_1 state of ketene is a case in which the problem is particularly severe, and in Chapter 4 a viable method for overcoming variational collapse is discussed and implemented.

(5) **Rydberg-valence mixing.** When an electronic state of valence character lies sufficiently near a Rydberg state of the same symmetry, Rydberg-valence mixing can occur. A classic example is the $(\pi\rightarrow\pi^*)^1$ state of ethylene, which is somewhat more diffuse in spatial extent than its triplet counterpart but nonetheless predominantly valence in character if enough electron correlation is included in the theoretical description. The question of Rydberg-valence mixing also arises for the 2^1A_1 state of ketene, and the analysis in Chapter 4 indicates that it is predominantly a $(\pi\rightarrow 3p_x)^1$ Rydberg state with a moderate amount of $(\pi\rightarrow\pi^*)^1$ character.

In the following chapters (2-4) much attention is paid to these and other general features of excited electronic states as they are encountered in the ketene molecule. Afterwards in Chapter 5 a retrospective view is given of the dominant theme: ketene as a paradigm of features exhibited by excited electronic states.

Chapter 2 A Survey of the Low-Lying Electronic States of Ketene

2.1 INTRODUCTION

In recent years the low-lying electronic states of ketene (CH_2=C=O) have been of interest in several areas of chemical research. Thermal and photochemical Wolff rearrangements of

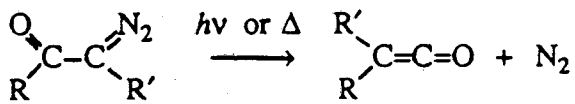

diazoketones to form ketenes have long been of synthetic utility in organic chemistry,[1,2] and several recent theoretical and experimental sdtudies have been performed to elucidate the mechanisms involved.[3,4] Perhaps even greater attention has been focused on ketenes as a convenient source of carbenes,

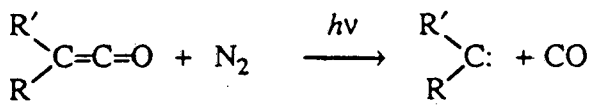

and particularly on ketene itself as a source $\tilde{a}^1A_1$ and $\tilde{X}^3B_1$ methylene.[5,6] Obviously for such processes a detailed theoretical understanding of the photochemistry of ketene and the nature of its low-lying electronic states is of much importance. Indeed, in a recent experimental paper concerning ketene photofragmentation, Moore and co-workers[7] state that "the complete description of [ketene fragmentation dynamics] will require parallel theoretical efforts towards characterizing the ground and excited state potential surfaces on which internal conversion and fragmentation processes occur."

The ground state of ketene has a C_{2v} equilibrium geometry with the orbital occupancy[8]

$1a_1^2 2a_1^2 3a_1^2 4a_1^2 5a_1^2 6a_1^2 7a_1^2 1b_2^2 1b_1^2 2b_2^2 2b_1^2$

The $3b_2$ orbital is the lowest unoccupied molecular orbital (LUMO) followed by the $3b_1$ and $8a_1$ orbitals. Thus, single excitations from the $2b_1$ orbital yield $^3A_2$, $^1A_2$, $^3A_1$, 2^1A_1, $^3B_1$, and $^1B_1$ states under the C_{2v} point group. Experimental attempts to characterize these states have not been entirely successful. Several experimental studies of the electronic spectrum of ketene have appeared[9–16]; however, the electronic absorption spectrum of gaseous ketene below 50000 cm^{-1} consists only of broad, diffuse bands with relatively little structure. No fluorescence from the excited states has been reported, and determinations of equilibrium geometry and vibrational energy levels for the excited states have not been possible. Since Dykstra and Schaefer[1,8] have discussed these experimental results in some detail, only the salient points will be reviewed here. No new attempts to analyze the electronic spectrum of ketene have occurred within the last ten years.

In Table I vertical excitation energies from several experimental and theoretical studies are listed. Both the $^3A_2$ and $^1A_2$ states appear to have in-plane bent C-C-O skeletons since long progressions in bending vibrations have been observed. Thus, the first two excited states of ketene are actually $^3A''$ and $^1A''$ states with $...4a'^2 5a'^2 6a'^2 7a'^2 8a'^2 1a''^2 9a'^2 2a'' 10a'$ electronic configurations. Laufer and Keller[14] disagree with Dixon and Kirby[12] on whether the $^3A''$ state is actually observed, on the adiabatic excitation energies for the $^3A''$ and $^1A''$ states, and on the reason the observed bands are diffuse. Laufer and Keller argue that the $^3A''$ and $^1A''$ states are less than 19200 and 21300 cm^{-1}, respectively, above the $\tilde{X}^1A_1$ state while Dixon and Kirby suggest adiabatic excitation energies of 21100 and 26300 cm^{-1}. Other experimental studies have investigated the $^3A_1$, $^1B_1$, and $^3B_1$ states. Using electron-impact energy-loss spectroscopy, Frueholz, Flicker, and Kuppermann,[17] observed a differential cross section feature with onset at 4.7 eV (38000 cm^{-1}) and maximum at

5.3 eV (43000 cm^{-1}) which was assigned to the $\tilde{X}^1A_1 \rightarrow {}^3A_1$ transition. Frueholz *et al.* also ascertained a value of 5.86 eV (47300 cm^{-1}) for the $\tilde{X}^1A_1 \rightarrow {}^1B_1$ vertical transition, and in another electron-impact spectroscopic study, Vogt, Jungen, and Beauchamp[18] suggest 46800 cm^{-1} for the analogous $\tilde{X}^1A_1 \rightarrow {}^3B_1$ transition. However, the effects of geometry relaxation for the ${}^3A_1$, ${}^1B_1$, and ${}^3B_1$ states are not known from available experimental analyses. Price, Teegan, and Walsh[11] and Rabelais, McDonald, Scherr, and McGlynn[13] report four diffuse bands spaced ≈1050 cm^{-1} apart in the 46900-51000 cm^{-1} region of the electronic spectrum but do not assign them to either the $\tilde{X}^1A_1 \rightarrow {}^1B_1$ or $\tilde{X}^1A_1 \rightarrow {}^3B_1$ transition. Finally, the location of the 2^1A_1 state remains in doubt. Price *et al.* assigned six observed transitions between 54680 and 75180 cm^{-1} as n=3,4,5,6,7, and 8 members of a $\pi \rightarrow ns$ Rydberg series. However, according to Herzberg's interpretation of the same data, the upper states in this series are ${}^1A_1$ rather than the ${}^1B_1$ states, even though the quantum defect δ=1.07 is typical of *ns* Rydberg series.[15] Accordingly, Herzberg places the 2^1A_1 state at 54680 cm^{-1}.

There have been a myriad of *ab initio* and semiempirical calculations on ketene.[3,4,8,12,13,19–38,50] The ground state C_2H_2O potential surface has been examined in great detail.[3,4,31] In particular, high levels of theory have been used to compute the stabilites of ketene, hydroxyacetylene, oxirene, formylmethylene, hydroxyvinylidene, and oxiranylidene as well as the barriers to the interconversion of these isomers.[3,4] However, the excited state potential surfaces have not been examined in such detail. Harding and Goddard[26] used GVB and GVB-CI wave functions computed with a double ζ (DZ) basis at the $\tilde{X}^1A_1$ experimental equilibrium geometry to obtain $\tilde{X}^1A_1 \rightarrow {}^{3,1}A_2$ and $\tilde{X}^1A_1 \rightarrow {}^3A_1$ vertical excitation energies. Using double ζ, double ζ plus Rydberg (DZ+R), and double ζ plus polarization (DZ+P) basis sets, Dykstra and Schaefer[8] computed vertical excitation energies for 18 excited electronic states at the

self-consistent-field (SCF) level of theory. Some of these results are shown in Table I along with those of Harding and Goddard, where good agreement among the experimental and theoretical results is seen, especially if one considers the levels of theory used. An early study of Del Bene[27] and the later study by Dykstra and Schaefer dealt explicitly with the effect of geometry relaxation on excitation energies. Dykstra and Schaefer performed DZ SCF geometry optimizations for the seven lowest electronic states. Consistent with the experimental results mentioned previously,[12,14] the $^3A_2$ and $^1A_2$ states become $^3A''$ and $^1A''$ states with C_s^{II} geometries as shown in Fig. 2. At the SCF level of theory, T_e values of 11700 and 13900 cm^{-1} were found for these states. For the $^3A_1(^3A')$ and $2^1A_1(2^1A')$ states, C_s^I (Fig. 3) optimum geometries were located, and T_e values of 15200 and 18100 cm^{-1}, respectively, were obtained. It must be noted that the $2^1A_1(2^1A')$ calculation was nonvariational in the sense that the computed energy was not an upper bound for the true energy of the first excited $^1A'$. Thus, the T_e value for the $2^1A_1(2^1A')$ state is unreliable. Finally, the $^3B_1$ and $^1B_1$ states were found to dissociate directly to CH_2 + CO without a barrier within the constraint of C_{2v} symmetry. Other authors have also reached this conclusion.[24,25] The reader is referred to Ref. 1 for additional discussions.

Integrally related to the studies which have sought to characterize the excited states of ketene are the numerous experimental and the theoretical studies which have dealt directly with ketene photofragmentation.[7,39–55] Several important predictions can be made by considering the state correlation diagrams of Yamabe and Morokuma[50] for $CH_2CO \rightarrow CH_2+CO$. (1) Least-motion C_{2v} dissociation paths are not allowed for the $\tilde{X}^1A_1$, $^{3,1}A_2$, $^3A_1$, and 2^1A_1 states. (2) Along bent in-plane C_s^{II} paths (Fig. 2) the $^{3,1}A''$ ketene states lead favorably to $^{3,1}B_1CH_2 + \tilde{X}^1\Sigma^+CO$, while $CH_2CO(\tilde{X}^1A_1) \rightarrow CH_2(^1A_1) + CO(^1\Sigma^+)$ is forbidden. (3) Finally, along bent out-of-plane C_s^I paths (Fig. 3) the $^{3,1}A'(^{3,1}A_1)$ ketene states cross the $^{3,1}A''$ states and corre-

late to $^{3,1}B_1CH_2 + \tilde{X}^1\Sigma^+CO$, while $CH_2CO(\tilde{X}^1A_1) \rightarrow CH_2(^1A_1) + CO(^1\Sigma^+)$ proceeds with little or no barrier. Various theoretical and experimental studies confirm these predictions,[7,24,25,50,53] and the mechanisms for the production of $^1A_1$ and $^3B_1$ CH_2 by photodissociation of ketene are reasonably well extablished.[45–48,51] Irradiation at 308 nm (32500 cm^{-1}), for example, initiates $\tilde{X}^1A_1 \rightarrow {}^1A''$ transitions followed by rapid internal conversion to high vibrational levels of the ground state with subsequent dissociation to yield $^1A_1$ CH_2. On the other hand, *direct* production of $^3B_1$ CH_2 must occur on the $^3A''$ excited state surface. At wavelengths where production of both $^1A_1$ and $^3B_1$ CH_2 is possible energetically, $^1A_1$ CH_2 is typically the dominant product although triplet/singlet CH_2 ratios at various wavelengths are the subject of controversy.[44,47,49,54,55]

In summary, several important questions regarding ketene photochemistry remain. Among these questions are: (1) Which low-lying states of ketene have local energy minima? (2) What are the adiabatic excitation energies and equilibrium geometries for these states? (3) What are the corresponding force constants and vibrational frequencies? (4) Where does the 2^1A_1 state lie? (5) Are $\tilde{X}^1A_1 \rightarrow {}^3A''$ transitions observed in the electronic spectrum, thus implying the direct production of $^3B_1$ CH_2? (6) Why has no fluorescence from the excited states of ketene been observed? and (7) In what regions of the electronic spectrum should fluorescence be expected? In this survey these and other questions are addressed using *ab initio* theoretical methods in a continued effort to ascertain the details of ketene photochemistry.

2.2 THEORETICAL METHODS

The important features of the potential energy surfaces ot the $\tilde{X}^1A_1$, $^3A_2(^3A'')$, $^1A_2(^1A'')$, $^3A_1(^3A')$, $^1B_1(2^1A')$, and 2^1A_1 states of ketene were investigated. A standard Huzinaga and Dunning[56,57] double zeta plus polarization (DZP) basis set was employed in all calculations. This is a C(9s5p1d/4s2p1d), O(9s5p1d/4s2p1d), and H(4s1p/2s1p) basis set consisting of 58 contracted Gaussian functions (CGFs). It is identical to that used by Dykstra and Schaefer[8] except that the polarization functions have been changed. In Ref. 8, α_d(C)=0.75, α_d(O)=0.80, and α_p(H)=1.0 were used, whereas α_d(C)=0.75, α_d(O)=0.85, and α_p(H)=0.75 were used here. To calculate the vertical excitation energies for the five excited states of interest, the DZP basis was augmented with two sets of diffuse s and p functions on each C and O atom, giving a total of 82 CGFs. The orbital exponents for these Rydberg functions were also taken from Ref. 8.

Stationary points on the potential energy surfaces were located at the single-configuration restricted Hartree-Fock (RHF) self-consistent-field (SCF) level of theory[58] using analytic energy gradients and the variable metric method of Murtaugh and Sargent.[59] At all stationary points so located, the internal coordinates were optimized to 10^{-7} Å or radians, and the largest component of the Cartesian energy gradient was less than 10^{-6} hartree/bohr. At these stationary points analytic SCF second derivatives[60–62] were computed in Cartesian coordinates using the atomic orbital coupled-perturbed Hartree-Fock (AOCPHF) formalism[63] and transformed to give internal-coordinate force constants. The GF matrix method[64] was then used to obtain vibrational frequencies and normal mode eigenvectors. Final energies were obtained by performing configuration interaction singles and doubles (CISD) calculations for *several* of the states of interest at *each* stationary point. The three lowest

occupied orbitals, corresponding to carbon and oxygen 1s orbitals, and the three highest unoccupied orbitals, corresponding to 1s virtual orbitals, were frozen in the CI calculations. Otherwise, all singly and doubly excited configurations with respect to the SCF reference configurations were included in the CI wave functions.

Special methods were required for examination of the open-shell singlet 2^1A_1 states.[65–66] This excited state has the same spin and spatial symmetry as the ground state for all nuclear configurations. In such cases normal SCF calculations for the excited state are nonvariational in the sense that the calculated energy is not an upper bound for the true energy of the excited state. This arises from the fact that normal SCF methods do not constrain the excited state to be orthogonal to the ground state except by symmetry, and the excited state SCF wave function frequently collapses to become only a poor description of the ground state.[67–69] To avert such difficulties in this study the excited state SCF method of Davidson and Stenkamp[70,71] was utilized. Since Fitzgerald and Schaefer[66] have recently published a paper dealing with this excited state SCF method, only a brief description will be given here. The wave function is written in the usual open-shell singlet form

$$\Psi = \frac{1}{\sqrt{2}} A \{(\text{core})a\bar{b}\} - \frac{1}{\sqrt{2}} A \{(\text{core})\bar{a}b\} \quad , \tag{1}$$

except that the two open-shell orbitals |a> and |b> are allowed to have nonzero overlap S. (In the above equation A is the antisymmetrizer operator for the electrons.) Thus, one minimizes $E=\langle\Psi|H|\Psi\rangle/(1+S^2)$ subject to the constraints

$$\langle i|j\rangle = \delta_{ij} + (\delta_{ia}\delta_{jb} + \delta_{ib}\delta_{ja})S \quad , \tag{2}$$

where the indices i and j run over both the closed- and open-shell orbitals and S is allowed to vary. The resulting equations[66] are solved by the sequential orthogonalization method of Davidson[71] to obtain either closed-shell singlet ground state solutions (with overlap S=1) or open-shell singlet excited state solutions (with overlap S=0). If one defines the orthonormal orbitals

$$|u\rangle = \frac{(|a\rangle + |b\rangle)}{\sqrt{2(1+S)}} \quad \text{and} \quad |v\rangle = \frac{(|a\rangle - |b\rangle)}{\sqrt{2(1-S)}} \quad , \tag{3}$$

the wave function in Eq. (1) can be written (after normalization) in the form

$$\Psi = C_1 A\{(\text{core})u\bar{u}\} - C_2 A\{(\text{core})v\bar{v}\} \quad , \tag{4}$$

where

$$C_1 = (1+S)/\sqrt{2(1+S^2)} \quad \text{and} \quad C_2 = (1-S)/\sqrt{2(1+S^2)} \quad . \tag{5}$$

From Eq. (4) it is apparent that ground state solutions and excited state solutions can be considered to be TCSCF wave functions since both the orbitals and the overlap S (and hence C_1 and C_2) are fully optimized. Any three-configuration MCSCF wave function,

$$\begin{aligned}\Psi = {} & C'_1 A\{(\text{core})x\bar{x}\} + C'_2 A\{(\text{core})y\bar{y}\} \\ & + C'_3 A\{(\text{core})(x\bar{y} - \bar{x}y)\}/\sqrt{2} \quad ,\end{aligned} \tag{6}$$

can be written in the two-configuration form of Eq. (4) by performing the orbital rotation

$$|u\rangle = \cos\theta\,|x\rangle + \sin\theta\,|y\rangle \quad \text{and} \quad |v\rangle = \sin\theta\,|x\rangle - \cos\theta\,|y\rangle \quad , \tag{7}$$

where

$$\tan 2\theta = \frac{\sqrt{2}C'_3}{C'_1 - C'_2} \quad \text{and} \quad S = \pm\frac{C'_1 + C'_2}{\sqrt{(C'_1 - C'_2)^2 + 2C'^2_3}} \quad . \tag{8}$$

Thus, the excited state SCF procedure gives solutions identical to the roots of the three configuration MCSCF in Eq. (6). In particular, the open-shell singlet ($S \approx 0$, $C'_3 \approx 1$) solution typically appears as the second root of this three-configuration MCSCF and thus is variational, giving an energy which is an upper bound to the true excited state energy. Analytic first and second derivatives for either the ground or excited state can be computed conveniently using Eq. (4) and existing TCSCF methods.[61,72–74] Finally, by performing a two-reference CISD calculation based on

Eq. (4) and taking the second root, one can include electron correlation in the description of the excited state.[69] This topic is discussed in greater detail in the fourth chapter of this dissertation.

2.3 RESULTS AND DISCUSSION

2.3.1 The $^1A_1$ ground state

The internal coordinates for the C_{2v} equilibrium geometry are depicted in Fig. 1, and the optimum geometries and total energies from this study and previous studies are listed in Table II. As seen in Table II, two DZP SCF optimizations were actually performed, one with $\alpha_d(O)=0.85$ and the other with $\alpha_d(O)=0.80$, the value used in Ref. 8. Since the $\alpha_d(O)=0.85$ result is 0.64 mH (H = hartree) lower in energy, this value for the oxygen d-function exponent was used in all subsequent calculations. The best DZP SCF energy (-151.756673 H) is slightly higher (5.58 mH) than that of Tanaka and Yoshimine,[3] probably because their hydrogen basis contained an additional 1s primitive, although their C and H polarization functions were also different from those used here. The current DZP CISD wave function contained 16979 configuration state functions (CSFs) and gave an energy of -152.153102 H at the DZP SCF optimum geometry. Tanaka and Yoshimine obtained a CISD energy 6.98 mH lower with another 16979 SCF wave function determined at their DZP CISD optimum geometry.

The experimental ground state equilibrium geometry is well established from microwave and infrared studies.[75–80] The current DZP SCF geometrical parameters (virtually identical to those of Tanaka and Yoshimine) are in good agreement with experiment, the largest discrepancy being in the C-O bond length, which is predicted to be 0.014 Å too short. Such errors are expected since DZP SCF calculations usually underestimate equilibrium bond lengths. As shown in Table II, the main effect of reoptimizing the geometry at the DZP CISD level[3] is to increase the C-C and C-O bond lengths to values slightly above the experimental ones. Unlike Tanaka and Yoshimine, the geometry was not reoptimized here at the CI level, but to obtain sem-

iquantitative estimates of the effects of geometry reoptimization on adiabatic excitation energies, CISD calculations were also performed at the DZ optimum geometry of Dykstra and Schaefer[8] and the experimental geometry of Moore and Pimentel.[79] These results are shown in Table III. The energies labeled E(CIDVD) were obtained using Davidson's formula[81] to estimate the correlation energy correction due to the unlinked cluster contribution from quadruple excitations. At the experimental geometry, E(CISD) and E(CIDVD) are lowered by 201 and 334 cm^{-1}, respectively. In the CISD reoptimization of Tanaka and Yoshimine, similar reductions of 213 and 399 cm^{-1} were obtained. Thus, in Table III the energies at the experimental geometry are quite reasonable estimates of the CISD and CIDVD energies one would obtain upon reoptimizing the geometry at the CISD level using the DZP basis set selected here.

The ground state SCF quadratic force constants relative to the C_{2v} symmetrized internal coordinates are given in Table V with the experimental force fields of Mallinson and Nemes.[80] The symmetrized internal coordinates for ketene C_{2v}, C_s^I, and C_s^{II} geometries are defined in Table IV. Finally, in Tavle VI the DZP SCF harmonic frequencies and potential energy distributions are listed with the ketene fundamental frequencies observed by Moore and Pimentel.[79] It is well known[82,83] that DZP-type harmonic SCF frequencies are usually about 8%-13% above experimental fundamental frequencies. As shown inTable VI, the a_1 and b_2 frequency errors do indeed fall with great consistency within the expected range. For this reason the agreement between theory and experiment is to be considered quite good. Scaling the SCF force constants by $(0.9)^2$=0.81 allows reproduction of the experimental results with an average error of 2.1% overall and only 0.8% for the a_1 and b_2 frequencies. The b_1 frequency results are less encouraging, both being about 18% too high, presumably because electron correlation effects are of somewhat more importance for these out-

of-plane modes. Nevertheless, the SCF potential energy distributions in Table VI (defined in footnote c) are in exceptional agreement with those of Moore and Pimentel. Finally, a few comments concerning Table V are warranted. As usual, in the experimental analysis[80] it was necessary to constrain certain force constants. In particular, F_{13}, F_{14}, and F_{79} were constrained to 0, and F_{34} was required to equal 0.041 F_{33}. Thus, only the b_1 force constants are uniquely determined. The comparison in Table V reveals that the first three constraints are quite good approximations while the F_{34} constraint is less reasonable. However, the largest discrepancy is in the F_{23} constant. The DZP SCF result suggests a deficiency here in the empirical force field. In this regard it should be noted that in previous normal coordinate analyses[77–79] good fits were obtained with F_{23} constrained to zero, a reasonable assumption considering the *ab initio* prediction of a rather small value of F_{23}.

2.3.2 The $^3A''$ and $^1A''$ states

As mentioned above the $^3A''$ and $^1A''$ states have C_s^{II} optimum geometries. The C_s^{II} internal coordinates are defined in Fig. 2, and the optimum geometries and SCF energies for the $^3A''$ and $^1A''$ states are given in Table VII. Besides the ≈50° changes in the C-C-O angles, the largest changes in the DZP SCF $^{3,1}A''$ geometrical parameters relative to the $\tilde{X}^1A_1$ values are the 0.156 and 1.52 Å increases in the C-C bond lengths. These $^{3,1}A''$ values lie between the 1.34 and 1.53 Å C-C bond lengths in ethylene and ethane. Accordingly, a significant degree of C-C π bonding remains in the $^3A''$ and $^1A''$ states. The experimental $^{3,1}A''$ geometries are unknown, and the best previous theoretical results are the DZ SCF results of Dykstra and Schaefer, which are listed in Table VII. In general the DZ and DZP SCF results are in excellent agreement. However, as for the $\tilde{X}^1A_1$ state, the DZP carbon-oxygen bond lengths are somewhat shorter than the DZ values. Based on the ground state results,

one would expect the true C-O bond lengths to be intermediate between the DZP and DZ SCF results. Thus, the main effect of reoptimizing the $^{3,1}A''$ geometries at the DZP CISD level *should* be to increase the DZP SCF C-O bond lengths. None of the results in Table II and VII suggest significant changes in the other parameters.

At the $^3A''$ and $^1A''$ DZP SCF geometries, DZP CISD energies of -152.078127 and -152.067885 H were obtained, respectively, with wave functions consisting of 41336 and 41138 CSFs. Fixing all other geometrical parameters at the DZP SCF values and varying the C-O bond lengths gave the results listed in Table VIII. Parabolic interpolation yields 1.193 and 1.196 Å as estimates of the DZP CISD optimized C-O bond lengths for the $^3A''$ and $^1A''$ states. This lengthening of the C-O bonds (by ≈0.02 Å) due to electron correlation follows the suggestion of the previous paragraph. Comparing the estimates of CISD and CIDVD energy lowering in Tables III and VIII for the $\tilde{X}^1A_1$ and $^{3,1}A''$ states, it is difficult to envision the $^3A''$ T_0 values being as affected by over 200 cm^{-1} upon complete CISD reoptimization. Thus, the final vertical and adiabatic excitation energies listed in Table IX for the $^3A''$ and $^1A''$ states are based on DZP SCF optimum geometries. The corrections due to zero-point vibrational energies were obtained by scaling the SCF harmonic frequencies in Table VI and XI by 0.90.

From the results in Table IX the best estimates for the T_0 values of the $^3A''$ and $^1A''$ states are 16700 and 19000 cm^{-1}, respectively. These results support the 19200 and 21300 cm^{-1} experimental upper bounds of Laufer and Keller[14] for the $^3A''$ and $^1A''$ states. Due to poor Franck-Condon factors the lowest transition observed in the electronic spectrum of ketene occurs at 21119 cm^{-1},[12] which is above the theoretical $^1A''$ T_0 value. Therefore, $\tilde{X}^1A_1 \rightarrow {}^1A''$ transitions can account for all of the absorptions observed at low frequencies in the electronic spectrum, and no evidence of $\tilde{X}^1A_1 \rightarrow {}^3A''$ transitions is apparent. This conclusion is in agreement with several

other experimental studies[14,16,43] and questions the conclusions of Dixon and Kirby.[12] Nevertheless, the detection of $^3B_1$ CH_2 upon ketene photolysis can still be explained on the basis of $^1A'' \rightarrow {}^3A''$ CH_2CO intersystem crossing or collisional production of triplet CH_2 from $^1A_1$ CH_2.

To determine the spectral region in which fluorescence from the $^1A''$ should be expected, calculations for the $\tilde{X}^1A_1(\tilde{X}^1A')$ state were performed at the DZP SCF $^1A''$ optimum geometry. A single-reference CISD energy was computed for the $\tilde{X}^1A_1(\tilde{X}^1A')$ state which is only 3775 cm^{-1} below that of the $^1A''$ state at the DZP SCF $^1A''$ geometry. The corresponding CIDVD energy difference is 5530 cm^{-1}. TCSCF calculations were also performed for the $\tilde{X}^1A_1(\tilde{X}^1A')$ state. The configuration $\cdots 4a'^2 5a'^2 6a'^2 7a'^2 8a'^2 1a''^2 9a'^2 10a'^2$ is necessary to obtain proper dissociation of $\tilde{X}^1A_1$ CH_2CO to $^1A_1$ CH_2 + $^1\Sigma^+$ CO along C_s^{II} paths. Since the C-C π bond is largely broken (Tables II and VII) in the $^1A''$ structure, inclusion of this second configuration could be necessary to insure reliable $\tilde{X}^1A'$ energies. However, this is not the case here since TCSCF CI coefficients of C_1=0.998 and C_2=-0.057 were found. In fact, the most important second configuration in the description of the $\tilde{X}^1A'$ state was found to be $\cdots 4a'^2 5a'^2 6a'^2 7a'^2 8a'^2 1a''^2 9a'^2 3a''^2$, which gives TCSCF CI coefficients of C_1=0.978 and C_2=-0.206. As shown in Fig. 6, a two-reference (64889 CSF) CISD calculation based on these TCSCF orbitals gave a $\tilde{X}^1A_1$–$^1A''$ separation of 5820 cm^{-1}. The corresponding CIDVD energy difference is 6703 cm^{-1} when the Davidson-like correction to the two-reference $\tilde{X}^1A'$ energy is computed according to the formula[84]

$$\Delta E = (1 - C_1^2 - C_2^2)(E_{CISD} - E_{TCSCF}) \quad . \tag{9}$$

Therfore, according to the Franck-Condon principle, any peak in fluorescence from the ground vibrational level of the $^1A''$ state should occur around 5500-7000 cm^{-1}. Hence, after irradiation of ketene at 23000 cm^{-1}, for example, it might be possible to

observe fluorescence in the 9500-11000 cm^{-1} region. As pointed out by Laufer and Keller,[14] it is possible that fluorescence has never been reported for ketene because it has never been searched for in the near-infrared region.

The $^3A''$ and $^1A''$ DZP SCF quadratic force constants are shown in Table X. The corresponding harmonic vibrational frequencies and potential energy distributions appear in Table XI. Since no other theoretical or experimental results for these quantities exist, relatively little discussion is warranted. However, one crucial point must be addressed. At C_s^{II} geometries the $^1A''$ is orthogonal to the $\tilde{X}^1A'$ state by symmetry and thus is unperturbed by it. Hence the seven a′ modes for the $^1A''$ and $^3A''$ states have very similar frequencies. Moreover, the $^1A''$ a′ frequencies can be computed in the "usual" way without reference to the $\tilde{X}^1A'$ state.[62] In contrast, along a″ modes C_s symmetry is broken, and the $^1A''$ and $\tilde{X}^1A'$ states mix, perhaps strongly. As a result it is possible that the a″ frequencies for the $^1A''$ and $^3A''$ states will be quite different. Along these modes, $\tilde{X}^1A'$ interactions must be incorporated in the theoretical description to prevent the open-shell $^1A''$ wave function from collapsing to a poor description of the ground state.

One approach to dealing with this technical problem is to employ the excited state SCF method mentioned above without symmetry restrictions. At C_s^{II} geometries this method gives wave functions identical to those obtained by ordinary SCF methods. Computing analytic second derivatives using the TCSCF formalism described above (method A) yields a′ frequencies identical to those obtained either by finite differences of analytic gradients or by existing open-shell singlet second derivative formalisms (method B).[62] Furthermore, method A would correct the deficiencies of method B in the computation of the a″ frequencies if the correct ordering of the $^1A''$ and $\tilde{X}^1A'$ states were maintained. With the excited state SCF formalism it is possible to converge a TCSCF wave function for the $\tilde{X}^1A'$ state with an energy

below that of the $^1A''$ state (Fig. 5). However, with the $^1A''$ orbitals the $\tilde{X}^1A'$ state appears as a higher-energy root of the three-configuration CI described previously, and one must be cautious in relying on the method A results. As shown in Table XI, method A gives a″ frequencies of 1383 and 483 cm^{-1} while method B (which is theoretically less satisfactory) gives 599 and 427 cm^{-1}, values much closer to the $^3A''$ results.

After encountering difficulties in applying state-averaged MCSCF techniques to this problem, a qualitative check of the TCSCF a″ frequencies was performed by recomputing the 2×2 a″ internal-coordinate force constant matrix using double finite differences of CI energies obtained at geometries displaced from the $^1A''$ DZP SCF geometry (method C). Molecular orbitals were obtained from SCF calculations for the $^3A(^3A'')$ state. The CI consisted of all single excitations from three references, the open-shell singlet reference in which the open-shell orbitals ϕ_a and ϕ_b are both singly occupied, and the two closed-shell references in which ϕ_a and ϕ_b are doubly occupied. At all geometries considered the open-shell singlet state appeared as the second root of the CI. In particular, at the $^1A''$ C_s^{II} geometry, energies of -151.726438 and -151.712247 H were obtained for the $\tilde{X}^1A'$ and $^1A''$ states. The a″ force constants based on the second roots of these CI's gave values of 1498 and 557 cm^{-1} for the a″ frequencies. Because these (method C) results were obtained in a manner not precisely equivalent to method A, it is not surprising that they differ from the TCSCF values. Nevertheless, the method C results qualitatively confirm the method A prediction of a″ frequencies for the $^1A''$ state dramatically above those of the $^3A''$ state. However, since configuration interaction more than doubles the $\tilde{X}^1A'$-$^1A''$ energy separation, one must be cautious about the quantitative reliability of the method A a″ frequencies.[88]

2.3.3 The $^3A'$ state

In Fig. 3 internal coordinates for the C_s^I $^3A'$ stationary point are defined, and in Table XII the C_s^I SCF optimum geometry and total energy are listed. Note in Table XII that a C-C distance (1.52 Å) appropriate for a single bond is predicted with both basis sets while the C-O distance is only about 0.019 Å longer than in the ground state. Apparently, in the C_s^I structure the presence of H atoms above and below the C-C-O plane disrupts the partial C-C π bonding found for the planar $^{3,1}A''$ states. For the angles α and γ, rather large differences appear between the DZ and DZP SCF optimum values, indicating significant sensitivity of these parameters to the inclusion of polarization functions. Finally, one might wonder whether another stationary point exists with the hydrogen atoms *trans* to the oxygen. A careful search of *trans* geometries dispelled the possibility of such double-well behavior of the potential energy as a function of γ (Fig. 3). Setting γ=-32.6° while keeping all other parameters fixed gave an SCF energy of -151.678971 H, an increase of 1355 cm^{-1} over the *cis* structure.

The DZP CISD wave function for the $^3A'$ state included 40266 CSFs and at the SCF C_s^I optimum geometry an energy of -152.063861 H was computed. Hence, the following T_e values were obtained: T_e (SCF)=15699 cm^{-1}, T_e (CISD)=19586 cm^{-1}, and T_e (CIDVD)=20172 cm^{-1}. DZP SCF harmonic frequencies and potential energy distributions for the $^3A'$ state are listed in Table XIII. The results are somewhat striking. The C_s^I stationary point for the $^3A'$ state is actually a transition state and not a local minimum! The 388*i* cm^{-1} mode is of a″ symmetry and consists primarily of torsional motion of the C-C-O plane relative to the H-C-H plane. Following this a″ mode and performing a careful geometry optimization without symmetry restrictions produced no C_1 minimum. In fact, the C_s^I $^3A'$ state was found to lead *smoothly* to the C_s^{II} $^3A''$ state without a barrier.

According to group theory the $^3A''$ state correlates to the $^3A_2$ C_{2v} state along C_s^{II} paths while the $^3A'$ state correlates to the $^3A_1$ C_{2v} state along C_s^I paths. Thus, since the $^3A''$ and $^3A'$ states correlate to *different* C_{2v} states, at first glance the connection of the $^3A''$ and $^3A'$ states along C_1 paths is perplexing. A resolution of the problem is apparent in Figs. 4-6. As shown in Table XIV and Fig. 6, the $^3A_2(^3A'')$ and $^3A_1(^3A')$ states have DZP CISD relative energies of 30325 and 45585 cm^{-1}, respectively, at the $\tilde{X}^1A_1$ C_{2v} geometry. However, along C_s^I paths the $^3A''$ and $^3A'$ curves cross. At the $^3A'$ stationary point the $^3A'$ state has a DZP CISD energy 19928 cm^{-1} *lower* than that of the $^3A''$ state. Along C_s^{II} paths the $^3A''$ and $^3A'$ curves do not *cross*. The $^3A'$ CISD energy at the $^3A''$ geometry is 28466 cm^{-1} *above* the $^3A''$ value. Therefore, as shown in Fig. 4, we have a classic example of a conical intersection of two potential surfaces.[85–87] In fact, due to the symmetry of the molecule, two conical intersections are present. In Fig. 4 the two lowest triplet surfaces of ketene are depicted, the total energy being shown as a function of coordinates Q^I and Q^{II}. $(Q^I, Q^{II})=(0,0)$ corresponds to the $\tilde{X}^1A_1$ C_{2v} geometry while $(Q^I, Q^{II})=(\pm1,0)$ and $(Q^I, Q^{II})=(0,\pm1)$ correspond to the $^3A'$ C_s^I and $^3A''$ C_s^{II} geometries, respectively. Figure 4 reveals that the upper state, which corresponds to the $^3A_1$ C_{2v} state, achieves local energy minima at the conical intersections, where the derivatives of the potential energy are singular and non-Born-Oppenheimer phenomena are expected. Thus, the upper state has no "valid" energy minimum. Furthermore, the C_s^I $^3A'$ and C_s^{II} $^3A''$ states are actually the same electronic state since they both correspond to different regions on the lowest triplet surface. Figure 4 shows that the C_s^I $^3A'$ state is actually the transition state for the interconversion of the two equivalent $^3A''$ C_s^{II} minima by rotation about the C-C axis. At the CISD level of theory this rotation barrier is 3131 cm^{-1} (Fig. 6) or about 9 kcal/mol, which as discussed above is roughly the energy stabilization of the $^3A''$ state due to C-C π bonding. Recall that a

typical C-C π bond energy is ≈63 kcal/mol.

2.3.4 The 2^1A_1 and $^1B_1$ states

In the nonvariational DZ SCF calculation of Dykstra and Schaefer, a vertical excitation energy of 39700 cm^{-1} was computed for the 2^1A_1 state, a value only 1670 cm^{-1} above that of the $^3A_1$ state. With the excited state (variational) SCF method of Davidson and Stenkamp, a vertical excitation energy of 76003 cm^{-1} (Table XIV) was obtained with the DZP basis set, giving a $^3A_1$-2^1A_1 splitting of 34305 cm^{-1}! Therefore, the previous nonvariational results[8] are unreliable, a possibility raised by Dykstra and Schaefer. At the DZP CISD level of theory vertical excitation energis of 45585 and 71690 cm^{-1} were computed for the $^3A_1$ and 2^1A_1 states. DZP SCF and CISD calculations were also performed for the $^1B_1$ state at the $\tilde{X}^1A_1$ geometry. As shown in Table XIV, the $^1B_1$ state is 692 cm^{-1} *below* the 2^1A_1 state in the SCF calculation but 2334 cm^{-1} *above* it in the CISD calculation. Dykstra and Schaefer showed that the $^1B_1$ state has significant Rydberg character and is drastically affected by the addition of diffuse functions to the basis set. With a DZ+R basis set they computed an SCF vertical excitation energy of 45930 cm^{-1} for the $^1B_1$ state. They also found that Rydberg functions were unimportant for the $^3A_1$ and 2^1A_1 states. However, since the 2^1A_1 state was greatly raised in energy in the excited state SCF calculation, it seemed quite possible that it too would have significant Rydberg character. Therefore, using the 82-CGF DZP+Rydberg basis set described previously, SCF and CISD vertical excitation energies were computed at the DZP SCF $\tilde{X}^1A_1$ geometry for both the $^1B_1$ and 2^1A_1 states and, for the sake of completeness, the $^3A_2$, $^1A_2$, and $^3A_1$ states as well.

In Table XIV the DZP and DZP+R vertical excitation energies for the five states of interest are compared. The DZP+R CISD energies for the $\tilde{X}^1A_1$, $^1B_1$, and 2^1A_1

states were obtained with wave functions consisting of 40859, 50958, and 80500 CSFs, respectively. It is evident in Table XIV that both the $^1B_1$ and 2^1A_1 states do indeed have significant Rydberg character. The $^1B_1$ state certainly lies below the 2^1A_1 state, the respective CIDVD excitation energies being 46719 and 56294 cm^{-1}. It is concluded that Frueholz et al.[17] were correct in assigning their 5.86 eV (47300 cm^{-1}) peak to the $\tilde{X}^1A_1 \rightarrow {}^1B_1$ transition. Furthermore, the 11000 cm^{-1} $^3A_1$–2^1A_1 splitting obtained here explains why only $\tilde{X}^1A_1 \rightarrow {}^3A_1$ transitions were observed in the electron-impact energy-loss spectrum.

The 46900-51000 cm^{-1} absorptions in the ketene electronic spectum (Table I) also appear to be due to $\tilde{X}^1A_1 \rightarrow {}^1B_1$ transitions. In the Rydberg series observed by Price, Teegan, and Walsh,[11] the n=4,5,6,7, and 8 members were fit very accurately with the formula

$$\nu_0(n) = 77491 - \frac{R}{(n-1.07)^2} \quad , \tag{10}$$

where ν_0 is in cm^{-1} and R is the Rydberg constant. However, for n=3, ν_0=48039 cm^{-1} was calculated, but a 54680 cm^{-1} band was assigned as the n=3 member. If one accepts the interpretation of Price et al. that the Rydberg series is of $\pi \rightarrow$ns ($\tilde{X}^1A_1 \rightarrow$m $^1B_1$)-type, then the current theoretical results suggest that the 54680 cm^{-1} band is due to $\tilde{X}^1A_1 \rightarrow 2^1A_1$ transitions while the 47200 cm^{-1} $\tilde{X}^1A_1 \rightarrow {}^1B_1$ band corresponds to the first (n=3) member of the Rydberg series. However, the interpretation of Herzberg[15] that the Rydberg series is of $\tilde{X}^1A_1 \rightarrow$m $^1A_1$-type seems more plausible. In accord with the assignments suggested by the theoretical results, the 54680 cm^{-1} band would still arise from $\tilde{X}^1A_1 \rightarrow 2^1A_1$ transitions but would also correspond to the first member of the Rydberg series. Subsequently, the poor fit of the 54680 cm^{-1} band to Eq. (10) could be explained (as in Ref. 11) on the basis of the antibonding character of the nb_1 orbital for n=3 relative to n greater than 3.

Both the 2^1A_1 and $^1B_1$ states become $^1A'$ states at C_s^I geometries. Since the $^1B_1$ state lies below the 2^1A_1 state, it follows that the $^1B_1$ state actually correlates to the $2^1A'$ state in C_s^I symmetry. Thus, the correlation diagrams of Yamabe and Morokuma[50] should be modified slightly. In particular, it is the $^1B_1(2^1A')$ state which crosses the $^1A''$ state and correlates to $^1B_1$ CH_2 + $^1\Sigma^+$ CO. As mentioned earlier, along C_{2v} paths the $^1B_1$ state was found in previous theoretical studies[8,24,25] to dissociate directly to CH_2 + CO, i.e., the dissociation curve decreased monotonically. Thus, it is quite possible that the $^1B_1$ $(2^1A')$ state also dissociates directly along C_s^I paths. Attempts were made to perform excited state SCF calculations for the $2^1A'$ state along the C_s^I path defined by the coordinate Q^I mentioned above. However, for values of Q^I over 0.60 severe convergence problems were encountered which at the time could not be overcome. Because of the paucity of data which is available, it cannot be stated that a C_s^I $2^1A'$ stationary point does not exist. However, the possibility of a stationary point, similar to that of the $^3A'$ state, lying below the $^1B_1$ CH_2 + $^1\Sigma^+$ CO threshold seems quite remote. A DZP SCF energy of 29714 cm^{-1} was obtained for the $^1B_1$ CH_2 + $^1\Sigma^+$ CO system with the optimized geometrical parameters of r(C=O)=1.1174 Å, r(C-H)=1.0701 Å, and θ(H-C-H)=142.65°. Hence, referring to Figs. 5 and 6 one sees that if a $2^1A'$ C_s^I stationary point exists, it surely occurs after the $^1A''$ curve crossing. Thus, it would merely be a transition state for the interconversion of the two equivalent C_s^{II} $^1A''$ minima by rotation about the C-C axis.

2.4 CONCLUSIONS

(1) Vertical excitation energies based on DZP+R CISD results (Tables I and XIV) are in very good agreement with experiment. The following values were obtained: $\tilde{X}^1A_1 \rightarrow {}^3A_2$ 29800 cm^{-1}, $\tilde{X}^1A_1 \rightarrow {}^1A_2$ 30900 cm^{-1}, $\tilde{X}^1A_1 \rightarrow {}^3A_1$ 44700 cm^{-1}, $\tilde{X}^1A_1 \rightarrow {}^1B_1$ 46600 cm^{-1}, and $\tilde{X}^1A_1 \rightarrow 2^1A_1$ 56100 cm^{-1}.

(2) Of the five lowest-lying states of ketene, only the $\tilde{X}^1A_1$, $^3A''$, and $^1A''$ states have valid local energy minima. All three of these minima lie well below the CH_2CO $(\tilde{X}^1A_1) \rightarrow CH_2(\tilde{X}^3B_1) + CO(^1\Sigma^+)$ dissociation energy.

(3) The predicted T_0 values for the $^3A''$ and $^1A''$ states are 16700 and 19000 cm^{-1}, respectively, at the highest levels of theory considered here. These predictions favor the experimental analysis of Laufer and Keller,[14] rather than that of Dixon and Kirby.[12] Equilibrium geometries, quadratic force constants, and vibrational frequencies for the $\tilde{X}^1A_1$, $^3A''$, and $^1A''$ states appear in Tables II, V, VI, VII, X, and XI.

(4) The $^1A''$ T_0 value of 19000 cm^{-1} predicted here suggests that Laufer and Keller[14] are indeed correct in concluding that no $\tilde{X}^1A_1 \rightarrow {}^3A''$ transitions have been observed in the electronic absorption spectrum of ketene. Accordingly, the electronic spectra of ketene observed to date neither preclude nor imply *direct* photoproduction of $^3B_1$ CH_2.

(5) The 2^1A_1 C_{2v} state of ketene is quite high lying. A CISD $\tilde{X}^1A_1 \rightarrow 2^1A_1$ vertical excitation energy of 56100 cm^{-1} (Fig. 6) was computed, giving a $^3A_1$–2^1A_1 splitting of 11400 cm^{-1}. These theoretical results support the interpretation that the $\tilde{X}^1A_1 \rightarrow 2^1A_1$ transition initiates a Rydberg series at 54680 cm^{-1} in the experimental electronic spectrum of ketene.

(6) At the $^1A''$ optimum geometry, the $\tilde{X}^1A_1(\tilde{X}^1A')$ state is predicted to lie only 5500-7000 cm^{-1} below the $^1A''$ state and appears to have a significant effect on the

$^1A''$ out-of-plane frequencies. Franck-Condon factors suggest it might be possible to observe fluorescence in the near-infrared region.

2.5 ACKNOWLEDGEMENTS

Dr. Michael J. Frisch is thanked for helpful discussions as is the research group of Professor C.B. Moore at Berkeley. This material is based upon work supported under a National Science Foundation Graduate Fellowship held by W.D.A. from 1983-86. This research was primarily supported by the Director, Office of Energy Research, Office of Basic Energy Sciences, Chemical Sciences Division of the U.S. Department of Energy under Contract No. DE-AC03-76SF00098. The Berkeley theoretical chemistry minicomputer was supported by the U.S. National Science Foundation, Grant No. CHE-8218785.

2.6 REFERENCES AND NOTES

[1] *The Chemistry of Ketenes, Allenes, and Related Compounds*, edited by S. Patai (Wiley, New York, 1980). For theoretical aspects, see especially C. E. Dykstra and H.F. Schaefer III, pp. 1-44 therein.

[2] F.A. Carey and R.J. Sundberg, *Advanced Organic Chemistry Part B: Reactions and Synthesis* (Plenum, New York, 1977), pp. 322-325.

[3] See K. Tanaka and M. Yoshimine, J. Am. Chem. Soc. **102**, 7655 (1980), and references contained therein.

[4] See W.J. Bouma, R.H. Nobes, L. Radom, and C. E. Woodward, J. Org. Chem. **47**, 1869 (1982), and references contained therein.

[5] A.H. Laufer, Rev. Chem. Int. **4**, 225 (1981).

[6] W. Kirmse, *Carbene Chemistry*, 2nd ed. (Academic, New York, 1971).

[7] D.J. Nesbitt, H. Petek, M.F. Foltz, S.V. Filseth, D.J. Bamford, and C.B. Moore, J. Chem. Phys. **83**, 223 (1985).

[8] C.E. Dykstra and H.F. Schaefer III, J. Am. Chem. Soc. **98**, 2689 (1976).

[9] G.C. Lardy, J. Chim. Phys. Phys.-Chim. Biol. **21**, 353 (1924).

[10] R.G.W. Norrish, H.G. Crone, and O. Saltmarsh, J. Chem. Soc. **1933**, 1533.

[11] W.C. Price, J.M. Teegan, and A.D. Walsh, J. Chem. Soc. **1951**, 920.

[12] R.N. Dixon and G.H. Kirby, Trans. Faraday Soc. **62**, 1406 (1966).

[13] J.W. Rabelais, J.M. McDonald, V. Scherr, and S.P. McGlynn, Chem. Rev. **71**, 73 (1971).

[14] A.H. Laufer and R.A. Keller, J. Am. Chem. Soc. **93**, 61 (1971).

[15] G. Herzberg, *Electronic Spectra of Polyatomic Molecules* (Van Nostrand, Princeton, 1966), pp. 341, 530, 622.

[16] M. Grossman, G.P. Semeluk, and I. Unger, Can. J. Chem. **47**, 3079 (1969).

[17] R.P. Frueholz, W.M. Flicker, and A. Kuppermann, Chem. Phys. Lett. **38**, 57 (1976).

[18] J. Vogt, M. Jungen, and J. L. Beauchamp, Chem. Phys. Lett. **40**, 500 (1976).

[19] J.H. Letcher, M.L. Unland, and J.R. Van Wazer, J. Chem. Phys. **50**, 2185 (1969).

[20] J.-M. André, M. Cl. André, G. Leroy, and J. Weiler, Int. J. Quantum Chem. **3**, 1013 (1969).

[21] Z. Yoshida and T. Kobayashi, Bull. Chem. Soc. Jpn. **45**, 742 (1972); J. Chem. Phys. **58**, 334 (1973).

[22] D.D. Shillady and C. Trindle, Int. J. Quantum Chem. Symp. **7**, 269 (1973).

[23] A.C. Hopkinson, J. Chem. Soc. Perkin Trans. II **1973**, 795.

[24] H. Basch, Theor. Chim. Acta **28**, 151 (1973); Jerusalem Symp. Quant. Chem. **6**, 183 (1974).

[25] P. Pendergast and W.H. Fink, J. Am. Chem. Soc. **98**, 648 (1976).

[26] L.B. Harding and W.A. Goddard III, J. Am. Chem. Soc. **98**, 6093 (1976).

[27] J.E. Del Bene, J. Am. Chem. Soc. **94**, 3713 (1972).

[28] O.P. Strausz, R.K. Gosavi, and H.E. Gunning, J. Chem. Phys. **67**, 3057 (1977).

[29] A.C. Hopkinson, M. Lien, K. Yates, and I.G. Csizmadia, Prog. Theor. Org. Chem. **2**, 230 (1977).

[30] O.P. Strausz, R.K. Gosavi, and H.E. Gunning, Chem. Phys. Lett. **54**, 510 (1978).

[31] C.E. Dykstra, J. Chem. Phys. **68**, 4244 (1978).

[32] M. Torres, E.M. Lown, H.E. Gunnning, and O.P. Strausz, Pure Appl. Chem. **52**, 1623 (1980).

[33] C.E. Dykstra, Annu. Rev. Phys. Chem. **32**, 25 (1981).

[34] H. Huber and J. Vogt, Chem. Phys. **64**, 399 (1982).

[35] D. Cremer, J. Comput. Chem. **3**, 154, 165 (1982).

[36] J. Breulet and J. Lievin, Theor. Chim. Acta **61**, 59 (1982).

[37] G. De Alti, P. Decleva, and A. Lisini, Chem. Phys. **76**, 185 (1983).

[38] O. Kysel and J. Danciger, Chem. Zvesti **38**, 289 (1984).

[39] The references listed below which deal with ketene photofragmentation are by no means complete but are intended to illustrate the available literature. See H. Okabe, *Photochemistry of Small Molecules* (Wiley-Interscience, New York, 1978), pp. 309-314 for a concise review of pertinent ketene results.

[40] K. Knox, R.G. Norrish, and G. Porter, J. Chem. Soc. **1952**, 1477.

[41] W.A. Noyes, Jr., and I. Unger, Pure Appl. Chem. **9**, 461, (1964).

[42] P.G. Bowers, J. Chem. Soc. A **1967**, 466.

[43] M.A. Voisey, Trans. Faraday Soc. **64**, 3058 (1968).

[44] G.B. Kistiakowsky and T.A. Walter, J. Phys. Chem. **72**, 3952 (1968).

[45] R.L. Russell and F.S. Rowland, J. Am. Chem. Soc. **92**, 7508 (1970).

[46] D.C. Montague and F.S. Rowland, J. Am. Chem. Soc. **93**, 5381 (1971).

[47] V. Zabransky and R.W. Carr, Jr., J. Phys. Chem. **79**, 1618 (1975).

[48] D. Feldmann, K. Meier, H. Zacharias, and K.H. Welge, Chem. Phys. Lett. **59**, 171 (1978).

[49] J.W. Simons and R. Curry, Chem. Phys. Lett., **38**, 171 (1976).

[50] S. Yamabe and K. Morokuma, J. Am. Chem. Soc. **100**, 7551 (1978).

[51] G.T. Fujimoto, M.E. Umstead, and M.C. Lin, Chem. Phys. **65**, 197 (1982).

[52] A.O. Langford, H. Petek, and C.B. Moore, J. Chem. Phys. **78**, 6650 (1983).

[53] B.I. Sonobe and R.N. Rosenfeld, J. Am. Chem. Soc. **105**, 7528 (1983).

[54] C.C. Hayden, D.M. Neumark, K. Shobatake, R.K. Sparks, and Y.T. Lee, J. Chem. Phys. **76**, 3607 (1982). In this study Lee and co-workers found only $^1A_1$ CH_2 and no evidence of $^3B_1$ CH_2 upon irradiation of ketene at 308 nm.

[55] C.E. Canosa-Mas, H.M. Frey, and R. Walsh, J. Chem. Soc. Faraday Trans. 2 **80**, 561 (1984); **81**, 283 (1985).

[56] S. Huzinaga, J. Chem. Phys. **42**, 1293 (1965).

[57] T.H. Dunning, Jr., J. Chem. Phys. **53**, 2823 (1970).

[58] C.C.J. Roothaan, Rev. Mod. Phys. **23**, 69 (1951); **32**, 179 (1960).

[59] B.A. Murtaugh and R.W.H. Sargent Comput J. **13**, 185 (1970).

[60] J.A. Pople, R. Krishnan, H.B. Schlegel, and J.S. Binkley, Int. J. Quantum Chem. Symp. **13**, 225 (1979).

[61] P. Saxe, Y. Yamaguchi, and H.F. Schaefer III, J. Chem. Phys. 77, 5647 (1982).

[62] Y. Osamura, Y. Yamaguchi, P. Saxe, M.A. Vincent, J.F. Gaw, and H.F. Schaefer III, Chem. Phys. 72, 131 (1982).

[63] Y. Osamura, Y. Yamaguchi, P. Saxe, D.J. Fox, M.A. Vincent, and H.F. Schaefer III, J. Mol. Struct. Fukui Festschrift **103**, 183 (1983).

[64] E.B. Wilson, Jr., J.C. Decius, and P.C. Cross, *Molecular Vibrations* (McGraw-Hill, New York, 1955).

[65] G.B. Fitzgerald, Ph.D. thesis, Univ. of California, Berkeley, 1984.

[66] G.B. Fitzgerald and H.F. Schaefer III, J. Chem. Phys. **83**, 1162 (1985).

[67] P.M. Morse and H. Feshbach, *Methods of Theoretical Physics* (McGraw-Hill, New York, 1953), pp. 1113-1114, 1153-1155.

[68] E.R. Davidson and L.E. McMurchie, Excited States **5**, 1 (1982).

[69] E.R. Davidson and L.E. Nitzsche, J. Am. Chem. Soc. **101**, 6524 (1979).

[70] E.R. Davidson and L.Z. Stenkamp, Int. J. Quantum Chem. Symp. **10**, 21 (1976).

[71] E.R. Davidson, Chem. Phys. Lett. **21**, 565 (1973).

[72] J.D. Goddard, N.C. Handy, and H.F. Schaefer III, J. Chem. Phys. **71**, 1525 (1979).

[73] Y. Yamaguchi, Y. Osamura, G. Fitzgerald, and H.F. Schaefer III, J. Chem. Phys. 78, 1607 (1983).

[74] Y. Yamaguchi, Y. Osamura, and H.F. Schaefer III, J. Am. Chem. Soc. **105**, 7506 (1983).

[75] A.P. Cox, L.F. Thomas, and J. Sheridan, Spectrochim. Acta **15**, 542 (1959).

[76] J.W.C. Johns, J.M.R. Stone, and G. Winnewisser, J. Mol. Spectrosc. **42**, 523 (1972).

[77] W.H. Fletcher and W.T. Thompson, J. Mol. Spectrosc. **25**, 240 (1968).

[78] D.C. McKean and J.L. Duncan, Spectrochim. Acta Part A **27**, 1879 (1971).

[79] C.B. Moore and G.C. Pimentel, J. Chem. Phys. **38**, 2816 (1963).

[80] P.D. Mallinson and L. Nemes, J. Mol. Spectrosc. **59**, 470 (1976).

[81] S.R. Langhoff and E.R. Davidson, Int. J. Quantum Chem. **8**, 61 (1974).

[82] M.M. Francl, W.J. Pietro, W.J. Hehre, J.S. Binkley, M.S. Gordon, D.J. DeFrees, and J.A. Pople, J. Chem. Phys. **77**, 3654 (1982).

[83] Y. Yamaguchi and H.F. Schaefer III, J. Chem. Phys. **73**, 2310 (1980).

[84] R.J. Buenker and S.D. Peyerimhoff in *New Horizons of Quantum Chemistry*, edited by P.-O Löwdin and B. Pullman (Reidel, London, 1983), pp. 183-219.

[85] E. Teller, J. Phys. Chem. **41**, 109 (1937).

[86] G.H. Herzberg and H.C. Longuet-Higgins, Discuss. Faraday Soc. **35**, 77 (1963).

[87] E.R. Davidson and W.T. Bordon, J. Phys. Chem. **87**, 4783 (1983).

[88] Additional confidence in the method A results for $^1A''$ ketene can be obtained by comparing method A, B, and C results for the open-shell $^1A''$ state of formaldehyde, which has a bent out-of-plane equilibrium geometry and two a″ normal modes. Method B DZ SCF frequencies appear in Ref. 62. Applying the excited state (TCSCF) method to the $\tilde{X}^1A_1(\tilde{X}^1A')$ and $^1A''$ states at the DZ SCF $^1A''$ geometry of Ref. 62 gives $E(\tilde{X}^1A')=-113.840427$ H and $E(^1A'')=-113.765690$ H. This 16403 cm^{-1} $\tilde{X}^1A'-{}^1A''$ separation is much larger than the corresponding 2861 cm^{-1} separation (Fig. 5) in ketene. For the a″ C-H stretch mode in formaldehyde, methods A, B, and C give frequencies of 3463, 3463, and 3446 cm^{-1}, respectively, while for the a″ CH_2 rock, values of 1087, 1069, and 1082 cm^{-1} are predicted. This excellent agreement for $^1A''$ formaldehyde indicates that the high method A a″ frequencies for $^1A''$ ketene do indeed result from the small $\tilde{X}^1A'-{}^1A''$ separation.

TABLE I.

Experimental and theoretical vertical excitation energies (cm^{-1}) of ketene.

	$\tilde{X}^1A_1 \rightarrow {}^3A_2$	$\tilde{X}^1A_1 \rightarrow {}^1A_2$	$\tilde{X}^1A_1 \rightarrow {}^3A_1$	$\tilde{X}^1A_1 \rightarrow {}^1B_1$	$\tilde{X}^1A_1 \rightarrow 2{}^1A_1$
Price *et al.*[a]	-	31300	-	47200[c]	54680[c]
McGlynn *et al.*[a]	-	31000	-	46900[c]	-
Dixon and Kirby[a]	27000?	31000	-	-	-
Laufer and Keller[a]	-	30300	-	-	-
Frueholz *et al.*[b]	-	30000	43000	47300	-
Dykstra and Schaefer[d]	25600	27500	40800	45900	(42900)[g]
Harding and Goddard[e]	29200	29800	43500	-	-
This work[f]	29800	30900	44700	46600	56100

For comparison, Lee and co-workers (Ref. 54) found the following dissociation energies:
$\tilde{X}^1A_1$ $CH_2CO \rightarrow \tilde{X}^3B_1$ $CH_2 + {}^1\Sigma^+$ CO, 27160 cm^{-1}
and $\tilde{X}^1A_1$ $CH_2CO \rightarrow {}^1A_1$ $CH_2 + {}^1\Sigma^+$ CO, 30140 cm^{-1}.

[a] Electronic absorption spectra, Refs. 11-14.

[b] Electronic-impact energy-loss spectrum, Ref. 17.
Similar electron-impact spectroscopic results appear in Ref. 18.

[c] Observed but not assigned to the transition listed.

[d] DZP or DZ+R SCF results, Ref. 8.

[e] GVB-CI results, Ref. 26.

[f] See the text and Table XIV.

[g] Nonvariational SCF result.

TABLE II.

Equilibrium geometrical parameters[a] and total energies for $\tilde{X}^1A_1$ ketene.

	Expt.[b]	DZ SCF[d]	DZP SCF(1)[c]	DZP SCF(2)[c]	CISD[e]
r_1(C=O)	1.161(2)	1.171	1.1476	1.1466	1.167
r_2(C=C)	1.316(2)	1.311	1.3100	1.3101	1.319
$t_1=t_2$(C-H)	1.0780(10)	1.070	1.0735	1.0735	1.077
α(H-C-H)	122.01	120.1	122.0	122.99	122.2
Total energies	-	-151.6753	-151.75603	-151.75667	-152.16008

[a] Bond lengths in Å and bond angles in degrees.

[b] Reference 80, r_0 parameters.

[c] This work, (1) α_d(O)=0.80, (2) α_d(O)=0.85.

[d] Reference 8.

[e] Reference 3.

TABLE III.

Total energies of $\tilde{X}^1A_1$ ketene at various geometries.

	Geometry		
	DZP SCF[a]	DZ SCF[b]	Expt.[c]
E(SCF)	-151.756673 (0 cm^{-1})	-151.755592 (237 cm^{-1})	-151.756153 (114 cm^{-1})
E(CISD)	-152.153102 (0 cm^{-1})	-152.153892 (-173 cm^{-1})	-152.154015 (-201 cm^{-1})
E(CIDVD)	-152.197335 (0 cm^{-1})	-152.198860 (-335 cm^{-1})	-152.198856 (-334 cm^{-1})

[a] This work, DZP SCF(2) geometry in Table II.

[b] Reference 8.

[c] Reference 79, r(C=O)=1.161 Å, r(C=C)=1.314 Å, r(C-H)=1.079 Å, and α=122.3°.

TABLE IV.
Symmetrized internal coordinates for ketene C_{2v}, C_s^I, and C_s^{II} geometries.[a]

C_{2v}		C_s^I		C_s^{II}	
A_1	$S_1 = r_1$	A′	$S_1 = r_1$	A′	$S_1 = r_1$
	$S_2 = r_2$		$S_2 = r_2$		$S_2 = r_2$
	$S_3 = (t_1 + t_2)/\sqrt{2}$		$S_3 = (t_1 + t_2)/\sqrt{2}$		$S_3 = t_1$
	$S_4 = (\beta_1 + \beta_2)/\sqrt{2}$		$S_4 = \delta$		$S_4 = t_2$
			$S_4 = (\beta_1 + \beta_2)/\sqrt{2}$		$S_4 = \delta$
B_1	$S_5 = \gamma$		$S_6 = \gamma$		$S_6 = \beta_1$
	$S_6 = \phi$				$S_7 = \beta_2$
			$S_7 = (t_1 - t_2)/\sqrt{2}$		
	$S_7 = (t_1 - t_2)/\sqrt{2}$	A″	$S_8 = (\beta_1 - \beta_2)/\sqrt{2}$	A″	$S_8 = \gamma$
B_2	$S_8 = (\beta_1 - \beta_2)/\sqrt{2}$		$S_9 = (\tau_1 + \tau_2)/\sqrt{2}$		$S_9 = \tau_2$
	$S_9 = \theta$				

[a] δ: C_3–C_2–O_1 angle. γ: C_2–C_3 out of H_4–C_3–H_5 plane angle. θ: C_3–C_2–O_1 linear bend in H_4–C_3–H_5 plane. ϕ: C_3–C_2–O_1 linear bend perpendicular to H_4–C_3–H_5 plane. τ_1: Torsional angle between H_4–C_3–C_2 and C_3–C_2–O_1 planes. τ_2: Torsional angle between H_5–C_3–C_2 and C_3–C_2–O_1 planes. Refer to Figs. 1-3 for additional definitions.

TABLE V.

Experimental and DZP SCF theoretical force fields for $\tilde{X}^1A_1$ ketene.[a]

		Experimental[b]		DZP SCF theoretical
		Anharmonic[c]	Harmonic[d]	Harmonic[e]
	F_{11}	16.578	15.384	19.2569
	F_{12}	0.954	0.515	1.2145
	F_{13}[f]	0	0	-0.0964
	F_{14}[f]	0	0	0.0027
A_1	F_{22}	8.387	9.219	10.5452
	F_{23}	1.487	1.590	0.1165
	F_{24}	0.413	0.407	0.4979
	F_{33}	5.547	6.080	6.4101
	F_{34}[f]	-0.226	-0.249	-0.0653
	F_{44}	1.194	1.236	1.3987
	F_{55}	0.118	0.121	0.1293
B_1	F_{56}	0.113	0.115	0.1067
	F_{66}	0.664	0.681	0.7948
	F_{77}	5.332	5.754	6.3680
	F_{78}	0.120	0.069	0.1919
B_2	F_{79}[f]	0	0	0.0123
	F_{88}	0.348	0.354	0.4501
	F_{89}	0.133	0.144	0.1571
	F_{99}	0.667	0.696	0.7651

[a] Units: $F_{rr'}$:mdyn/Å, $F_{r\theta}$:mdyn, $F_{\theta\theta'}$:mdyn Å.

[b] From Ref. 80, where $S_4'=\alpha$ as opposed to $S_4=(\beta_1+\beta_2)/\sqrt{2}$ in this study (see Fig. 1). At C_{2v} geometries, $\alpha+\beta_1+\beta_2=2\pi$, so to convert off-diagonal S'_4 force constants one multiplies by $-\sqrt{2}$, and to convert the diagonal S'_4 force constants one multiplies by 2.

[c] Based on anharmonic frequency data.

[d] Based on harmonized frequency data.

[e] Analytic SCF quadratic force constants.

[f] Constrained in the experimental analysis.

TABLE VI.

Experimental and theoretical vibrational frequencies and potential energy distributions for $\tilde{X}^1A_1$ ketene.

	Frequencies (cm^{-1})				Qualitative description	Potential energy distributions[c]	
	Expt.[a]	DZP SCF[b]		% Error		Expt.[a]	DZP SCF
$\nu_1(a_1)$	3070	3355	(26.5)	9.3	C-H stretch	$F_{33}(99)$	$F_{33}(99)$
$\nu_2(a_1)$	2152	2360	(1087)	9.7	C=O stretch	$F_{11}(74),F_{22}(26)$	$F_{11}(73),F_{22}(27)$
$\nu_3(a_1)$	1388	1537	(21.6)	10.7	HCH bend	$F_{22}(16),F_{33}(82)$	$F_{22}(16),F_{44}(81)$
$\nu_4(a_1)$	1118	1245	(3.3)	11.4	C=C stretch	$F_{11}(20),F_{22}(65)$	$F_{11}(21),F_{22}(63)$
$\nu_5(b_1)$	591	702	(152.6)	18.8	CH_2 wag	$F_{55}(82),F_{66}(18)$	$F_{55}(100)$
$\nu_6(b_1)$	525	618	(31.6)	17.7	C=C=O bend	$F_{66}(93)$	$F_{66}(93)$
$\nu_7(b_2)$	3166	3467	(5.1)	9.5	C-H stretch	$F_{77}(100)$	$F_{77}(100)$
$\nu_8(b_2)$	977	1094	(9.5)	12.0	CH_2 rock	$F_{88}(79),F_{99}(21)$	$F_{88}(81),F_{99}(19)$
$\nu_9(b_2)$	438	486	(8.6)	11.0	C=C=O bend	$F_{88}(33),F_{99}(67)$	$F_{88}(31),F_{99}(68)$

[a] Reference 79.

[b] Analytically computed IR intensities (km/mol) given in parentheses.

[c] The potential energy distributions in percent among the diagonal elements of the symmetrized force constant matrix F defined by $2V=S^TFS$ where V is the potential energy and the S elements are from Table IV.

TABLE VII.

Equilibrium geometrical parameters[a] and total energies for the $^3A''$ and $^1A''$ states of ketene.

	$^3A''$		$^1A''$	
	DZ SCF[b]	DZP SCF[c]	DZ SCF[b]	DZP SCF[c]
r_1(C=O)	1.200	1.1716	1.201	1.1742
r_2(C=C)	1.459	1.4660	1.455	1.4620
t_1(C-H_4)	1.076[d]	1.0735	1.076[d]	1.0728
t_2(C-H_5)	1.076[d]	1.0780	1.076[d]	1.0766
δ(C-C-O)	131.7	129.25	130.9	129.81
β_1(H_4-C-C)	121.1[d]	119.94	120.9[d]	120.02
β_2(H_5-C-C)	121.1[d]	119.60	120.9[d]	118.99
Total energy	-151.6219	-151.698510	-151.6118	-151.687466

[a] Bond lengths in Å and bond angles in degrees.

[b] Reference 8.

[c] This work.

[d] Constrained to be equal in the geometry optimization in Ref. 8.

TABLE VIII.

Total energies of $^3A''$ and $^1A''$ ketene at various geometries.

The $^3A''$ state				
r_1(C=O) (Å)[a]	1.1716	1.1856	1.2000	1.1927[b]
E(SCF)	-151.698510 (0 cm^{-1})	-151.698128 (84 cm^{-1})	-151.696982 (335 cm^{-1})	-151.697662 (186 cm^{-1})
E(CISD)	-152.078127 (0 cm^{-1})	-152.078860 (-161 cm^{-1})	-152.078853 (-160 cm^{-1})	-152.078953 (-181 cm^{-1})
E(CIDVD)	-152.119781 (0 cm^{-1})	-152.120985 (-264 cm^{-1})	-152.121469 (-371 cm^{-1})	-152.121318 (-337 cm^{-1})
The $^1A''$ state				
r_1(C=O) (Å)[a]	1.1742	1.1882	1.2010	1.1965[b]
E(SCF)	-151.687466 (0 cm^{-1})	-151.687084 (84 cm^{-1})	-151.686102 (299 cm^{-1})	-151.686519 (208 cm^{-1})
E(CISD)	-152.067885 (0 cm^{-1})	-152.068680 (-175 cm^{-1})	-152.068769 (-194 cm^{-1})	-152.068808 (-203 cm^{-1})
E(CIDVD)	-152.110247 (0 cm^{-1})	-152.111570 (-290 cm^{-1})	-152.112151 (-418 cm^{-1})	-152.112014 (-388 cm^{-1})

[a] All other geometrical parameters were held fixed at the DZP SCF optimum values.

[b] Interpolated CISD minimum listed with interpolated energies.

TABLE IX.
Theoretical vertical and adiabatic excitation energies (cm^{-1}) for $^3A''$ and $^1A''$ ketene.

	$^3A''$			$^1A''$		
	Vertical	T_e	T_0	Vertical	T_e	T_0
DZP SCF	26659	12765	12463	28587	15189	15091
DZP CISD	30325	16455	16153	31405	18703	18605
DZP CIDVD	31128	17021	16719	31866	19113	19015

TABLE X.
DZP SCF quadratic force constants for $^3A''$ and $^1A''$ ketene.[a]

		$^3A''$	$^1A''$		$^3A''$	$^1A''$
	F_{11}	17.5503	17.5138	F_{34}	0.0002	0.0012
	F_{12}	1.1685	0.8977	F_{35}	0.0500	0.0453
	F_{13}	-0.0063	-0.0111	F_{36}	-0.0016	-0.0018
	F_{14}	0.0747	0.0484	F_{37}	-0.1221	-0.1225
	F_{15}	0.1992	0.2146	F_{44}	6.2053	6.2667
	F_{16}	0.0761	0.0687	F_{45}	-0.0792	-0.0749
A′	F_{17}	0.0597	0.0441	F_{46}	-0.1167	-0.1175
	F_{22}	5.0960	5.5473	F_{47}	-0.0156	-0.0070
	F_{23}	0.0501	0.0605	F_{55}	1.1570	1.1434
	F_{24}	0.0543	0.0551	F_{56}	0.1246	0.1214
	F_{25}	0.3211	0.2752	F_{57}	-0.1483	-0.1457
	F_{26}	0.2713	0.2952	F_{66}	1.0565	1.0666
	F_{27}	0.1841	0.2133	F_{67}	0.4656	0.4592
	F_{33}	6.4061	6.4295	F_{77}	0.9921	1.0005
A″	F_{88}	0.1204	0.1439	F_{99}	0.1201	0.8462
	F_{89}	0.0464	0.2185			

[a] Units: $F_{rr'}$:mdyn/Å, $F_{r\theta}$:mdyn, $F_{\theta\theta'}$:mdyn Å.

TABLE XI.

DZP SCF vibrational frequencies and potential energy distributions for $^3A''$ and $^1A''$ ketene.

	Frequencies (cm^{-1})		Qualitative description	Potential energy distributions[a]	
	$^3A''$	$^1A''$		$^3A''$	$^1A''$
$\nu_1(a')$	3458	3469	asym. C-H stretch	$F_{33}(69),F_{44}(30)$	$F_{33}(66),F_{44}(34)$
$\nu_2(a')$	3319	3332	sym. C-H stretch	$F_{33}(30),F_{44}(70)$	$F_{33}(34),F_{44}(66)$
$\nu_3(a')$	2093	2108	C=O stretch	$F_{11}(93),F_{22}(4)$	$F_{11}(92),F_{22}(6)$
$\nu_4(a')$	1554	1556	HCH bend	$F_{66}(53),F_{77}(40)$	$F_{66}(53),F_{77}(39)$
$\nu_5(a')$	1158	1189	CH_2 rock	$F_{22}(25),F_{66}(27),F_{77}(36)$	$F_{22}(34),F_{66}(22),F_{77}(33)$
$\nu_6(a')$	1027	1052	C-C stretch	$F_{22}(51),F_{66}(27),F_{77}(20)$	$F_{22}(39),F_{66}(32),F_{77}(26)$
$\nu_7(a')$	508	509	CCO bend	$F_{55}(63),F_{66}(16),F_{77}(20)$	$F_{55}(65),F_{66}(15),F_{77}(19)$
$\nu_8(a'')$	680	1383	CH_2 wag	$F_{88}(59),F_{99}(41)$	$F_{88}(8),F_{99}(92)$
			or		
$\nu_9(a'')$	396	483	HCCO torsion	$F_{88}(30),F_{99}(70)$	$F_{88}(85),F_{99}(15)$

[a] See footnote c of Table VI.

TABLE XII.

Equilibrium geometrical parameters[a] and total energies for the $^3A'$ state of ketene.

	DZ SCF[b]	DZP SCF[c]		DZ SCF[b]	DZP SCF[c]
r_1(C=O)	1.190	1.1652	δ(C-C-O)	126.7	125.47
r_2(C-C)	1.519	1.5163	α(H-C-H)	124.1	117.66
$t_1=t_2$(C-H)	1.069	1.0788	γ	23.9	32.62
Total energy	-151.6060	-151.685145			

[a] Bond lengths in Å and bond angles in degrees.

[b] Reference 8.

[c] This work.

TABLE XIII.

DZP SCF vibrational frequencies and potential energy distributions for $^3A'$ ketene.

	Frequencies (cm^{-1})	Qualitative description	Potential energy distributions[a]
ν_1(a')	3288	C-H stretch	F_{33}(100)
ν_2(a')	2137	C=O stretch	F_{11}(95)
ν_3(a')	1508	H-C-H bend	F_{55}(95)
ν_4(a')	1060	C-C stretch	F_{22}(85),F_{44}(14)
ν_5(a')	806	CH_2 wag	F_{55}(29),F_{66}(65)
ν_6(a')	517	C-C-O bend	F_{44}(50),F_{66}(26)
ν_7(a'')	3409	C-H stretch	F_{66}(100)
ν_8(a'')	916	CH_2 rock	F_{88}(100)
ν_9(a'')	388 i	H-C-C-O torsion	F_{99}(98)

[a] See footnote c of Table VI.

TABLE XIV.

Theoretical vertical excitation energies (cm^{-1}) for the low-lying electronic states of ketene.[a]

	$^3A_2$	$^1A_2$	$^3A_1$	$^1B_1$	2^1A_1
DZP SCF	26659	28587	41698	75311	76003
DZP CISD	30325	31405	45585	74024	71690
DZP CIDVD	31128	31866	46446	73195	68959
DZP+R SCF	26215	28163	40928	44299	53083
DZP+R CISD	29830	30904	44677	46589	56051
DZP+R CIDVD	30628	31346	45502	46719	56294

[a] Obtained at the DZP SCF $\tilde{X}^1A_1$ geometry. The DZP+R SCF and CISD energies for the $\tilde{X}^1A_1$ state at this geometry are -151.758947 and -152.158510 hartree, respectively.

[b] Computed according to Eq. (9) of the text.

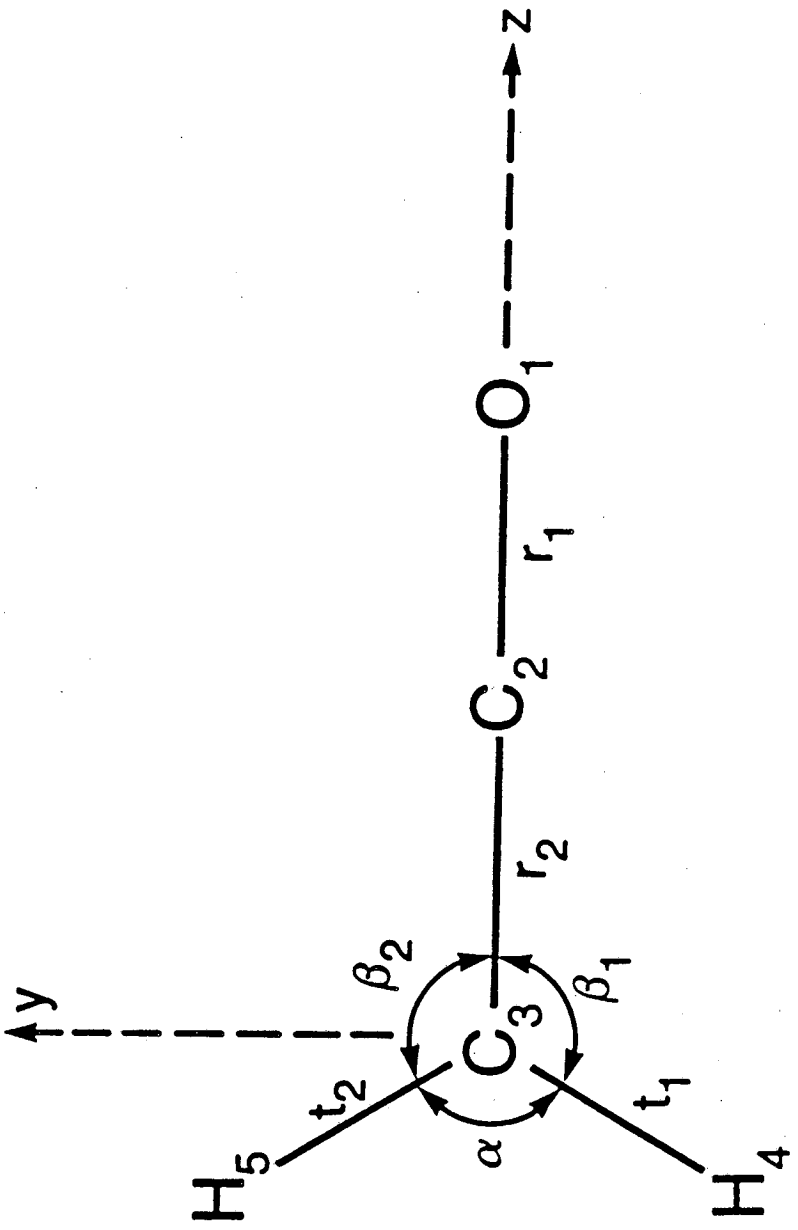

Figure 1. The C_{2v} equilibrium geometry and internal coordinates for the $\tilde{X}^1A_1$ state of ketene.

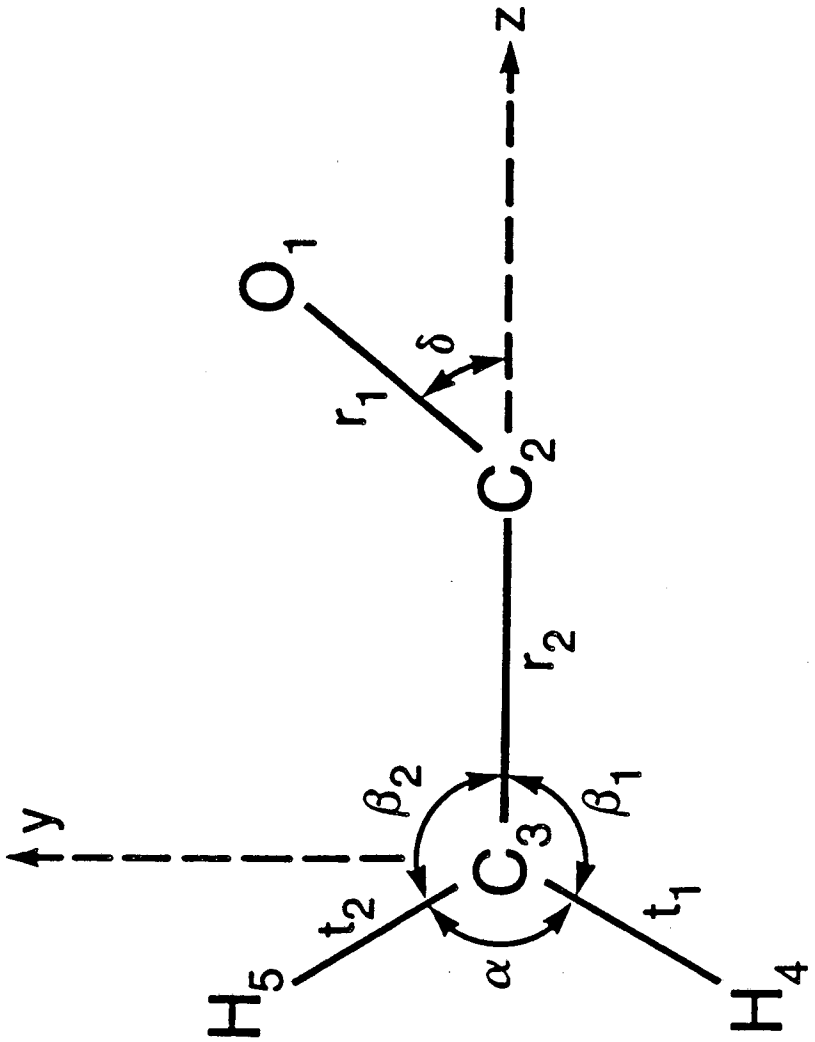

Figure 2. The C_s^{II} equilibruim geometry and internal coordinates for the $^3A''$ and $^1A''$ states of ketene.

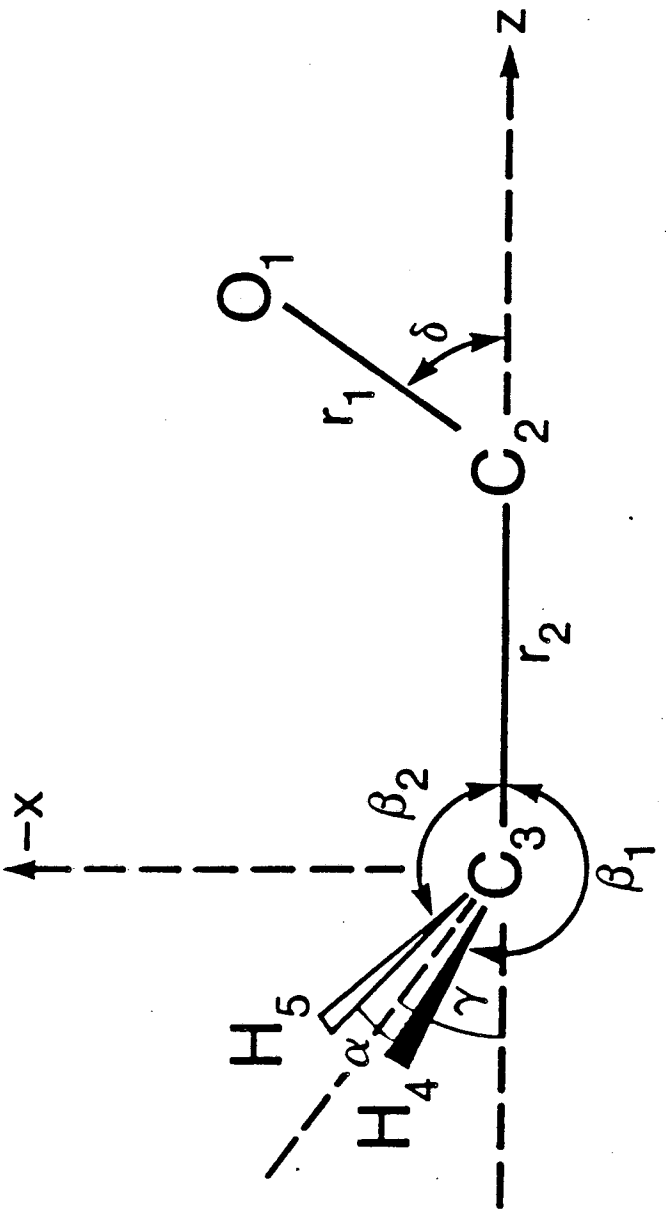

Figure 3. The C_s^1 geometry and internal coordinates for the $^3A'$ state of ketene.

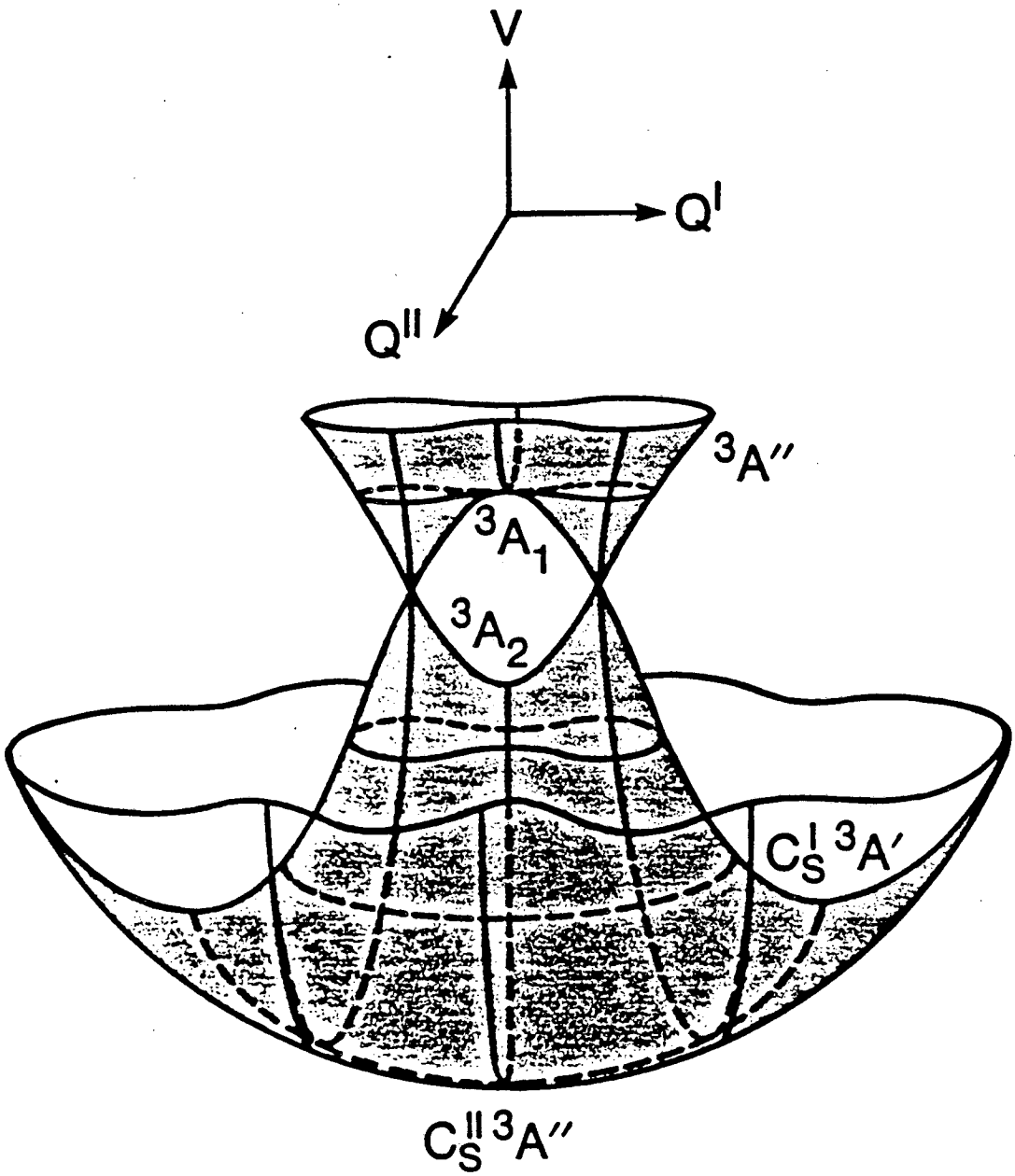

Figure 4. A sketch of the two lowest triplet surfaces of ketene. The potential energy is shown as a function of the coordinates Q^I and Q^{II} defined in the text.

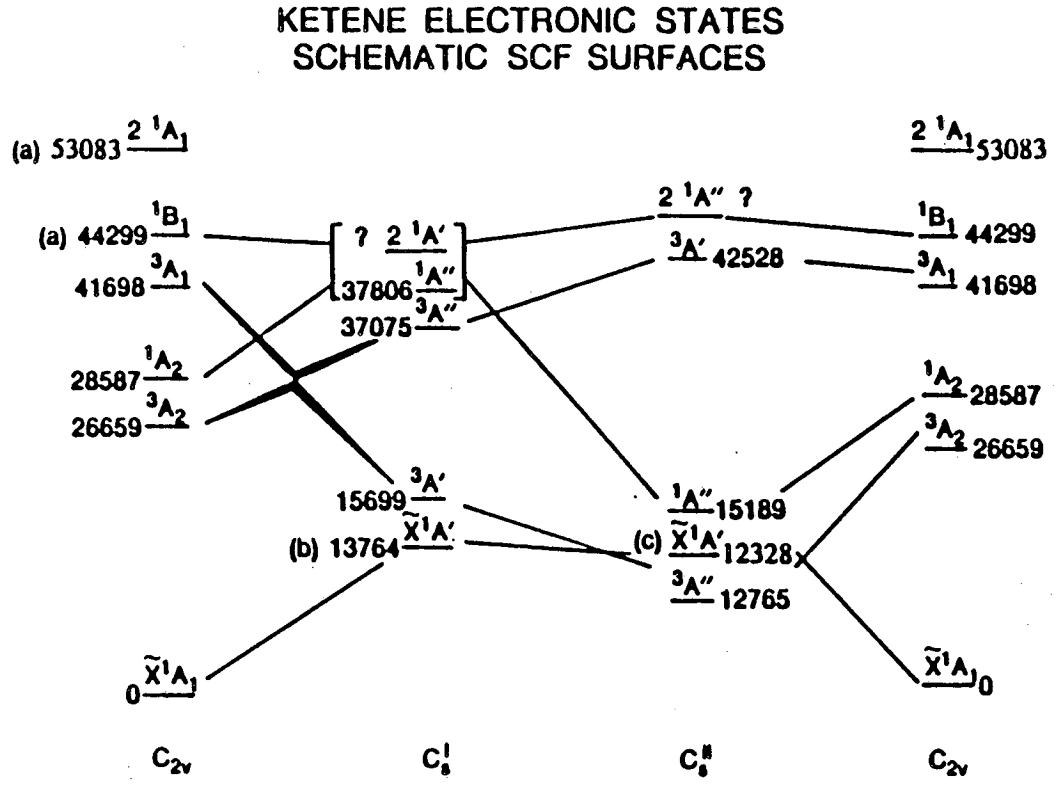

Figure 5. Relative SCF energies (in cm^{-1}) are shown for the low-lying electronic states of ketene at C_{2v}, C_s^I, and C_s^{II} geometries. The C_{2v} and C_s^I geometries are the DZP SCF optimum geometries for the $\tilde{X}^1A_1$ and $^3A'$ states, respectively. For singlet states the C_s^{II} geometry is the DZP SCF optimum geometry for the $^1A''$ state while for triplet states it is the corresponding DZP SCF $^3A''$ geometry. The energies listed are single-configuration DZP SCF values except for the following: (a) DZP+R SCF and excited state SCF results. (b) DZP TCSCF values with the second configuration $1a'^2 2a'^2 3a'^2 4a'^2 5a'^2 6a'^2 7a'^2 8a'^2 1a''^2 2a''^2 10a'^2$ (C_1=0.895 and C_2=-0.446). (c) DZP TCSCF values with the second configuration $1a'^2 2a'^2 3a'^2 4a'^2 5a'^2 6a'^2 7a'^2 8a'^2 1a''^2 9a'^2 3a''^2$ (C_1=0.978 and C_2=-0.206). Note that the $\tilde{X}^1A'$ and $^3A''$ energies are essentially equal.

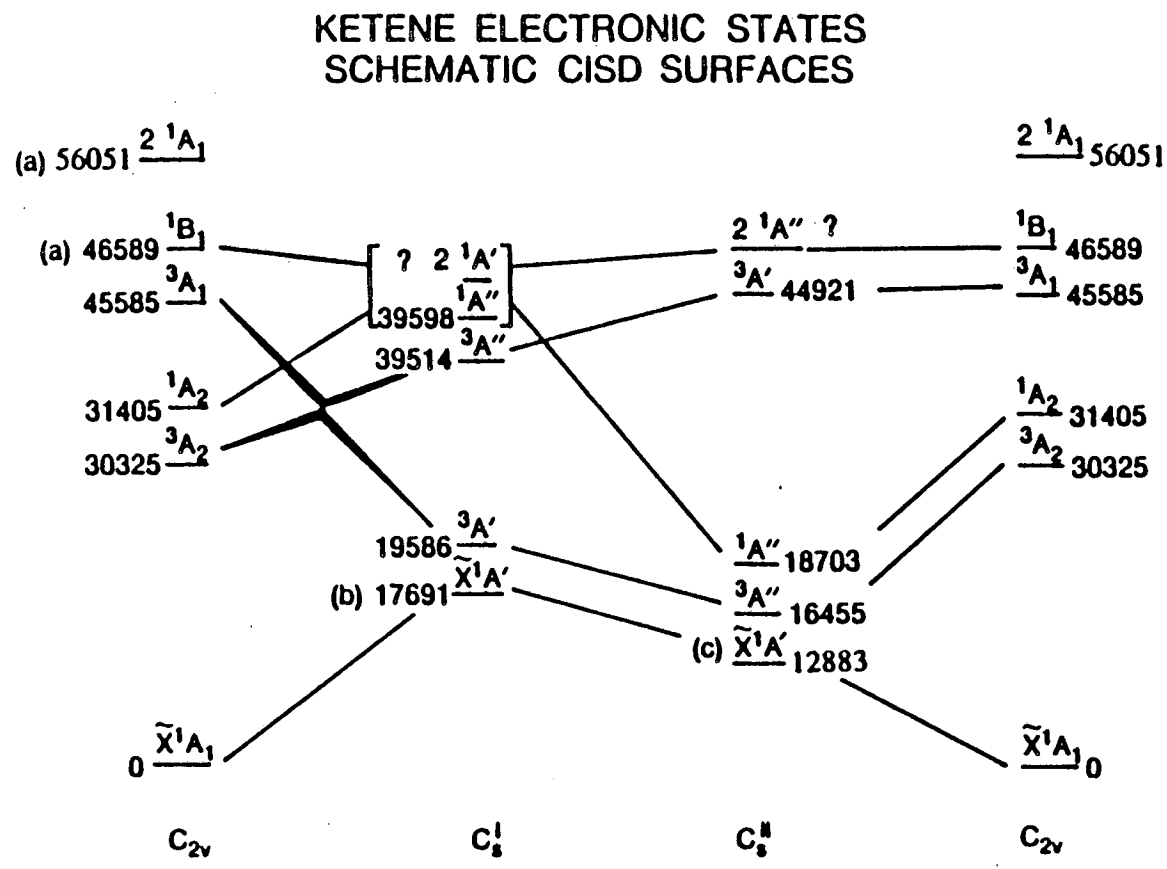

Figure 6. Relative CISD energies (in cm^{-1}) are shown for the low-lying electronic states of ketene at C_{2v}, C_s^I, and C_s^{II} geometries (identical to those in Fig. 5). The energies listed are single-reference DZP CISD values except for the special cases mentioned in the caption to Fig. 5: (a) DZP+R one- and two-reference CISD results. (b), (c) Two-reference CISD values corresponding to the DZP TCSCF results in Fig. 5.

Chapter 3 An Investigation of Reaction Paths for the Dissociation $\tilde{a}^3A''\ CH_2CO \rightarrow \tilde{X}^3B_1\ CH_2 + \tilde{X}^1\Sigma^+\ CO$

3.1 INTRODUCTION

Recent experimental determinations of photofragment energy state distributions for molecules such as H_2CO,[1] NCNO,[2–4] HNCO,[5–9] and CH_2CO[6,10,11] have provided valuable insights into the potential energy surfaces of these molecules and the dynamical processes which occur upon them. Fragment state distributions (near threshold) for bond fissions on ground state potential surfaces without barriers are matched well by simple phase space theory (PST) statistical models,[12,13] which assume that all product states allowed by conservation of total energy and angular momentum are equally probable. Thus, energy is randomized as the products separate slowly. In contrast, dissociations which occur with a barrier in the exit channel lead to nonstatistical fragment distributions,[1,11] as evidenced by poor agreement with phase space theory. Once the transition state for dissociation is reached, the fragments are repelled too rapidly for energy to be randomized.[13] Thus, the energy state distribution reflects the geometry of the transition state and the shape of the exit valley. In such cases simple impulse models may be applicable.[14–16] These models assume that the excess energy for dissociation is released as kinetic energy of the two atoms linked by the bond which is ruptured. In other words, the repulsive force is assumed to be directed along the breaking bond, and by conserving energy and momentum, the energy state distribution can be modeled. The crux is that the transition state geometry must be known, and *ab initio* theoretical predictions can be especially helpful in this regard.

The $\tilde{X}^1A_1$ and $\tilde{a}^3A''$ electronic states of ketene exhibit the two qualitatively different types of photofragmentation dynamics just mentioned. At 308 nm (32500 cm^{-1}) ketene is excited to the in-plane bent $\tilde{A}^1A''$ electronic state, but internal conversion to the ground state soon follows. On the S_0 surface, $\tilde{X}^1A_1$ CH_2CO dissociates to $\tilde{a}^1A_1$ CH_2 + $\tilde{X}^1\Sigma^+$ CO without a barrier along out-of-plane bent C_s^I paths. In 1985, Nesbitt, Petek, Foltz, Filseth, Bamford, and Moore[10] measured the rotational state distribution of nascent CO from ketene photolysis at 308 nm and found good agreement with phase space statistical theory. More recently, Bitto, Chen, and Moore[11] measured the CO rotational state distribution at 351 nm, or 28500 cm^{-1}, which is below the energy threshold for $\tilde{a}^1A_1$ CH_2 + $\tilde{X}^1\Sigma^+$ CO production. At 351 nm the $\tilde{A}^1A''$ state of ketene is still accessed initially, but intersystem crossing to the $\tilde{a}^3A''$ surface eventually occurs followed by dissociation to $\tilde{X}^3B_1$ CH_2 + $\tilde{X}^1\Sigma^+$ CO. The observed CO (v=0, J) rotational distribution exhibited a nonstatistical population inversion for $J < 13$, which was attributed to a barrier in the exit channel. Impulsive models were successful in describing the energy partitioning among the fragments, but the analysis was hampered by the lack of high-quality theoretical data. To quote Bitto, Chen, and Moore: "Parallel theoretical efforts are now needed, especially state-of-the-art *ab initio* calculations of the minimum energy paths and determination of the transition state geometries and vibrational frequencies." The current investigation is a response to this call.

Early theoretical studies of the photofragmentation curves of the low-lying electronic states of ketene were performed by Basch[17] and Pendergast and Fink.[18] However, Yamabe and Morokuma[19] were the first to report detailed MO and state correlation diagrams for all pertinent dissociation paths. By current standards the results of Yamabe and Morokuma are deficient in a quantitative sense because the STO-3G SCF level of theory was used throughout their study, but most of the qualitative

features of their dissociation curves are correct. Nonetheless, some modifications of the correlation diagrams are required based on the re-examination of the low-lying electronic states of ketene by Allen and Schaefer in 1986.[20]

In Fig. 1 appears a state correlation diagram for the C_{2v} dissociation of ketene to methylene and $\tilde{X}^1\Sigma^+$ CO. The vertical spacing in the diagram accurately reflects the relative energies of the initial and final states. The primary difference between Figs. 1-3 of this paper and Figs. 2-4 of Yamabe and Morokuma is the placement of the 2^1A_1 state of ketene above rather than below the $^{3,1}B_1$ states.[21] In the left- and right-hand columns of Fig. 1 the numbers of valence electrons in a_1, b_1, and b_2 orbitals are listed for each electronic state. Note that the ground state of ketene has an (a_1, b_1, b_2) occupation of (8,4,4) as opposed to (10,2,4) for $\tilde{a}^1A_1$ CH_2 + $\tilde{X}^1\Sigma^+$ CO. Therefore, a change in electronic configuration occurs along the C_{2v} dissociation path, and a large barrier is encountered on the S_0 surface. Such a reaction path is "forbidden" in the language of orbital symmetry conservation. The $^{3,1}A_2$, $^3A_1$, and 2^1A_1 states of ketene all have symmetries different from $^{3,1}B_1$ CH_2 + $^1\Sigma^+$ CO and thus correlate to higher-energy product states in C_{2v} symmetry. The states of ketene which do correlate to $^{3,1}B_1$ CH_2 + $^1\Sigma^+$ CO are the ($2b_1 \rightarrow 8a_1$) $^{3,1}B_1$ Rydberg states.[20] The electronic configurations of $^{3,1}B_1$ CH_2CO and $^{3,1}B_1$ CH_2 + $^1\Sigma^+$ CO are identical so that C_{2v} dissociation paths are "allowed". Indeed, several theoretical studies have found $^{3,1}B_1$ CH_2CO to dissociate monotonically.[17,18,22]

In Fig. 2 a state correlation diagram is shown for the in-plane bent dissociation of ketene. For consistency with Dykstra and Schaefer[22] and Allen and Schaefer,[20] this path is denoted C_s^{II}. The distributions of the valence electrons among the a′ and a″ orbitals are also listed in Fig. 2. Note that $\tilde{X}^1A_1$ $CH_2CO \rightarrow \tilde{a}^1A_1$ CH_2 + $\tilde{X}^1\Sigma^+$ CO is still "forbidden" while $^{3,1}A_2$ $CH_2CO \rightarrow {}^{3,1}B_1$ CH_2 + $^1\Sigma^+$ CO is "allowed". The spacing of the energy levels in Fig. 2 corresponds to the vertical excitation energies. If the geometries of the $^{3,1}A_2$ states are optimized, in-plane bent

C_s^{II} structures are obtained with total energies below those of $^{3,1}B_1$ CH_2 + $^1\Sigma^+$ CO.[20,22,23] Thus, the $^{3,1}A_2$ ($^{3,1}A''$) states of ketene lie in C_s^{II} potential energy wells which correlate to $^{3,1}B_1$ CH_2 + $^1\Sigma^+$ CO with small or nonexistent barriers. In reality, there is a small barrier (<4 kcal/mol)[11,24] for $^3A''$ CH_2CO dissociation in C_s^{II} symmetry, and this topic is the primary subject of this article.

In Fig. 3 appears a state correlation diagram for the out-of-plane bent (C_s^I) dissociation of ketene. Note that $\tilde{X}^1A_1$ $CH_2CO \rightarrow \tilde{a}^1A_1$ CH_2 + $\tilde{X}^1\Sigma^+$ CO is now "allowed", and as mentioned previously, dissociation of ketene on the S_0 surface proceeds without a barrier along C_s^I paths. The $^{3,1}A_2$ states become $^{3,1}A''$ in C_s^I symmetry and thus no longer correlate to the $^{3,1}B_1$ ($^{3,1}A'$) states of CH_2. It is the $^3A_1$ state which crosses the $^3A_2$ state and correlates to $^3B_1$ CH_2. This curve crossing manifests itself in at least two important ways. First, the $^3A_1$ state of ketene does not have a potential energy minimum which is valid in a Born-Oppenheimer sense. As shown in Fig. 4 of Ref. 20, a conical intersection of the two lowest triplet surfaces of ketene occurs, and the upper state achieves an energy minimum at the conical intersection. The $^3A_1$ state does correlate to a $^3A'$ stationary point in C_s^I symmetry, but because of the conical intersection, this $^3A'$ stationary point is actually a transition state for the interconversion of two equivalent $^3A''$ C_s^{II} minima through rotation about the C-C axis. The second manifestation of the ($^3A_2$, $^3A_1$) curve crossing is that any C_s^I transition state for the dissociation $^3A'$ $CH_2CO \rightarrow {}^3B_1$ CH_2 + $^1\Sigma^+$ CO is expected to actually be a super transition state for the interconversion of two equivalent $^3A''$ C_s^{II} transition states through rotation about the C-C axis. Consequently, the height of such a $^3A'$ C_s^I super transition state above a $^3A''$ C_s^{II} transition state for dissociation would be indicative of how tight or loose the $^3A''$ C_s^{II} transition state is.

An important modification in Fig. 3 relative to the C_s^I correlation diagram of Yamabe and Morokuma is that the $^1B_1$ rather than the 2^1A_1 state of ketene correlates

to $^1B_1$ CH_2 + $^1\Sigma^+$ CO. In analogy to the C_{2v} case, the $^1B_1$ state probably dissociates monotonically along C_s^I paths. In contrast, the 2^1A_1 state, which is predominantly Rydberg in character, achieves a minimum in C_{2v} symmetry similar to that of $^2B_1$ CH_2CO^+ and correlates in C_s^I symmetry to products much higher in energy than $^1B_1$ CH_2 + $^1\Sigma^+$ CO.[25]

As stated above, the current study addresses the need[11] for high-quality *ab initio* predictions concerning the C_s^{II} and C_s^I dissociations of triplet ketene into triplet methylene and ground-state CO. This topic does not appear to have been studied theoretically in detail since the work of Yamabe and Morokuma[19] was performed at the STO-3G SCF level in 1978. Dramatic improvements in theoretical methodology over the last decade have provided the tools to investigate this problem with greater quantitative accuracy. The primary goal of this study is to precisely locate transition states for the C_s^{II} and C_s^I dissociation paths of triplet ketene. The geometrical structures of the transition states will provide reliable data for impulse model calculations, and with the associated vibrational frequencies, RRKM calculations are feasible. The accurate *ab initio* prediction of the energetics of the dissociation paths is a more difficult task, but by combining theoretical results with experimental data, the energy profiles can be firmly established.

3.2 THEORETICAL METHODS

The reaction paths for the C_s^{II} dissociation $\tilde{a}^3A''$ CH_2 CO $\rightarrow$ $\tilde{X}^3B_1$ CH_2 + $\tilde{X}^1\Sigma^+$ CO and its C_s^I counterpart $^3A'$ CH_2CO $\rightarrow$ $\tilde{X}^3B_1$ CH_2 + $\tilde{X}^1\Sigma^+$ CO were investigated at the restricted Hartree-Fock (RHF) self-consistent-field (SCF) and configuration interaction singles and doubles (CISD) levels of theory. A standard Huzinaga[26] and Dunning[27] double-zeta plus polarization (DZP) basis set was used

throughout most of this study. This atomic-orbital basis is a C(9s5p1d/4s2p1d), O(9s5p1d/4s2p1d), and H(4s1p/2s1p) set consisting of 58 contracted Gaussian functions (CGFs). It is identical to that used by Allen and Schaefer[20] in their recent survey of the low-lying electronic states of ketene. The hydrogen s-function exponents were scaled by the usual factor of 1.2^2=1.44. Selected CISD energy points were obtained with a basis set of quadruple-zeta plus double-polarization (QZ2P) quality in the valence space consisting of 107 CGFs. For carbon and oxygen this QZ2P basis is a Huzinaga[26] and Dunning[28] (10s6p2d/5s4p2d) set with α_d(C)= 1.20, 0.40 and α_d(O)= 1.35, 0.45. For hydrogen the (6s2p/4s2p) basis used in Ref. 29 was employed with α_p(H)= 1.00, 0.30. In all configuration interaction wave functions the carbon and oxygen 1s core and 1s virtual orbitals were frozen. Consequently, the ketene $^3A''$ C_s^{II} and $^3A'$ C_s^{I} DZP CISD wave functions included 41336 and 40266 configuration state functions (CSFs), respectively.

Stationary points corresponding to the $^3A''$ and $^3A'$ optimum geometries, their transition states for dissociation, and the corresponding fragmentation products were located precisely (to 10^{-6} Å or radians in the internal coordinates) by using SCF and CISD analytic energy gradient methods. Harmonic vibrational frequencies and quadratic force constants were determined either with analytic second derivative techniques (SCF)[30] or by taking finite differences of analytic gradients (CISD).[31] For additional discussion of analytic derivative techniques the reader is referred to two recent reviews.[32,33] In the finite-difference procedures the quadratic force constants (F_{ij}) were obtained by displacing fully symmetrized internal coordinates (Table I) ±0.005 Å or ±0.01 rad. The cubic contaminations were removed from all numerical F_{ij} constants, and quartic contaminations were extracted from the F_{ii} values. The final harmonic frequencies determined from these numerical force constants are expected to differ from the analytic values by no more than 0.1 cm^{-1}.

3.3 RESULTS AND DISCUSSION

3.3.1 The $\tilde{X}^1A_1$ State of Ketene

In order to provide a reference for comparing the total energies, geometrical structures, and vibrational frequencies of the $^3A''$ and $^3A'$ states and to construct a standard for assessing the accuracy of these predictions, DZP CISD theoretical data were obtained for the $\tilde{X}^1A_1$ state of ketene. The $\tilde{X}^1A_1$ DZP CISD results are presented in Table II along with analogous DZP SCF data from Ref. 20.

The DZP CISD geometrical parameters are in good agreement with the CISD results of Tanaka and Yoshimine,[36] who obtained r_e(C-O) = 1.167 Å, r_e(C-C) = 1.319 Å, r_e(C-H) = 1.077 Å, and α_e(H-C-H) = 122.2° with a DZP basis containing an additional hydrogen 1s primitive and different C and H polarization function exponents. The errors in the DZP CISD C-O and C-C r_e distances in Table II are only +0.007 and +0.004 Å, respectively, when compared to experimental r_0 values.[34] The r_e(C-H) = 1.0785 Å result is in even better agreement with experiment (1.078 Å) but is also seen to be an overestimate if zero-point vibrational effects are considered. This overestimation of r_e(C-O), r_e(C-C), and r_e(C-H) can be ascribed primarily to basis set incompleteness, since large-basis CISD predictions of bond lengths are frequently slight *underestimates*. In Ref. 20 an estimate of -152.154015 was made for the optimum DZP CISD $\tilde{X}^1A_1$ energy in order to appraise the effects of geometry reoptimization on adiabatic excitation energies. The actual value of -152.154138 is only 27 cm^{-1} lower in energy, thus validating the previous prediction *post facto*.

As discussed in Ref. 20, seven of the nine DZP SCF $\tilde{X}^1A_1$ harmonic vibrational frequencies are between 9 and 12% above the experimental anharmonic frequencies, such agreement being typical of DZP SCF predictions. The remaining two frequencies, the b_1 CH_2 wag (ν_5) and the b_1 C-C-O out-of-plane bend (ν_6), are 18.8 and

17.7%, respectively, above experiment. The average error of all of the SCF frequencies 12.2%.

The most salient feature of the CISD frequencies is that the errors for $\nu_5(b_1)$ and $\nu_6(b_1)$ are only 2.5 and 0.8%. Thus, the primary deficiency in the DZP SCF description of the b_1 normal modes appears to be the lack of incorporation of electron correlation. The largest DZP CISD frequency error (8.1%) occurs for $\nu_7(b_2)$, the asymmetric C-H stretch. However, C-H stretching frequencies typically have anharmonicities of roughly 5%; thus, when compared to the experimental harmonic vibrational frequency for this mode, the ν_7 = 3422 cm^{-1} result should be comparable in accuracy to the $\nu_5(b_1)$ prediction mentioned above, for which anharmonicity is expected to be less significant. By appending SCF anharmonic corrections to the DZP CISD harmonic frequencies, one presumably could arrive at final predictions with an average error of roughly 2-4%.[37,38] Without such corrections the DZP CISD frequencies exhibit an average error of 5.3%. These $\tilde{X}^1A_1$ frequencies prove to be quite useful in scaling the frequencies for the $^3A''$ and $^3A'$ states in a mode-specific manner.

In Table III DZP SCF and CISD quadratic force constants for $\tilde{X}^1A_1$ ketene appear. The appropriate C_{2v} internal coordinates are defined in Table I and depicted in Fig. 4. The attention of the reader is directed to Ref. 20 for a discussion of the DZP SCF force field. The DZP CISD results apparently comprise the first published theoretical force field obtained with the inclusion of electron correlation.

3.3.2 The C_s^{II} Dissociation Path of $^3A''$ Ketene

In Table IV are given DZP SCF theoretical data for the C_s^{II} dissociation of $^3A''$ ketene, and in Fig. 5 the $^3A''$ transition state for dissociation is represented pictorially. The $^3A''$ equilibrium geometry and vibrational frequencies in Table IV are taken from Ref. 20, where they are discussed in some detail. Note that the DZP SCF

C-C distance increases from 1.4660 Å to 1.9472 Å in going from the equilibrium structure to the transition state. The DZP SCF vibrational analysis confirms the identification of the transition state for dissociation in that only one imaginary frequency is obtained [$\omega_6(a') = 871\,i$], which corresponds to C-C stretching motion. Upon inclusion of zero-point vibrational effects, the DZP SCF energy for the transition state is 20.16 kcal/mol above the value for the $^3B_1$ CH_2 + $^1\Sigma^+$ CO fragments, and the depth of the $^3A''$ potential energy well is only 2.56 kcal/mol. However, one would not expect DZP SCF theory to provide accurate energetics for this dissociation curve,[39] and indeed this expectation is borne out upon comparison with results which include electron correlation.

In Table V appear the DZP CISD data for the C_s^{II} dissociation of $^3A''$ ketene. Since these results are our best theoretical predictions, attention to some of the details is warranted. While the C-C distance in the equilibrium structure (1.4658 Å) is in close agreement with the SCF prediction, the C-C distance in the transition state (2.0708 Å) is over 0.12 Å longer than the SCF value. Hence, the transition state has shifted to a location farther out in the exit channel. The C-O bond length transforms smoothly from the 1.1930 Å value in the equilibrium structure to the 1.1386 Å value predicted for carbon monoxide. Concomitantly the H-C-H angle increases monotonically from 120.11° in $^3A''$ CH_2CO to 131.14° in the $^3B_1$ CH_2 fragment. In accord with the STO-3G SCF results of Yamabe and Morokuma,[19] the deviation of the C-C-O angle from linearity becomes larger as the molecule passes through the transition state. Specifically, the deviation increases [δ(C-C-O) decreases] from 50.75° to 62.33° at the DZP CISD level of theory.

The $^3A''$ equilibrium values r_e(C-O) = 1.1930 Å and E(CISD) = −152.079129 give confirmation of the r_e(C-O) = 1.1927 Å and E(CISD) = −152.078953 estimates in Ref. 20. Consequently, the DZP CISD $T_e(^3A'')$ = 16463 cm^{-1} adiabatic excitation

energy computed here differs by only 8 cm^{-1} from the corresponding value from the previous study. As expected, the $^3A''$ CISD well depth (13.29 kcal/mol) is much larger than the SCF value, and the corresponding barrier height for dissociation (10.68 kcal/mol) is much smaller. The addition of the Davidson correction to the CISD relative energies further increases the well depth to 14.92 kcal/mol and decreases the barrier height to 8.41 kcal/mol. Final predictions of these quantities are deferred until Section 3.3.4.

Consistent with the large reduction of the barrier height upon inclusion of electron correlation, the DZP CISD $\omega_6(a') = 560\ i\ cm^{-1}$ in the transition state is a 35.7% reduction from its SCF counterpart. The CH_2 rock (ω_5) and the C-C-O bend (ω_7) are also reduced significantly, reflecting a looser transition state at the DZP CISD level. Final scaled vibrational frequencies for the transition state, the equilibrium structure, and the fragments are listed in Table VI. These frequencies were obtained by constructing a one-to-one correspondence (i,j) between the normal modes of $^3A''$ CH_2CO (at the various stages along the C_s^{II} dissociation path) and those of $\tilde{X}^1A_1$ CH_2CO (at its equilibrium geometry); thence $\nu_{i,scaled}(^3A'') = \nu_{j,expt}(^1A_1) \cdot [\omega_{i,theory}(^3A'')/\omega_{j,theory}(^1A_1)]$ was employed. The data in Table VI should be quite reliable for use in, for example, RRKM calculations. In this regard it is worth noting that the $\nu_0(^1\Sigma^+$ CO) = 2136 cm^{-1} value in Table VI is in excellent agreement with the experimental value[41] of 2143 cm^{-1}, even though the scaling procedure used here is least applicable to the CO and CH_2 fragments. The agreement for the fundamentals of $^3B_1$ CH_2 appears to be somewhat poorer,[42] but considering that some question exists over the C-H stretching frequencies of triplet methylene,[43] a final judgement should perhaps be reserved.

The (unscaled) DZP SCF and CISD quadratic force constants pertinent to the C_s^{II} dissociation of $^3A''$ ketene are tabulated in Table VII. The appropriate C_s^{II}

internal coordinates are defined in Table I and depicted in Fig. 5.

Finally, a qualitative comparison of the electronic structural effects involved in the C_s^I $\tilde{X}^1A_1$ and C_s^{II} $^3A''$ dissociations is merited. As shown in Figs. 2 and 3, both processes are allowed according to conservation of orbital symmetry, but a qualitative difference exists in that the C_s^{II} $^3A''$ dissociation channel has a small barrier while the C_s^I $\tilde{X}^1A_1$ channel does not. This occurrence can be rationalized using simple bonding concepts. In the C_s^I formation of $\tilde{X}^1A_1$ ketene, the carbon lone pair in CO is donated into the empty p orbital in $^1A_1$ CH_2 while the lone pair in the methylene moiety is donated into a CO π^* orbital. The out-of-plane bending into C_s^I symmetry allows these processes to occur in different regions of space, and conformations in which the CO and CH_2 lone pairs are pointed directly at one another are avoided. Accordingly, a smooth transition occurs between the electronic structure of the CH_2 and CO fragments and that of $\tilde{X}^1A_1$ CH_2CO; hence, no barrier is encountered. The difference in the C_s^{II} formation of $^3A''$ CH_2CO arises because $^3B_1$ CH_2 does not have an empty p orbital available to receive electron density. The in-plane, singly-occupied orbital ($3a_1$) in $^3B_1$ CH_2 must shift onto the CO carbon atom while the carbon lone pair in CO (5σ) is simultaneously donated into the methylene carbon center. The decrease in the C-C-O angle at the transition state relative to that in the $^3A''$ equilibrium structure apparently decreases the interaction of these CH_2 ($3a_1$) and CO (5σ) electrons but is not sufficient to avert a small barrier along C_s^{II} paths due to electron reorganization. Once the transition state is passed in the C_s^{II} formation of $^3A''$ ketene, a larger equilibrium value of the C-C-O angle is approached as governed by Walsh-type ideas.[44,45] Specifically, the reduction of the C-C-O angle from 180° is driven by the large stabilization of the singly-occupied $3b_2$ ($10a'$) orbital in the $^3A_2$ ($^3A''$) state and counterbalanced by moderate destabilizations of several other occupied valence orbitals.

3.3.3 The C_s^I Dissociation Path of $^3A'$ Ketene

In Table VIII DZP SCF theoretical data are given for the C_s^I dissociation of $^3A'$ ketene, and in Fig. 6 the $^3A'$ transition state for dissociation is depicted. The pertinent correlation diagram appears in Fig. 3, where the $^3A_1$ state is shown to become the $^3A'$ state in C_s^I symmetry and correlate to $^3B_1$ methylene. Actually, the correlation of $^3A_1$ CH_2CO to $^3B_1$ CH_2 + $^1\Sigma^+$ CO is a little more subtle than indicated in Fig. 3. Using the DZP+R basis set of Ref. 20, the following vertical excitation energies are predicted: $^3A_1$ CH_2CO, E(CISD) = 44677 cm^{-1}, E(CIDVD) = 45502 cm^{-1}; $^3B_1$ CH_2CO, E(CISD) = 44967 cm^{-1}, E(CIDVD) = 45094 cm^{-1} (CIDVD = Davidson-corrected CISD). Therefore, the $^3A_1$ valence state and the $^3B_1$ Rydberg state are close in energy, and the $^3B_1$ state may actually be lower. However, the actual vertical ordering of the states is a moot point. The DZP SCF optimum C_{2v} geometry for the $^3A_1$ state is r_e (C-O) = 1.1833 Å, r_e (C-C) = 1.5150 Å, r_e (C-H) = 1.0696 Å, and α_e(H-C-H) = 124.63°. At this geometry the DZP+R energies of the $^3A_1$ and $^3B_1$ states relative to the $\tilde{X}^1A_1$ optimum value are: $^3A_1$, E(CISD) = 36592 cm^{-1}, E(CIDVD) = 37009 cm^{-1}; and $^3B_1$, E(CISD) = 44937 cm^{-1}, E(CIDVD) = 44282 cm^{-1}. Thus, the $^3A'$ state whose optimum C_s^I geometry is listed in Table VIII should be unambiguously associated with the valence $^3A_1$ state. In this sense the correlation $^3A_1$ $CH_2CO \rightarrow {}^3A'$ $CH_2CO \rightarrow {}^3B_1$ CH_2 + $^1\Sigma^+$ CO is apt.

The DZP SCF C-C distance for $^3A'$ ketene increases from 1.5163Å to 1.9444 Å in going from the optimum C_s^I structure to the transition state. The latter value differs from the analogous $^3A''$ distance by only 0.0028 Å. The DZP SCF vibrational analysis actually indicates two imaginary frequencies for the "transition state": $\omega_4(a') = 903i$ cm^{-1} (C-C stretch) and $\omega_9(a'') = 163i$ cm^{-1} (H-C-C-O torsion).[66] This phenomenon is in accord with the expectation stated in the introduction section of

this paper, viz., because of the ($^3A_2$,$^3A_1$) curve crossing, any C_s^I transition state for the dissociation of $^3A'$ ketene is actually a super transition state for the interconversion of two equivalent $^3A''$ C_s^{II} transition states for dissociation. Indeed, by following the $^3A'$ normal mode corresponding to $\omega_9(a'') = 163i$ cm^{-1}, one eventually arrives at the $^3A''$ C_s^{II} transition state discussed in the previous section. At the SCF level and including zero-point vibrational energy, the rotational barrier for the interconversion of the two equivalent $^3A''$ transition states is only 21.75 – 20.16 = 1.59 kcal/mol (cf. Tables IV and VIII). For comparison, the rotational barrier for the $^3A''$ equilibrium structure is 7.65 kcal/mol at the same level of theory.

The DZP CISD data for the C_s^I dissociation of $^3A'$ ketene are listed in Table IX. The C-C distance in the $^3A'$ optimum structure is 1.5180 Å as compared to 2.0544 Å in the transition state. Recall that the corresponding $^3A''$ lengths are 1.4658 and 2.0708 Å. The DZP CISD r_e(C-O), r_e(C-H), and δ_e(C-C-O) values in the $^3A'$ transition state are all in close proximity to the $^3A''$ parameters and also exhibit monotonic variations as the C_s^I dissociation path is traversed. A similar statement holds for the α_e(H-C-H) angle, despite the predictions at the SCF level. In this regard note that the inclusion of electron correlation reduces the H-C-H angle in the transition state substantially from 133.00° to 126.98°. Electron correlation also reduces the CH_2 wagging angle γ (Fig. 6) significantly from 30.44° to 23.06°. The differences in the $^3A'$ and $^3A''$ well depths are 7.98 and 8.02 kcal/mol at the DZP CISD and CIDVD levels, respectively, indicating a moderate rotational barrier for the interconversion of the two equivalent $^3A''$ C_s^{II} minima. The analogous CISD and CIDVD rotational barriers for the $^3A''$ transition state are only 1.25 and 1.10 kcal/mol. Therefore, the transformation of the H-C-C-O torsional motion in the transition state from harmonic oscillator to free rotor behavior can occur for rather small values of the excess energy for dissociation, and this fact should be taken into account in theoretical models for

the reaction rate.

Final scaled DZP SCF and CISD vibrational frequencies for the $^3A'$ C_s^I optimum structure, transition state, and fragments are given in Table X. These frequencies were obtained as for the $^3A''$ state by using mode-specific scale factors based on $\tilde{X}^1A_1$ results. Unscaled DZP SCF and CISD quadratic force constants for $^3A'$ ketene are tabulated in Table XI. The C_s^I internal coordinates are defined in Table I and illustrated in Fig. 6.

3.3.4 Final Energetics for $^3A''$ Ketene Dissociation

No direct experimental values exist for the $\tilde{a}^3A''$ $CH_2CO \rightarrow \tilde{X}^3B_1$ CH_2 + $\tilde{X}^1\Sigma^+$ CO dissociation energy, but through a combination of experimental and theoretical results a reliable estimate is obtained in this section. In 1982 Hayden, Neumark, Shobatake, Sparks, and Lee[24] measured fragment velocities from ketene photodissociation at 351 and 308 nm in a molecular beam and obtained values of $D_0(^3B_1)$ = 27160 and $D_0(^1A_1)$ = 30140 cm^{-1}, respectively, for the $\tilde{X}^1A_1$ $CH_2CO \rightarrow \tilde{X}^3B_1$ CH_2 + $\tilde{X}^1\Sigma^+$ CO and $\tilde{X}^1A_1$ $CH_2CO \rightarrow \tilde{a}^1A_1$ CH_2 + $\tilde{X}^1\Sigma^+$ CO dissociation energies. Moore and co-workers[46] have recently obtained a more precise experimental value for the singlet threshold, viz., $D_0(^1A_1)$ = 30116 ± 1 cm^{-1}. When combined with the best known value (T_0 = 9.02 ± 0.01 kcal/mol)[47–51] for the singlet-triplet splitting in methylene, the new result of Moore et al. yields $D_0(^3B_1)$ = 26961 ± 5 cm^{-1}, which is accepted here as the experimental $\tilde{X}^1A_1$ $CH_2CO \rightarrow \tilde{X}^3B_1$ CH_2 + $\tilde{X}^1\Sigma^+$ CO dissociation energy. Thus, in order to arrive at a D_0 value for $\tilde{a}^3A''$ $CH_2CO \rightarrow \tilde{X}^3B_1$ CH_2 + $\tilde{X}^1\Sigma^+$ CO, an accurate determination of the $\tilde{X}^1A_1 \rightarrow \tilde{a}^3A''$ CH_2CO adiabatic excitation energy is needed.

In Table XII results for T_e of $^3A''$ CH_2CO are presented for several levels of theory. The DZP CISD and CIDVD values are 16463 and 17036 cm^{-1}, respectively.

Augmenting the one-particle basis by employing the QZ2P set described in Section 3.2 yields T_e(QZ2P CISD) = 17365 cm^{-1} and T_e(QZ2P CIDVD) = 18004 cm^{-1}. Since the amount of correlation energy which is missing at the single-reference CISD level of theory should be several kcal/mol greater for the $\tilde{X}^1A_1$ state than for the $^3A''$ state, the T_e = 17365 cm^{-1} prediction can be considered a lower bound. An important second configuration which is needed to provide a more consistent treatment of the $\tilde{X}^1A_1$ state relative to the $^3A''$ state arises from the $\pi \rightarrow \pi^*$ ($2b_1 \rightarrow 3b_1$) double excitation.[52] If a $\pi^2 \rightarrow \pi^{*2}$ QZ2P TCSCF reference wave function (C_2 = – 0.162) is employed for the ground state, T_e(QZ2P TCSCF) = 17879 cm^{-1}, T_e(QZ2P 2R CISD) = 19007 cm^{-1}, and T_e(QZ2P 2R CIDVD) = 18908 cm^{-1} are predicted (2R = two-reference). Note that the two-reference Davidson correction[53] actually reduces the 2R CISD T_e result by a small amount (99 cm^{-1}), and indeed the 19007 cm^{-1} QZ2P 2R CISD prediction may be an overestimate of the QZ2P full CI value since the calculation could now be biased slightly in favor of the ground state. However, further expansion of the one-particle basis set is expected to increase the $\tilde{X}^1A_1$–$^3A''$ splitting further, so the final proposal favored here is $T_e(^3A'') \approx 18900$ cm^{-1}. Utilizing the scaled DZP CISD $^3A''$ vibrational frequencies in Table VI and the observed $\tilde{X}^1A_1$ fundamentals in Table II, one finds a zero-point vibrational energy (ZPVE) correction to T_e of –255 cm^{-1}. Therefore, an adiabatic excitation energy of $T_0 \approx 18650$ cm^{-1} is predicted for the $^3A''$ state of ketene.

The $T_0(^3A'')$ = 18650 cm^{-1} estimate is in accord with values (Table XII) from other theoretical methods based on Møller-Plesset perturbation theory.[54,55] The most elaborate of these methods is BAC-MP4,[56–58] which utilizes 6-31G** MP4(SDTQ)//6-31G* SCF *ab initio* data and empirical bond additivity corrections (BACs) to arrive at heats of formation. For a wide variety of H, C, N, and O containing molecules, the method gives ΔH_f° results within 3 kcal/mol of experiment

with an average difference of less than one kcal/mol. For example, the BAC-MP4 ΔH_f^o prediction for $\tilde{X}^1A_1$ CH_2CO at 0 K is –10.79 kcal/mol, which differs from the experimental value (–10.7 kcal/mol)[59] by only 0.1 kcal/mol. For $^3A''$ CH_2CO, $\Delta H_{f,0}^o$ = 43.30 kcal/mol is predicted (including ZPVE effects and corrections due to spin contamination in the $^3A''$ UHF reference wave function). Consequently, the BAC-MP4 scheme gives $T_0(^3A'')$ = 54.09 kcal/mol (18920 cm^{-1}), which is only 0.77 kcal/mol higher than the $T_0(^3A'')$ = 18650 cm^{-1} proposal made above.

An additional check of the $T_0(^3A'')$ = 18650 cm^{-1} estimate can be made by ascertaining the implications for T_0 of $\tilde{A}^1A''$ ketene. In Table XIII the DZP CISD C_s^{II} optimum geometry for the $\tilde{A}^1A''$ state is given along with DZP and QZ2P CISD and CIDVD total energies. Since the single-reference CISD level of theory should provide consistent treatments of the $^3A''$ and $^1A''$ states, the $^3A''$ – $^1A''$ splitting is expected to be more accurate than the corresponding $\tilde{X}^1A_1$ – $^1A''$ value. The QZ2P CISD and CIDVD $^3A''$ – $^1A''$ separations are 2224 and 2045 cm^{-1}, respectively, as compared to the analogous DZP predictions of 2231 and 2048 cm^{-1}. The ZPVE effect on the $^3A''$ – $^1A''$ splitting is rather difficult to ascertain because the a″ vibrational frequencies (ν_8 and ν_9) for the $^1A''$ state appear to be strongly perturbed by the close-lying $\tilde{X}^1A'$ state. In the 1986 study of Allen and Schaefer,[20] ω_8 = 599 cm^{-1} and ω_9 = 427 cm^{-1} were obtained for the $^1A''$ state from a conventional open-shell singlet SCF analytic second derivative approach, and ω_8 = 1383 cm^{-1} and ω_9 = 483 cm^{-1} were predicted using an excited-state SCF (SCFX) wave function equivalent to a two-electron-in-two-orbital CASSCF. The first pair of frequencies is less satisfactory theoretically due to the possibility of variational collapse while ω_8 in second pair is probably too large because configuration interaction more than doubles the SCFX $\tilde{X}^1A'$ – $^1A''$ energy separation. Averaging the two ω_8 and ω_9 possibilities, combining them with the a′ frequencies in Table XI of Ref. 20, and multiplying by a scale

factor of 0.90 gives a ZPVE correction to the $^3A'' - {}^1A''$ splitting of +211 cm^{-1}. Subsequently, $T_0(^1A'') - T_0(^3A'') = 2256$ cm^{-1} results from the QZ2P CIDVD energies, and this separation suggests a final estimate of $T_0(^1A'') = 18650 + 2256 = 20906$ cm^{-1}. Not only is this $T_0(^1A'')$ estimate in accord with the experimental $T_0(^1A'') < 21300$ cm^{-1} upper bound of Laufer and Keller[60] but it is also tantalizingly close to the lowest $\tilde{X}^1A_1 \rightarrow {}^1A''$ absorption (21119 cm^{-1}) observed by Dixon and Kirby.[61] One concludes that if the 21119 cm^{-1} $^1A''$ energy level does not correspond to the lowest vibrational level on the $^1A''$ surface, then it must involve only one quantum (or at most two) in the $\nu_7(a')$ C-C-O bending mode.

Accepting the $T_0(^3A'') = 18650$ cm^{-1} value, then as a result of our deliberations a $^3A''$ $CH_2CO \rightarrow {}^3B_1$ $CH_2 + {}^1\Sigma^+$ CO dissociation energy of 26961 – 18650 = 8311 cm^{-1} (23.76 kcal/mol) is obtained. This "experimental" number is to be compared with the results listed in Tables V and XIV from several levels of theory. Recall that the DZP CISD and CIDVD $^3A''$ CH_2CO dissociation energies (Table V) are 13.29 and 14.92 kcal/mol, and thus the $^3A''$ well depth is predicted to be 10.47 and 8.84 kcal/mol too small, respectively, at these levels of theory.

The effect of incorporating additional electron correlation into the DZP CI predictions was investigated as follows. First, iterative natural orbitals based on the CISD configuration space were determined, the DZP NO-CISD energy at each geometry being converged to less than 10^{-6} hartrees. Multi-reference (MR) CISD energies were then obtained using the iterative natural orbitals. The references consisted of all possible configuration state functions (a total of 61 CSFs) generated by distributing six electrons among the 9a′, 10a′, 11a′, 1a″, 2a″, and 3a″ orbitals. Under this partitioning the most dominant configurations appearing in the NO-CISD wave functions at each geometry were included as references. All single and double excitations relative to the reference set were included in the final multi-reference CI wave functions.

To make such a calculation feasible, the three carbon and oxygen 1s core orbitals were frozen as were all natural orbitals with occupation numbers less than 0.00050. Thus, relative to the SCF reference configuration, seven doubly occupied, two singly occupied, and 32 unoccupied orbitals were active. The total number of configuration state functions included in the DZP MR CISD procedure was then 1 028 883. The 15 most important configurations in the $^3A''$ CH_2CO and $^3B_1$ CH_2 + $^1\Sigma^+$ CO DZP MR CISD wave functions are listed in Table XV.

As shown in Table XIV, the DZP MR CISD $^3A''$ well depth is 15.65 kcal/mol, which is still 8.11 kcal/mol too small. Somewhat better agreement with experiment is obtained by employing the size-extensive MP2, MP3, and MP4 methods. The highest-order perturbation theory treatment (6-31G** UMP4) gives a $^3A''$ CH_2CO dissociation energy of 16.75 kcal/mol, which is an improvement of 1.1 kcal/mol relative to the DZP MR CISD value. Nevertheless, it is obvious that it is necessary to use a one-particle basis set much larger than DZP in order to obtain accurate energetics for the $^3A''$ $CH_2CO \rightarrow {}^3B_1$ CH_2 + $^1\Sigma^+$ CO dissociation. Indeed, in recent years a rather large body of theoretical data has been compiled which clearly indicates the necessity of using large basis sets including higher angular momentum functions in order to recover a sufficient amount of the correlation energy to achieve chemical accuracy. For example, Jankowski, Becherer, Scharf, Schiffer, and Ahlrichs[62] found an increase of 2.7 kcal/mol in their MR-CI-6 D_e value for F_2 upon enlarging the one-particle basis from (10s6p3d/6s4p3d) to (10s6p2d 1f 1g/6s4p2d 1f 1g). Their most elaborate calculation, MR-CI-18 with a (10s6p2d1f/6s4p2d1f) basis, gave a D_e value for F_2 of 36.7 kcal/mol, which is 1.6 kcal/mol smaller than experiment. A more dramatic example is contained in an article by Frisch, Pople, and Binkley.[63] They found that the addition of f functions to a 6-311G(2d) basis increased the MP4 D_e value for N_2 from 212.2 to 221.3 kcal/mol, the latter value being 7.1 kcal/mol

smaller than experiment. Of course, the fact that N_2 contains a triple bond exacerbates the problem of theoretically predicting D_e, but one can nevertheless expect that f functions as well as g and multiple d functions will be important in obtaining an accurate dissociation energy for $^3A''$ CH_2CO.

Initial efforts toward ascertaining the basis set effects on the $^3A''$ ketene dissociation energy are detailed in Table XIV, where QZ2P SCF, CISD, and CIDVD results are given. It is interesting that the $^3A''$ CI well depths actually *decrease* by 0.1 – 0.2 kcal/mol relative to the DZP CI values. Additional studies at the CISD, MR CISD, and MP4 levels of theory are in progress with a QZ2P+f basis set. It is worth remarking that the use of large, general-contracted atomic natural orbital basis sets[64] in conjunction with MP4 or MR CISD methods may be required.

The problem of the inadequacy of the one-particle basis set and the lack of sufficient incorporation of electron correlation is accounted for in the BAC-MP4 method through the use of empirical bond additivity corrections. The BAC-MP4 number for the $^3A''$ CH_2CO well depth is 19.14 kcal/mol (Table XIV), which differs from the 23.76 kcal/mol "experimental" value by only 4.62 kcal/mol. Most of this error can be traced to the fact that the BAC-MP4 heat of formation for CO (–30.14 kcal/mol) is 2.94 kcal/mol too low.[65] In other words, use of the experimental $\Delta H^{\circ}_{f,0}(CO)$ would yield a $^3A''$ CH_2CO well depth of 22.08 kcal/mol. Given this fact, the BAC-MP4 prediction of 5.05 kcal/mol for the barrier height in the dissociation channel can be taken as an upper bound, in accord with experimental data[11,24] which indicate a barrier height less than 4 kcal/mol. A final theoretical prediction for the barrier height must be postponed until a purely *ab initio* level of theory is found which yields a $^3A''$ well depth near the 23.76 kcal/mol experimentally derived value proposed above.

3.4 SUMMARY

An *ab initio* investigation of the in-plane bent (C_s^{II}) $^3A''$ $CH_2CO \rightarrow \tilde{X}^3B_1$ CH_2 + $\tilde{X}^1\Sigma^+$ CO and the out-of-plane bent (C_s^I) $^3A'$ $CH_2CO \rightarrow \tilde{X}^3B_1$ CH_2 + $\tilde{X}^1\Sigma^+$ CO dissociation paths has been performed. Geometrical structures, vibrational frequencies, and quadratic force constants have been determined at the DZP SCF and CISD levels for the $\tilde{X}^1A_1$, $^3A''$, and $^3A'$ states of ketene and for the $^3A''$ and $^3A'$ transition states for dissociation. The DZP CISD structure for $\tilde{A}^1A''$ ketene is also reported.

The DZP CISD C_s^{II} transition state for $^3A''$ ketene dissociation has r_1(C-O) = 1.1481 Å, r_2(C-C) = 2.0708 Å, δ(C-C-O) = 116.26°, and one imaginary frequency for the C-C stretch, $\omega_6(a') = 560\ i\ cm^{-1}$. The corresponding C_s^I stationary point for $^3A'$ ketene has r_1(C-O) = 1.1488 Å, r_2(C-C) = 2.0544 Å, δ(C-C-O) = 117.74°, and a CH_2 wagging angle γ = 23.06°. This C_s^I stationary point has two imaginary frequencies, $\omega_4(a') = 588\ i\ cm^{-1}$ (C-C stretch) and $\omega_9(a'') = 152\ i\ cm^{-1}$ (rotation about the C-C axis). Following the ω_9 normal mode leads back to the $^3A''$ C_s^{II} transition state, which is only 1 kcal/mol lower in energy. This phenomenon is analogous to the behavior of the $^3A''$ and $^3A'$ states at their optimum geometries and is a consequence of a conical intersection of the $\tilde{a}^3A_2$ and $\tilde{b}^3A_1$ surfaces.

The final theoretical estimates for the adiabatic excitation energies of the $\tilde{a}^3A''$ and $\tilde{A}^1A''$ states of ketene are $T_0(^3A'') = 18650\ cm^{-1}$ and $T_0(^1A'') = 20910\ cm^{-1}$. The former value leads to an experimentally derived dissociation energy of 23.76 kcal/mol for $^3A''$ ketene. The purely *ab initio* results reported here which include electron correlation give $^3A''$ well depths between 13.0 and 17.5 kcal/mol and $^3A''$ barriers to dissociation between 6.4 and 10.8 kcal/mol. Therefore, higher-quality *ab initio* calculations are needed to accurately predict the energy profile for $^3A''$ ketene dissociation. The BAC-MP4 $^3A''$ well depth is 19.1 kcal/mol, and the barrier height

in the dissociation channel is 5.0 kcal/mol. The latter value can be considered an upper bound since the BAC-MP4 method overestimates the heat of formation of CO by 2.9 kcal/mol.

3.5 ACKNOWLEDGEMENTS

Mr. Bill Green of the research group of Professor C.B. Moore at Berkeley is thanked for helpful discussions, and Dr. Carl F. Melius of Sandia National Laboratories, Livermore, CA is acknowledged for provision of the previously unpublished BAC-MP4 results reported here. This research was supported by the Director, Office of Energy Research, Office of Basic Energy Sciences, Chemical Sciences Division of the U.S. Department of Energy under Contract No. DE-AC03-76SF00098.

3.6 REFERENCES AND NOTES

[1] D.J. Bamford, S.V. Filseth, M.F. Foltz, J.W. Hepburn, and C.B. Moore, J. Chem. Phys. 82, 3032 (1985).

[2] I. Nadler, M. Noble, H. Reisler, and C. Wittig, J. Chem. Phys. 82, 2608 (1985).

[3] C.X.W. Qian, M. Noble, I. Nadler, H. Reisler, and C. Wittig, J. Chem. Phys. 83, 5573 (1985).

[4] C. Wittig, I. Nadler, H. Reisler, M. Noble, J. Catanzarite, and G. Radhakrishnan, J. Chem. Phys. 83, 5581 (1985).

[5] W.S. Drozdoski, A.P. Baronavski, and J.R. McDonald, Chem. Phys. Lett. 64, 421 (1979).

[6] G.T. Fujimoto, M.E. Umstead, and M.C. Lin, Chem. Phys. 65, 197 (1982).

[7] T.A. Spiglanin, R.A. Perry, and D.W. Chandler, J. Phys. Chem. 90, 6184 (1986).

[8] T.A. Spiglanin, R.A. Perry, and D.W. Chandler, J. Chem. Phys. 87, 1568 (1987).

[9] T.A. Spiglanin and D.W. Chandler, J. Chem. Phys. 87, 1577 (1987).

[10] D.J. Nesbitt, H. Petek, M.F. Foltz, S.V. Filseth, D.J. Bamford, and C.B. Moore, J. Chem. Phys. 83, 223 (1985).

[11] H. Bitto, I.-C. Chen, and C.B. Moore, J. Chem. Phys. 85, 5101 (1986).

[12] H. Reisler and C. Wittig, Annu. Rev. Phys. Chem. 37, 307 (1986).

[13] H. Bitto, D.R. Guyer, W.F. Polik, and C.B. Moore, Faraday Discuss. Chem. Soc. 81, paper 8 (1986).

[14] K.E. Holdy, L.C. Klotz, and K.R. Wilson, J. Chem. Phys. 52, 4588 (1970).

[15] G.E. Busch and K.R. Wilson, J. Chem. Phys. 56, 3626 (1972).

[16] A.F. Tuck, J. Chem. Soc. Faraday Trans. 2 73, 689 (1977).

[17] H. Basch, Theor. Chim. Acta 28, 151 (1973).

[18] P. Pendergast and W. H. Fink, J. Am. Chem. Soc. 98, 648 (1976).

[19] S. Yamabe and K. Morokuma, J. Am. Chem. Soc. 100, 7551 (1978).

[20] W.D. Allen and H.F. Schaefer III, J. Chem. Phys. **84**, 2212 (1986). Chapter 2 of this dissertation is an updated version of Ref. 20.

[21] As discussed in Refs. 20 and 25, variational collapse is a severe problem when conventional SCF procedures are applied to the 2^1A_1 state of ketene. Consequently, the results given for the 2^1A_1 state in Ref. 19 are invalid. In footnote 23 of their paper, Yamabe and Morokuma allude to this problem but do not indicate its severity.

[22] C.E. Dykstra and H.F. Schaefer III, J. Am. Chem. Soc. **98**, 2689 (1976).

[23] J.E. Del Bene, J. Am. Chem. Soc. **94**, 3713 (1972).

[24] C.C. Hayden, D.M. Neumark, K. Shobatake, R.K. Sparks, and Y.T. Lee, J. Chem. Phys. **76**, 3607 (1982).

[25] W.D. Allen and H.F. Schaefer III, J. Chem. Phys., in press.

[26] S. Huzinaga, J. Chem. Phys. **42**, 1293 (1965).

[27] T.H. Dunning, Jr., J. Chem. Phys. **53**, 2823 (1970).

[28] T.H. Dunning, Jr., J. Chem. Phys. **55**, 716 (1971).

[29] W.D. Allen and H.F. Schaefer III, Chem. Phys. **108**, 243 (1986).

[30] Y. Osamura, Y. Yamaguchi, P. Saxe, M.A. Vincent, J.F. Gaw, and H.F. Schaefer III, Chem. Phys. **72**, 131 (1982).

[31] J.E. Rice, R.D. Amos, N.C. Handy, T.J. Lee, and H.F. Schaefer III, J. Chem. Phys. **85**, 963 (1986).

[32] J.F. Gaw and N.C. Handy, "Derivatives of the Potential Energy Hypersurface by Analytic Techniques", in *Annual Reports C, The Royal Society of Chemistry* (London, 1984), pp. 291-323.

[33] H.F. Schaefer III and Y. Yamaguchi, J. Mol. Struct. (Theochem) **135**, 369 (1986).

[34] P.D. Mallinson and L. Nemes, J. Mol. Spectrosc. **59**, 470 (1976).

[35] C.B. Moore and G.C. Pimentel, J. Chem. Phys. **38**, 2816 (1963).

[36] K. Tanaka and M. Yoshimine, J. Am. Chem. Soc. **102**, 7655 (1980).

[37] D.A. Clabo, Jr., W.D. Allen, R.B. Remington, Y. Yamaguchi, and H.F. Schaefer III, Chem. Phys., in press.

[38] T.J. Lee, W.D. Allen, and H.F. Schaefer III, J. Chem. Phys., in press.

[39] See, for example, W.J. Hehre, L. Radom, P.v.R. Schleyer, and J.A. Pople, *Ab initio Molecular Orbital Theory* (Wiley-Interscience, New York, 1986).

[40] G. Herzberg, *Electronic Spectra of Polyatomic Molecules* (Van Nostrand, New York, 1966), p. 583.

[41] K.P. Huber and G. Herzberg, *Constants of Diatomic Molecules* (Van Nostrand-Reinhold, New York, 1979).

[42] P.R. Bunker and P. Jensen, J. Chem. Phys. **79**, 1224 (1983).

[43] See C.W. Bauschlicher, Jr., S.R. Langhoff, and P.R. Taylor, J. Chem. Phys. **87**, 387 (1987) and references contained therein.

[44] A.D. Walsh, J. Chem. Soc. **1953**, 2260, 2266, 2288, 2296, 2301, 2306, 2318, 2321, 2325, 2330.

[45] R.S. Mulliken, Annu. Rev. Phys. Chem. **29**, 1 (1978).

[46] W.H. Green and C.B. Moore, private communication.

[47] D.G. Leopold, K.K. Murray, A.E.S. Miller, and W.C. Lineberger, J. Chem. Phys. **83**, 4849 (1985).

[48] P.R. Bunker and T.J. Sears, J. Chem. Phys. **83**, 4866 (1985).

[49] T.J. Sears, J. Chem. Phys. **85**, 3711 (1986).

[50] M.D. Marshall and A.R.W. McKellar, J. Chem. Phys. **85**, 3716 (1986).

[51] P.R. Bunker, P. Jensen, W.P. Kraemer, and R. Beardsworth, J. Chem. Phys. **85**, 3724 (1986).

[52] In going from the $\tilde{X}^1A_1$ to the $^3A''$ state, the C-C π bond is largely broken. In order to describe the π electron pair correlation in the $\tilde{X}^1A_1$ state which is not present in the $^3A''$ state, both the π^2 and π^{*2} $\tilde{X}^1A_1$ configurations must be included.

[53] The two-reference Davidson correction for the ground state is computed according to the formula $\Delta E = (1 - C_1^2 - C_2^2)(E_{2R\ CISD} - E_{TCSCF})$. See R.J. Buenker and S.D. Peyerimhoff in *New Horizons of Quantum Chemistry*, edited by P.-O. Löwdin and B. Pullman (Reidel, London, 1983) pp. 183-219.

[54] R. Krishnan and J.A. Pople, Int. J. Quantum Chem. **14**, 91 (1978).

[55] R. Krishnan, M.J. Frisch, and J.A. Pople, J. Chem. Phys. 72, 4244 (1980).

[56] C.F. Melius and J.S. Binkley, Twentieth Symp. (Internat.) on Comb., p. 575, The Comb. Inst. (1984).

[57] C.F. Melius and J.S. Binkley, ACS Combustion Symposium 249, 103 (1984).

[58] P. Ho, M.E. Coltrin, J.S. Binkley, and C.F. Melius, J. Phys. Chem. 89, 4647 (1985).

[59] R.L. Nuttall, A.H. Laufer, and M.V. Kilday, J. Chem. Thermodyn. 3, 167 (1978).

[60] A.H. Laufer and R.A. Keller, J. Am. Chem. Soc. 93, 61 (1971).

[61] R.N. Dixon and G.H. Kirby, Trans. Faraday Soc. 62, 1406 (1966).

[62] K. Jankowski, R. Becherer, P. Scharf, H. Schiffer, and R. Ahlrichs, J. Chem. Phys. 82, 1413 (1985).

[63] M.J. Frisch, J.A. Pople, and J.S. Binkley, J. Chem. Phys. 80, 3265 (1984).

[64] J. Almlöf and P.R. Taylor, J. Chem. Phys. 86, 4070 (1987).

[65] JANAF *Thermochemical Tables*, 2nd ed., edited by D.R. Stuhl and H. Prophet, Natl. Bur. Stand. Publ. 37 (1971).

[66] The term "transition state" is conventionally applied to stationary points which exhibit only one imaginary frequency. The $C_s^I\ ^3A'$ stationary point does not qualify as a true transition state under this criterion, but it does have only one totally symmetric imaginary frequency, which involves dissociation of the C-C bond. Technically the term "stationary point of Hessian index 2" is applicable, but such nomenclature is not used here because it is cumbersome.

Table I.
Symmetrized internal coordinates for ketene C_{2v}, C_s^I, and C_s^{II} geometries.[a]

	C_{2v}		C_s^I		C_s^{II}
A_1	$S_1 = r_1$		$S_1 = r_1$		$S_1 = r_1$
	$S_2 = r_2$		$S_2 = r_2$		$S_2 = r_2$
	$S_3 = (t_1 + t_2)/\sqrt{2}$	A'	$S_3 = (t_1 + t_2)/\sqrt{2}$		$S_3 = t_1$
	$S_4 = (\beta_1 + \beta_2)/\sqrt{2}$		$S_4 = \delta$	A'	$S_4 = t_2$
			$S_4 = (\beta_1 + \beta_2)/\sqrt{2}$		$S_4 = \delta$
B_1	$S_5 = \gamma$		$S_6 = \gamma$		$S_6 = \beta_1$
	$S_6 = \phi$				$S_7 = \beta_2$
			$S_7 = (t_1 - t_2)/\sqrt{2}$		
	$S_7 = (t_1 - t_2)/\sqrt{2}$	A''	$S_8 = (\beta_1 - \beta_2)/\sqrt{2}$	A''	$S_8 = \gamma$
B_2	$S_8 = (\beta_1 - \beta_2)/\sqrt{2}$		$S_9 = (\tau_1 + \tau_2)/\sqrt{2}$		$S_9 = \tau_2$
	$S_9 = \theta$				

[a] δ: C_3–C_2–O_1 angle. γ: C_2–C_3 out of H_4–C_3–H_5 plane angle (positive if H_4 and H_5 move in the -x direction). θ: C_3–C_2–O_1 linear bend in H_4–C_3–H_5 plane (positive if O_1 moves in the -y direction). ϕ: C_3–C_2–O_1 linear bend perpendicular to H_4–C_3–H_5 plane (positive if O_1 moves in the -x direction). τ_1: Torsional angle between H_4–C_3–C_2 and C_3–C_2–O_1 planes. τ_2: Torsional angle between H_5–C_3–C_2 and C_3–C_2–O_1 planes. Refer to Figs. 4-6 for pictorial definitions.

Table II.

Experimental and DZP theoretical geometrical structures and vibrational frequencies for $\tilde{X}^1A_1$ ketene

Geometrical structures[a]

	DZP SCF[b]	DZP CISD	Experiment[c]
r_1(C-O)	1.1466	1.1669	1.161
r_2(C-C)	1.3101	1.3195	1.316
$t_1=t_2$(C-H)	1.0735	1.0785	1.078
α(H-C-H)	121.99	121.83	122.01
Total energy	−151.756673	−152.154138	-

Vibrational frequencies (cm^{-1})[d]

$\nu_1(a_1)$	C-H stretch	3355 (9.3)	3305 (7.7)	3070
$\nu_2(a_1)$	C-O stretch	2360 (9.7)	2284 (6.1)	2152
$\nu_3(a_1)$	CH_2 scissor	1537 (10.7)	1477 (6.4)	1388
$\nu_4(a_1)$	C-C stretch	1245 (11.4)	1197 (7.1)	1118
$\nu_5(b_1)$	CH_2 wag	702 (18.8)	606 (2.5)	591
$\nu_6(b_1)$	C-C-O bend	618 (17.7)	529 (0.8)	525
$\nu_7(b_2)$	C-H stretch	3467 (9.5)	3422 (8.1)	3166
$\nu_8(b_2)$	CH_2 rock	1094 (12.0)	1036 (6.0)	977
$\nu_9(b_2)$	C-C-O bend	486 (11.0)	453 (3.4)	438

[a] Bond lengths in Å, bond angles in degrees, and total energies in hartrees. The geometrical parameters are defined pictorially in Fig. 4.

[b] Taken from Tables II and VI of Ref. 20.

[c] Reference 34, r_0 parameters.

[d] The percentage errors of the theoretical harmonic frequencies relative to the experimental anharmonic frequencies (from Ref. 35) are given in parentheses.

Table III.

DZP SCF and CISD quadratic force constants for $\tilde{X}^1A_1$ ketene[a]

		DZP SCF[b]	DZP CISD
	F_{11}	19.2569	17.2981
	F_{12}	1.2145	0.7914
	F_{13}	− 0.0964	− 0.0973
	F_{14}	0.0027	− 0.0106
A_1	F_{22}	10.5452	10.1129
	F_{23}	0.1165	0.0889
	F_{24}	0.4979	0.4835
	F_{33}	6.4101	6.2185
	F_{34}	− 0.0653	− 0.0699
	F_{44}	1.3987	1.3064
	F_{55}	0.1293	0.0915
B_1	F_{56}	0.1067	0.1069
	F_{66}	0.7948	0.6921
	F_{77}	6.3680	6.2036
	F_{78}	0.1919	0.1832
B_2	F_{79}	0.0123	0.0097
	F_{88}	0.4501	0.4176
	F_{89}	0.1571	0.1380
	F_{99}	0.7651	0.6650

[a] Relative to the C_{2v} internal coordinates defined in Table I. Units: mdyn/Å, mdyn/rad, and mdyn·Å / rad^2.

[b] Taken from Table V of Ref. 20.

Table IV.

DZP SCF theoretical data for the C_s^{II} dissociation $^3A''$ $CH_2CO \rightarrow {}^3B_1$ $CH_2 + {}^1\Sigma^+$ CO

Geometrical structures[a]

	$^3A''$ CH_2CO[b]	Transition State	$^3B_1$ $CH_2 + {}^1\Sigma^+$ CO
r_1(C-O)	1.1716	1.1315	1.1174
r_2(C-C)	1.4660	1.9472	∞
t_1(C-H)	1.0735	1.0742	1.0756
t_2(C-H)	1.0780	1.0781	1.0756
δ(C-C-O)	129.25	117.67	-
α(H-C-H)	120.46	126.98	129.36
β_1(H-C-C)	119.94	116.12	-
E(SCF)[c]	-151.698510	-151.657567	-151.687022
	(-2.56)	(20.16)	(0.00)

Vibrational frequencies (cm^{-1})

ω_1(a′)	asym C-H stretch	3458	3485	3494
ω_2(a′)	sym C-H stretch	3319	3282	3287
ω_3(a′)	C-O stretch	2093	2239	2424
ω_4(a′)	CH_2 scissor	1554	1346	1300
ω_5(a′)	CH_2 rock	1158	624	-
ω_6(a′)	C-C stretch	1027	871*i*	-
ω_7(a′)	C-C-O bend	508	316	-
ω_8(a″)	CH_2 wag	680	378	-
ω_9(a″)	H-C-C-O torsion	396	176	-

[a] Bond lengths in Å and bond angles in degrees. The geometrical parameters are defined pictorially in Fig. 5.

[b] Taken from Tables VII and XI of Ref. 20.

[c] Total energies in hartrees. Relative energies in kcal/mol are listed in parentheses. These relative energies include zero-point vibrational energy corrections of +1623 ($^3A''$ CH_2CO) and +585 (transition state) cm^{-1} as obtained from the scaled DZP SCF frequencies in Table VI.

Table V.

DZP CISD theoretical data for the C_s^{II} dissociation $^3A''$ $CH_2CO \rightarrow {}^3B_1$ $CH_2 + {}^1\Sigma^+$ CO

Geometrical structures[a]

	$^3A''$ CH_2CO	Transition State	$^3B_1$ $CH_2 + {}^1\Sigma^+$ CO[b]
r_1(C-O)	1.1930	1.1481	1.1386 (1.1412)
r_2(C-C)	1.4658	2.0708	∞
t_1(C-H)	1.0804	1.0813	1.0812 (1.0853)
t_2(C-H)	1.0855	1.0843	1.0812 (1.0853)
δ(C-C-O)	127.65	116.26	-
α(H-C-H)	120.11	128.21	131.14 (132.68)
β_1(H-C-C)	119.83	115.04	-
E(CISD)[c]	-152.079129	-152.035719	-152.050111
	(-13.29)	(10.68)	(0.00)
E(CIDVD)[c]	-152.121650	-152.079262	-152.090030
	(-14.92)	(8.41)	(0.00)

Vibrational frequencies (cm^{-1})

ω_1(a′)	asym C-H stretch	3394	3435	3456 (3408)
ω_2(a′)	sym C-H stretch	3250	3226	3239 (3193)
ω_3(a′)	C-O stretch	1954	2153	2267 (2245)
ω_4(a′)	CH_2 scissor	1502	1259	1206 (1167)
ω_5(a′)	CH_2 rock	1102	501	-
ω_6(a′)	C-C stretch	997	560*i*	-
ω_7(a′)	C-C-O bend	479	261	-
ω_8(a″)	CH_2 wag	710	375	-
ω_9(a″)	H-C-C-O torsion	382	155	-

[a] Bond lengths Å and bond angles in degrees. The geometrical parameters are defined pictorially in Fig. 5.

[b] The CISD and CIDVD results were obtained by treating the fragments as a supermolecule in order to account for the lack of size extensivity. A separation of r_2 = 1000 bohr was used. The geometrical structures and vibrational frequencies listed in parentheses were determined by treating the fragments individually.

[c] Total energies in hartrees. CIDVD = Davidson-corrected CISD. Relative energies in kcal/mol are listed in parentheses. These relative energies include zero-point vibrational energy corrections of +1720 ($^3A''$ CH_2CO) and +578 (transition state) cm^{-1} as obtained from the scaled DZP CISD frequencies in Table VI.

Table VI.

Scaled vibrational frequencies (cm^{-1}) for the C_s^{II} dissociation $^3A''$ $CH_2CO \rightarrow {}^3B_1$ $CH_2 + {}^1\Sigma^+$ CO [a]

		$^3A''$ CH_2CO	Transition State	$^3B_1$ $CH_2 + {}^1\Sigma^+$ CO
$\nu_1(a')$	asym C-H stretch	3140 (3158)	3178 (3182)	3197 (3191)
$\nu_2(a')$	sym C-H stretch	3019 (3037)	2997 (3003)	3009 (3008)
$\nu_3(a')$	C-O stretch	1841 (1909)	2029 (2042)	2136 (2210)
$\nu_4(a')$	CH_2 scissor	1411 (1403)	1183 (1216)	1133 (1174)
$\nu_5(a')$	CH_2 rock	1039 (1034)	472 (557)	-
$\nu_6(a')$	C-C stretch	931 (922)	523*i* (782*i*)	-
$\nu_7(a')$	C-C-O bend	463 (458)	252 (285)	-
$\nu_8(a'')$	CH_2 wag	692 (572)	366 (318)	-
$\nu_9(a'')$	H-C-C-O torsion	379 (336)	154 (150)	-

[a] Scaled DZP SCF frequencies are tabulated in parentheses along with the corresponding DZP CISD values without parentheses. Mode-specific scale factors were applied to the $^3A''$ DZP SCF and CISD harmonic frequencies in Tables IV and V based on the $\tilde{X}^1A_1$ theoretical and experimental frequencies in Table II. The correlation of $\nu_6(\tilde{X}^1A_1)$ with $\nu_9(^3A'')$ was made for lack of a better choice. The correspondence of the other eight modes of the two states is clear.

Table VII.

DZP SCF and CISD quadratic force constants for $^3A''$ ketene[a]

		Equilibrium		Transition State	
		DZP SCF[b]	DZP CISD	DZP SCF	DZP CISD
	F_{11}	17.5503	15.4516	21.0055	19.1757
	F_{12}	1.1685	1.2047	1.8012	0.9336
	F_{13}	-0.0063	-0.0015	0.0470	0.0285
	F_{14}	0.0747	0.0659	0.0851	0.0538
	F_{15}	0.1992	0.2615	0.1017	0.1253
	F_{16}	0.0761	0.0709	0.1596	0.1114
	F_{17}	0.0597	0.0315	0.1830	0.1149
	F_{22}	5.0960	4.7626	-2.4262	-1.0761
	F_{23}	0.0501	0.0420	-0.0567	-0.0312
	F_{24}	0.0543	0.0537	-0.0471	-0.0109
	F_{25}	0.3211	0.3233	0.4360	0.1787
	F_{26}	0.2713	0.2655	0.1198	0.0970
A′	F_{27}	0.1841	0.1774	-0.0230	0.0305
	F_{33}	6.4061	6.1744	6.3657	6.1476
	F_{34}	0.0002	-0.0113	-0.0630	-0.0737
	F_{35}	0.0500	0.0467	0.0164	0.0108
	F_{36}	-0.0016	-0.0045	-0.1045	-0.1104
	F_{37}	-0.1221	-0.1197	-0.1032	-0.1048
	F_{44}	6.2053	5.9496	6.1928	6.0213
	F_{45}	-0.0792	-0.0772	-0.0281	-0.0176
	F_{46}	-0.1167	-0.1179	-0.1060	-0.1088
	F_{47}	-0.0156	-0.0240	-0.1127	-0.1167
	F_{55}	1.1570	1.0371	0.5452	0.4013
	F_{56}	0.1246	0.1064	0.0181	0.0097
	F_{57}	-0.1483	-0.1247	-0.0988	-0.0738
	F_{66}	1.0565	0.9989	0.6697	0.5687
	F_{67}	0.4656	0.4455	0.4667	0.4363
	F_{77}	0.9921	0.9387	0.6564	0.5633
	F_{88}	0.1204	0.1368	0.0239	0.0271
A″	F_{89}	0.0464	0.0441	0.0046	0.0042
	F_{99}	0.1201	0.1109	0.0329	0.0226

[a] Relative to the C_s^{II} internal coordinates defined in Table I. Units: mdyn/Å, mdyn/rad, and mdyn·Å/rad^2.

[b] Taken from Table X of Ref. 20.

Table VIII.

DZP SCF theoretical data for the C_s^I dissociation $^3A'$ $CH_2CO \rightarrow {}^3B_1$ $CH_2 + {}^1\Sigma^+$ CO

Geometrical structures[a]

	$^3A'$ CH_2CO[b]	Transition State	$^3B_1$ $CH_2 + {}^1\Sigma^+$ CO
r_1(C-O)	1.1652	1.1325	1.1174
r_2(C-C)	1.5163	1.9444	∞
$t_1=t_2$(C-H)	1.0788	1.0775	1.0756
δ(C-C-O)	125.47	119.00	-
α(H-C-H)	117.66	133.00	129.36
γ	32.62	30.44	-
E(SCF)[c]	−151.685145	−151.654780	−151.687022
	(5.09)	(21.75)	(0.00)

Vibrational frequencies (cm^{-1})

$\omega_1(a')$	C-H stretch	3288	3273	3287
$\omega_2(a')$	C-O stretch	2137	2218	2424
$\omega_3(a')$	CH_2 scissor	1508	1351	1300
$\omega_4(a')$	C-C stretch	1060	903*i*	-
$\omega_5(a')$	CH_2 wag	806	555	-
$\omega_6(a')$	C-C-O bend	517	343	-
$\omega_7(a'')$	C-H stretch	3409	3459	3494
$\omega_8(a'')$	CH_2 rock	916	552	-
$\omega_9(a'')$	H-C-C-O torsion	388*i*	163*i*	-

[a] Bond lengths in Å and bond angles in degrees. The geometrical parameters are defined pictorially in Fig. 6.

[b] Taken from Tables XII and XIII of Ref. 20.

[c] Total energies in hartrees. Relative energies in kcal/mol are listed in parentheses. These relative energies include zero-point vibrational energy corrections of +1369 ($^3A'$ CH_2CO) and +532 (transition state) cm^{-1} obtained from the scaled DZP SCF frequencies in Table X.

Table IX.

DZP CISD theoretical data for the C_s^I dissociation $^3A'$ $CH_2CO \rightarrow {}^3B_1$ $CH_2 + {}^1\Sigma^+$ CO

Geometrical structures[a]

	$^3A'$ CH_2CO	Transition State	$^3B_1$ $CH_2 + {}^1\Sigma^+$ CO[b]
r_1(C-O)	1.1861	1.1488	1.1386 (1.1412)
r_2(C-C)	1.5180	2.0544	∞
$t_1=t_2$(C-H)	1.0841	1.0833	1.0812 (1.0853)
δ(C-C-O)	123.25	117.74	-
α(H-C-H)	118.64	126.98	131.14 (132.68)
γ	28.17	23.06	-
E(CISD)[c]	−152.064991	−152.033394	−152.050111
	(-5.31)	(11.93)	(0.00)
E(CIDVD)[c]	−152.107453	−152.077157	−152.090030
	(-6.90)	(9.51)	(0.00)

Vibrational frequencies (cm^{-1})

ω_1(a′)	C-H stretch	3242	3223	3239 (3193)
ω_2(a′)	C-O stretch	1993	2140	2267 (2245)
ω_3(a′)	CH_2 scissor	1448	1260	1206 (1167)
ω_4(a′)	C-C stretch	1015	588*i*	-
ω_5(a′)	CH_2 wag	687	414	-
ω_6(a′)	C-C-O bend	490	294	-
ω_7(a″)	C-H stretch	3371	3423	3456 (3408)
ω_8(a″)	CH_2 rock	869	447	-
ω_9(a″)	H-C-C-O torsion	411*i*	152*i*	-

[a] Bond lengths in Å and bond angles in degrees. The geometrical parameters are defined pictorially in Fig. 6.

[b] The CISD and CIDVD results were obtained by treating the fragments as a supermolecule in order to account for the lack of size extensivity. A separation of r_2 = 1000 bohr was used. The geometrical structures and vibrational frequencies listed in parentheses were determined by treating the fragments individually.

[c] Total energies in hartrees. CIDVD = Davidson-corrected CISD. Relative energies in kcal/mol are listed in parentheses. These relative energies include zero-point vibrational energy corrections of +1409 ($^3A'$ CH_2CO) and +502 (transition state) cm^{-1} obtained from the scaled DZP CISD frequencies in Table X.

Table X.

Scaled vibrational frequencies (cm^{-1}) for the C_s^I dissociation $^3A'\ CH_2CO \rightarrow {}^3B_1\ CH_2 + {}^1\Sigma^+\ CO$ [a]

		$^3A'\ CH_2CO$	Transition State	$^3B_1\ CH_2 + {}^1\Sigma^+\ CO$
$\nu_1(a')$	C-H stretch	3011 (3009)	2994 (2995)	3009 (3008)
$\nu_2(a')$	C-O stretch	1878 (1949)	2016 (2023)	2136 (2210)
$\nu_3(a')$	CH_2 scissor	1361 (1362)	1184 (1220)	1133 (1174)
$\nu_4(a')$	C-C stretch	948 (952)	549*i* (811*i*)	-
$\nu_5(a')$	CH_2 wag	670 (679)	404 (467)	-
$\nu_6(a')$	C-C-O bend	486 (439)	292 (291)	-
$\nu_7(a'')$	C-H stretch	3119 (3113)	3167 (3159)	3197 (3191)
$\nu_8(a'')$	CH_2 rock	820 (818)	422 (493)	-
$\nu_9(a'')$	H-C-C-O torsion	397*i* (350*i*)	147*i* (147*i*)	-

[a] Scaled DZP SCF frequencies are tabulated in parentheses along with the corresponding DZP CISD values without parentheses. Mode-specific scale factors were applied to the $^3A'$ DZP SCF and CISD harmonic frequencies in Tables VIII and IX based on the $\tilde{X}^1A_1$ theoretical and experimental frequencies in Table II. The correlation of $\nu_9(\tilde{X}^1A_1)$ with $\nu_9(^3A')$ was made for lack of a better choice. The correspondence of the other eight modes of the two states is clear.

Table XI.

DZP SCF and CISD quadratic force constants for $^3A'$ ketene[a]

		Equilibrium[b]		Transition State	
		DZP SCF	DZP CISD	DZP SCF	DZP CISD
	F_{11}	18.3984	16.2135	20.7270	19.0250
	F_{12}	0.7495	0.8380	1.9819	1.0395
	F_{13}	0.0385	0.0314	0.0764	0.0556
	F_{14}	0.2125	0.3091	0.0641	0.1034
	F_{15}	0.0869	0.0679	0.1798	0.1439
	F_{16}	− 0.0044	0.0040	− 0.0337	− 0.0144
	F_{22}	4.3774	4.0019	− 2.6228	− 1.2108
	F_{23}	0.0286	0.0097	− 0.0550	− 0.0321
	F_{24}	0.0485	0.0662	0.3721	0.1448
	F_{25}	0.3092	0.2859	0.2020	0.1360
A′	F_{26}	0.0764	0.0565	0.1128	0.0535
	F_{33}	6.1532	5.9865	6.1615	5.9885
	F_{34}	− 0.0575	− 0.0499	− 0.0298	− 0.0206
	F_{35}	− 0.2050	− 0.1820	− 0.2685	− 0.2537
	F_{36}	− 0.1716	− 0.1422	− 0.1055	− 0.0748
	F_{44}	1.1504	1.0567	0.5645	0.4159
	F_{45}	− 0.1061	− 0.0895	− 0.1284	− 0.0874
	F_{46}	− 0.0328	− 0.0449	− 0.0329	− 0.0267
	F_{55}	2.1487	1.7879	1.6504	1.2365
	F_{56}	0.7398	0.5171	0.5319	0.2996
	F_{66}	0.4298	0.2755	0.2375	0.1090
	F_{77}	6.1618	6.0184	6.2735	6.1279
	F_{78}	0.1094	0.1044	0.0025	− 0.0024
	F_{79}	− 0.0141	− 0.0169	− 0.0109	− 0.0089
A″	F_{88}	0.4713	0.4240	0.1802	0.1197
	F_{89}	− 0.0105	− 0.0104	− 0.0029	− 0.0023
	F_{99}	− 0.0522	− 0.0609	− 0.0106	− 0.0094

[a] Relative to the C_s^I internal coordinates defined in Table I. Units: mdyn/Å , mdyn/rad, and mdyn·Å /rad^2.

[b] As shown in Table VIII and discussed in Ref. 20, the $^3A'$ "equilibrium" geometry is actually a transition state for the interconversion of two equivalent $^3A''$ C_s^{II} minima through rotation about the C-C axis.

Table XII.

Adiabatic Excitation Energies for the $^3A''$ State of Ketene

Level of theory[a]	$\tilde{X}^1A_1$ Total Energy (hartrees)	$T_e(^3A'')$ (cm^{-1})
DZP SCF//DZP SCF	−151.756673	12765
DZP CISD//DZP CISD	−152.154138	16463
DZP CIDVD//DZP CISD	−152.199271	17036
QZ2P SCF//DZP CISD	−151.783701	13486
QZ2P CISD//DZP CISD	−152.242651	17365
QZ2P CIDVD//DZP CISD	−152.295825	18004
QZ2P TCSCF//DZP CISD[b]	−151.803717	17879
QZ2P 2R CISD//DZP CISD[b]	−152.250136	19007
QZ2P 2R CIDVD//DZP CISD[b]	−152.299946	18908
6-31G** SCF//6-31G* SCF[c]	−151.728761	11025
6-31G** MP2//6-31G* SCF[c]	−152.160534	19190
6-31G** MP3//6-31G* SCF[c]	−152.167027	17602
6-31G** MP4//6-31G* SCF[c]	−152.195623	18444
BAC-MP4[d]	−10.79	19173

Final predictions: $T_e \approx 18900\ cm^{-1}$, $T_0 = T_e - 255 \approx 18650\ cm^{-1}$

[a] // = at the geometry of, 2R=two-reference, CIDVD=Davidson-corrected CISD.

[b] Based on TCSCF, 2R CISD, and 2R CIDVD energies for the ground state and single-reference results for the $^3A''$ state. See the text for details.

[c] Based on RHF reference wave functions for the $\tilde{X}^1A_1$ state and UHF reference wave functions for the $^3A''$ state ($S^2 = 2.0400$).

[d] The predicted heat of formation at 0 K for $\tilde{X}^1A_1$ CH_2CO is listed in kcal/mol. The $\Delta H^\circ_{f,0}$ value for the $^3A''$ state is 43.30 kcal/mol. Thus, $T_0(^3A'') = 54.09$ kcal/mol, and $T_e = T_0 + 255 = 19173\ cm^{-1}$.

Table XIII.

Theoretical data for the $\tilde{A}^1A''$ state of ketene

DZP CISD C_s^{II} Geometry [a]

r_1(C-O) = 1.1972	δ(C-C-O) = 128.89
r_2(C-C) = 1.4550	α(H-C-H) = 120.43
t_1(C-H) = 1.0798	β_1(H-C-C) = 119.99
t_2(C-H) = 1.0849	

Total Energy [b]

E(DZP SCF) = –151.686333	E(QZ2P SCF) = –151.710926 (2486)
E(DZP CISD) = –152.068965 (2231)	E(QZ2P CISD) = –152.153398 (2224)
E(DZP CIDVD) = –152.112319 (2048)	E(QZ2P CIDVD) = –152.204478 (2045)

[a] Bond lengths in Å and bond angles in degrees. The geometrical parameters are defined pictorially in Fig. 5. DZP SCF results are given in Ref. 20.

[b] In hartrees, at the DZP CISD geometry. Energies (in cm^{-1}) relative to the $^3A''$ state are listed in parentheses.

Table XIV.

Energetics for the C_s^{II} dissociation $^3A''$ $CH_2CO \rightarrow {}^3B_1$ $CH_2 + {}^1\Sigma^+$ CO [a]

	$^3A''$ CH_2CO	Transition State	$^3B_1$ $CH_2 + {}^1\Sigma^+$ CO
DZP NO-CISD//DZP CISD[b]	−152.077953 (−13.45)	−152.034905 (10.29)	−152.048676 (0.00)
DZP MR CISD//DZP CISD[c]	−152.08670 (−15.65)	– –	−152.05392 (0.00)
6-31G** UHF//6-31G* UHF[d]	−151.678525 (−4.60)	−151.644468 (13.51)	−151.663361 (0.00)
6-31G** UMP2//6-31G* UHF	−152.073099 (−17.53)	−152.028360 (7.28)	−152.037323 (0.00)
6-31G** UMP3//6-31G* UHF	−152.086827 (−17.22)	−152.042103 (7.58)	−152.05155 (0.00)
6-31G** UMP4//6-31G* UHF	−152.111588 (−16.75)	−152.069474 (6.41)	−152.077057 (0.00)
BAC-MP4[e]	43.30 (−19.14)	67.49 (5.05)	62.44 (0.00)
QZ2P SCF//DZP CISD	−151.722255 (−0.78)	−151.685681 (18.90)	−151.713169 (0.00)
QZ2P CISD//DZP CISD	−152.163532 (−13.12)	−152.120283 (10.76)	−152.134789 (0.00)
QZ2P CIDVD//DZP CISD	−152.213794 (−14.82)	−152.171598 (8.39)	−152.182332 (0.00)

Proposed experimental $^3A''$ CH_2CO well depth from the text: 23.76 kcal/mol

Table XIV (continued)

[a] Total energies (in hartrees) are tabulated with relative energies (in kcal/mol) in parentheses. The latter values include the zero-point vibrational energy corrections (+1720 and +578 cm^{-1}) from footnote c of Table V.

[b] Iterative natural orbital results based on the CISD configuration space.

[c] Multi-reference CISD results based on iterative natural orbitals.

[d] In the UHF reference wave functions, S^2 = 2.040 for $^3A''$ CH_2CO, S^2 = 2.071 for the transition state, and S^2 = 2.015 for $^3B_1$ CH_2.

[e] Instead of total energies in hartrees, heats of formation at 0 K are listed in kcal/mol.

Table XV.

The 15 most important electronic configurations in the DZP MR CISD wave functions[a]

$^3A''$ CH_2CO [b]

I	C_I	9a′	10a′	11a′	1a″	2a″	3a″	Core
1	0.9354	2	1	0	2	1	0	
2	0.0824	2	1	0	0	1	2	
3	0.0617	1	2	0	1	1	1	
4	− 0.0529	2	1	0	1	1	1	
5	0.0428	2	1	0	0	2	1	
6	− 0.0383	1	2	0	1	1	1	
7	0.0362	2	1	1	1	1	1	$(6a')^1$
8	0.0346	2	1	0	1	1	1	$(8a')^1$ $(12a')^1$
9	− 0.0342	2	1	0	2	1	0	$(7a')^0$ $(14a')^2$
10	− 0.0336	2	1	0	1	1	1	
11	− 0.0323	1	2	0	1	2	0	
12	− 0.0291	1	2	0	2	1	0	$(8a')^1$ $(12a')^1$
13	0.0263	1	2	0	1	1	1	
14	0.0255	2	2	0	1	1	1	$(8a')^1$
15	− 0.0249	2	1	1	1	1	1	$(6a')^1$

$^3B_1$ CH_2 + $^1\Sigma^+$ CO [c]

I	C_I	9a′	10a′	11a′	1a″	2a″	3a″	Core
1	0.9399	2	1	0	2	1	0	
2	− 0.0848	0	1	2	2	1	0	
3	0.0848	2	1	0	0	1	2	
4	− 0.0615	1	1	1	1	1	1	
5	− 0.0533	2	1	0	2	1	2	$(8a')^0$
6	− 0.0533	2	1	2	2	1	0	$(8a')^0$
7	− 0.0517	1	1	1	1	1	1	
8	− 0.0472	2	1	0	1	1	1	$(6a')^1$ $(12a')^1$
9	− 0.0471	2	1	0	2	1	0	$(5a')^1$ $(7a')^1$ $(13a')^1$ $(14a')^1$
10	− 0.0459	2	1	0	2	1	0	$(7a')^0$ $(14a')^2$
11	0.0452	2	1	0	2	1	0	$(5a')^1$ $(13a')^1$
12	0.0445	1	1	1	2	1	0	$(6a')^1$ $(12a')^1$
13	− 0.0402	2	1	0	2	1	0	$(7a')^0$ $(13a')^2$
14	− 0.0382	2	1	0	2	1	0	$(5a')^0$ $(13a')^2$
15	0.0376	1	1	1	1	1	1	

Table XV (continued)

[a] The occupations of the orbitals which are active in the reference space are given explicitly. The occupation of the core is $(1a')^2(2a')^2(3a')^2(4a')^2(5a')^2(6a')^2(7a')^2(8a')^2$ unless otherwise indicated in the table.

[b] At the DZP CISD equilibrium geometry (Table V).

[c] At the DZP CISD supermolecule geometry (Table V).

C_{2v} Correlation Diagram

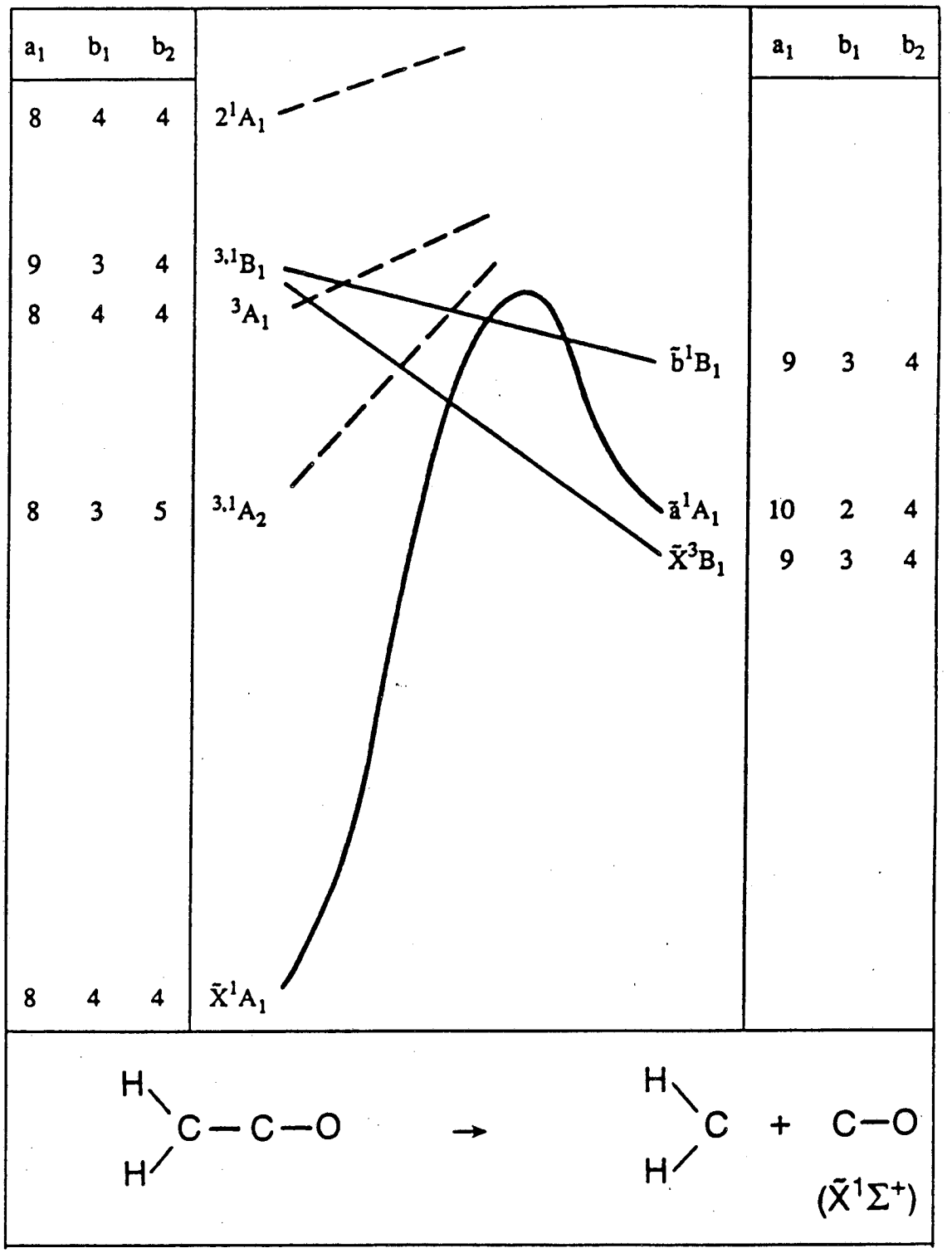

Figure 1

Figure 1 (continued)

A state correlation diagram for the C_{2v} dissociation of ketene to methylene and $\tilde{X}^1\Sigma^+$ CO. In the left- and right-hand columns, the total numbers of *valence* electrons in a_1, b_1, and b_2 orbitals are listed for each electronic state. The vertical spacing in the diagram reflects the relative energies of the initial and final states obtained as follows. From Table XIV of Ref. 20 the following vertical excitation energies (cm^{-1}) for the low-lying electronic states of ketene are found: $^3A_2$, 30600; $^1A_2$, 31300; $^3A_1$, 45500; $^1B_1$, 46700; 2^1A_1, 56300. (See also footnote 81 of Ref. 25.) Table I of Ref. 20 lists pertinent experimental vertical excitation energies. Hayden et al. (Ref. 24) have determined the following dissociation energies: $\tilde{X}^1A_1$ $CH_2CO \rightarrow \tilde{X}^3B_1$ CH_2 + $^1\Sigma^+$ CO, 27160 cm^{-1} and $\tilde{X}^1A_1$ $CH_2CO \rightarrow \tilde{a}^1A_1$ CH_2 + $^1\Sigma^+$ CO, 30140 cm^{-1}. Finally, from Ref. 40 the $\tilde{a}^1A_1 \rightarrow \tilde{b}^1B_1$ excitation energy in CH_2 is 7100 cm^{-1}.

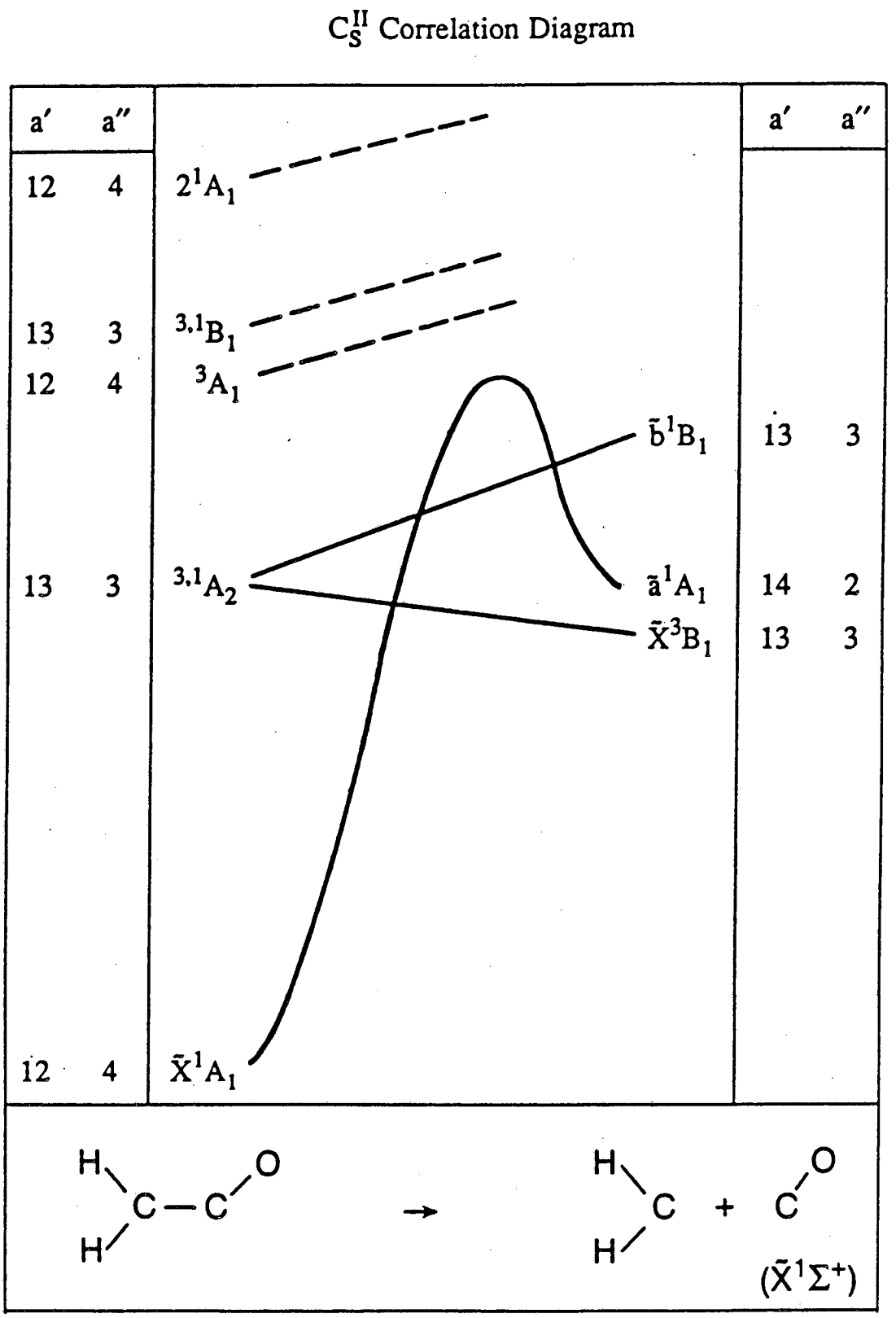

Figure 2. A state correlation diagram for the C_s^{II} dissociation of ketene to methylene and $\tilde{X}^1\Sigma^+$ CO. See the caption to Fig. 1.

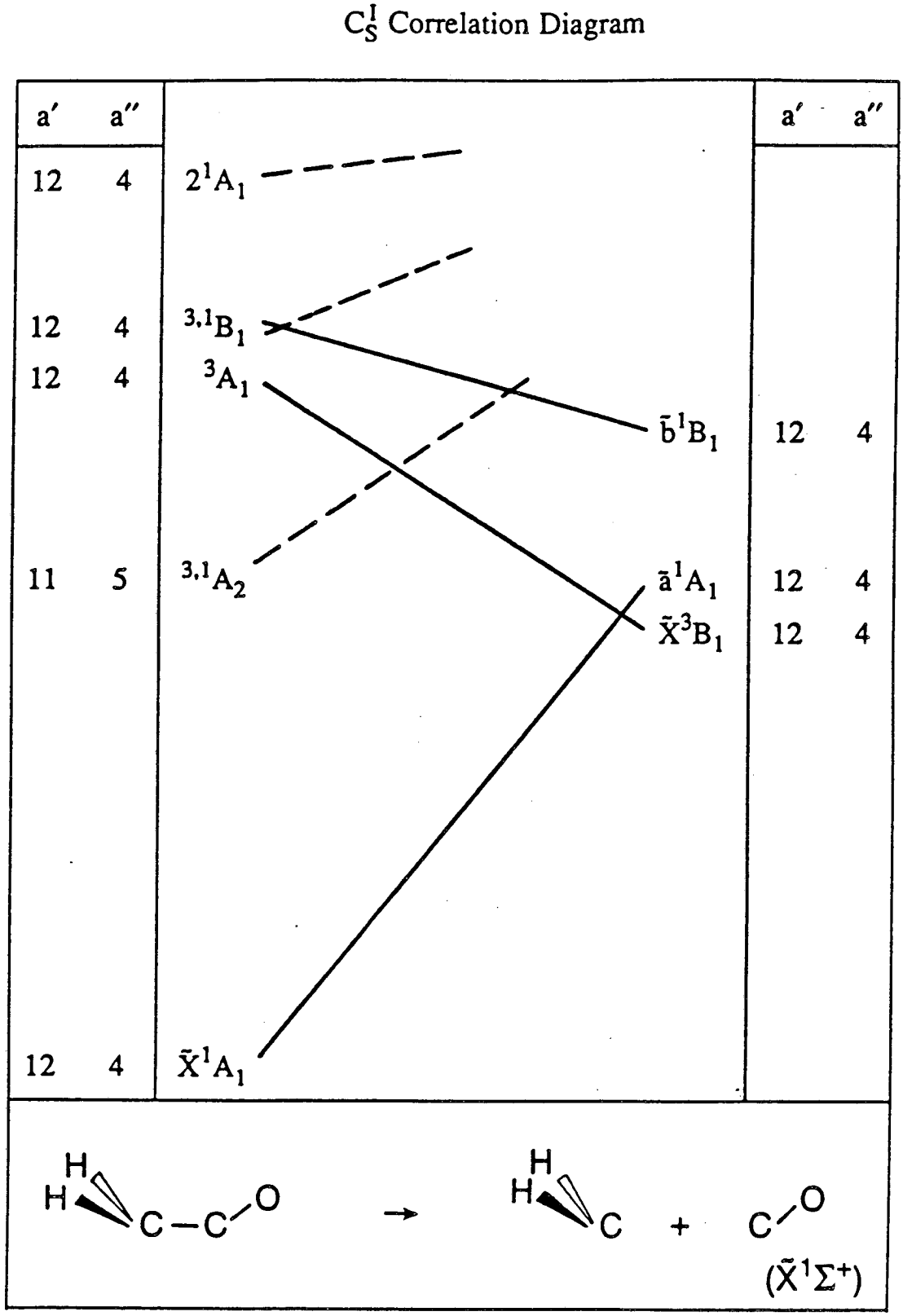

Figure 3. A state correlation diagram for the C_s^I dissociation of ketene to methylene and $\tilde{X}^1\Sigma^+$ CO. See the caption to Fig. 1.

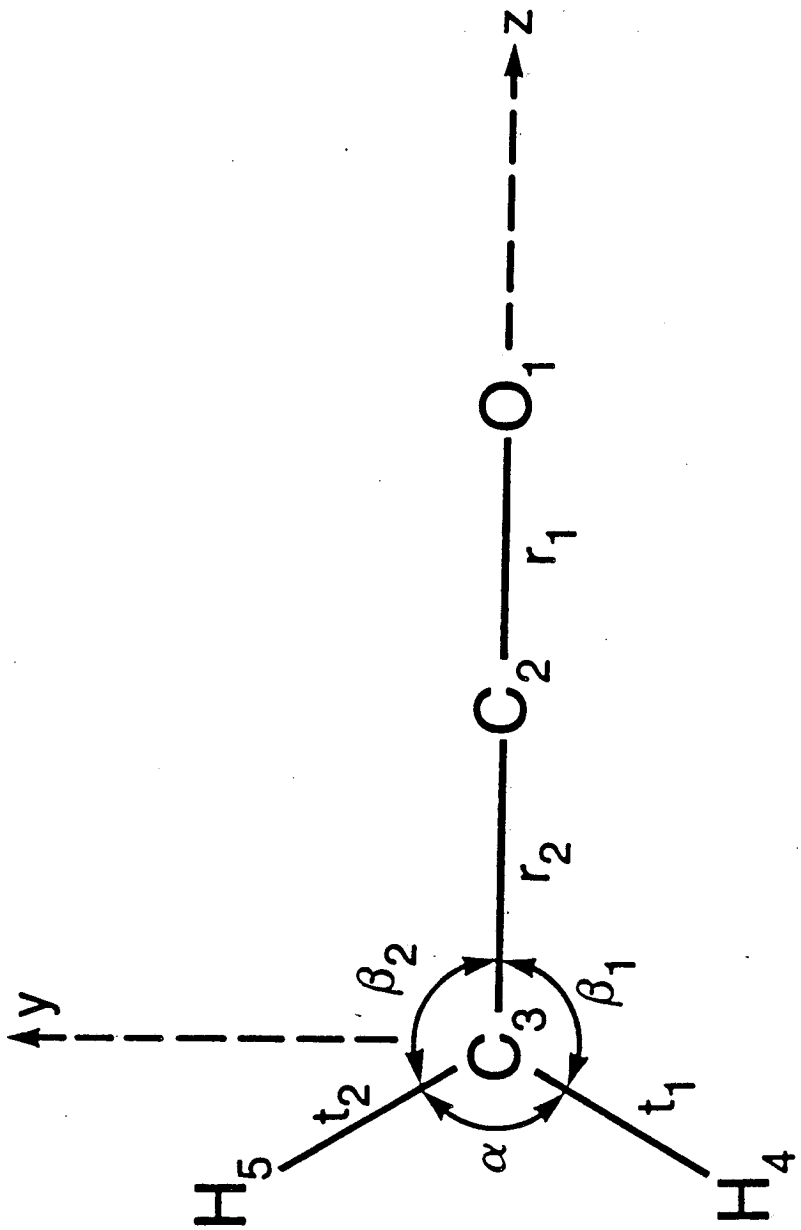

Figure 4. The C_{2v} equilibrium geometry and internal coordinates for $\tilde{X}^1A_1$ ketene.

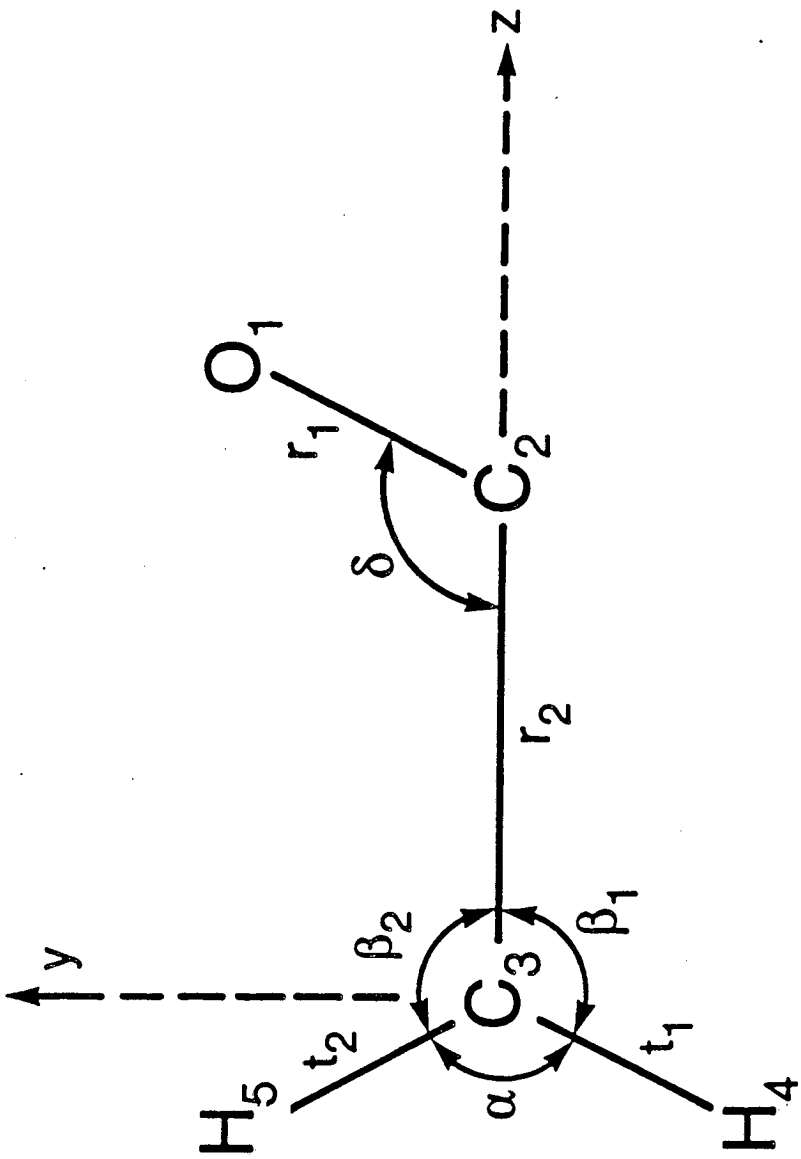

Figure 5. The C_s^{II} transition state and internal coordinates for the dissociation of $^3A''$ ketene.

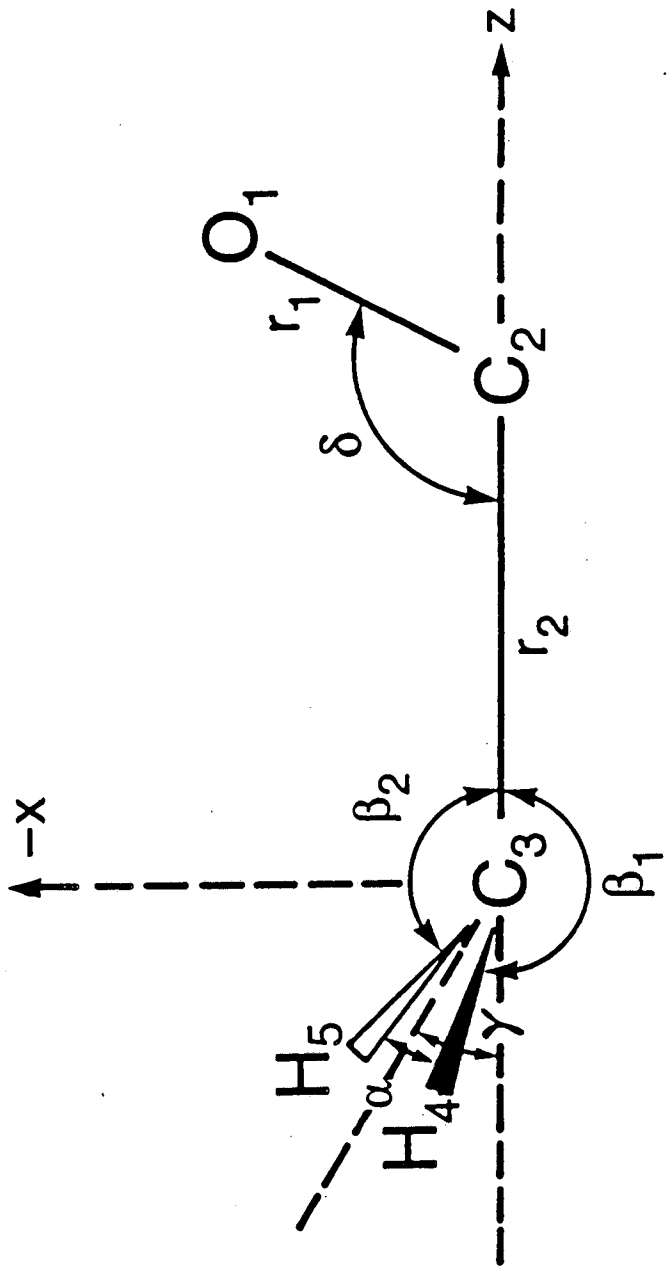

Figure 6. The C_s^1 transition state and internal coordinates for the dissociation of $^3A'$ ketene.

Chapter 4 Analytic Configuration Interaction Energy First Derivatives for Singlet Excited Electronic States of the Same Symmetry as the Ground State. Application to the 2^1A_1 States of Formaldehyde and Ketene

4.1 INTRODUCTION

In a 1982 review Davidson and McMurchie[1] discussed many of the difficulties involved in obtaining accurate *ab initio* predictions for excited electronic states and summarized results for 23 polyatomic molecules. A pervasive problem is that of variational collapse, i.e., wave functions optimized (in a variational sense) for excited states are frequently only poor descriptions of lower states of the same spin and spatial symmetry. The energy predicted for an excited state will be variational (an upper bound to the exact energy of the excited state) only if the excited-state wave function is orthogonal to the wave functions of all lower states.[2] Thus, conventional SCF and SCF-CI methods are applicable only to the lowest state of a given spin and spatial symmetry.

Davidson and Nitzsche[3] demonstrated this point in a study of the ($\pi\rightarrow\pi^*$) $2^1A'$ state of acrolein. A conventional (nonvariational) SCF calculation gave a vertical excitation energy of 3.24 eV, and a CI calculation using these orbitals gave a result of 11.31 eV. The experimental value is 6.5 eV.[4] The SCF excitation energy is much too low due to variational collapse, and the CI value is much too high because the SCF orbitals provide a poor description of the second root of the CI. The ($\pi\rightarrow\pi^*$) 2^1A_1 states of formaldehyde and ketene constitute other examples for which this phenomenon is observed. As discussed in Chapter 2, in the ketene case the nonvariational SCF method predicts a $^3A_1$ - 2^1A_1 splitting of 2100 cm^{-1} with a DZP basis set,

and the 2^1A_1 state appears to have little Rydberg character.[5] However, a variational excited-state SCF procedure gives a $^3A_1$ - 2^1A_1 splitting of 34300 cm^{-1} with virtually the same basis set, and the relative 2^1A_1 energy subsequently drops 23000 cm^{-1} when diffuse basis functions are added.[6]

These dramatic results clearly indicate that special methods are required to investigate, for example, the $2^1A'$ state of acrolein or the 2^1A_1 states of formaldehyde and ketene. In fact, such methods are required in general if all regions of the potential energy surface of an excited state are to be investigated, because polyatomic molecules almost always have displacements which wholly or partially remove spatial symmetry. This principle even applies to the prediction of vibrational frequencies for states which are otherwise accessible by conventional methods. For example, the optimum geometry and the a′ vibrational frequencies of the $^1A''$ state of ketene can be reliably predicted with a single-configuration, open-shell singlet, RHF SCF wave function, but the a″ frequencies obtained in this manner are of dubious quality because displacements along the a″ normal modes make the $^1A''$ state of the same symmetry as the close-lying ground state (see Section 2.3.2).

In an MCSCF or CI procedure, one can ensure an energy is an upper bound for the exact energy of the *n*th excited state by selecting the *n*th root of the corresponding secular equation.[7,8] In this way the problem of variational collapse can be circumvented, and MCSCF-CI techniques (perhaps state-averaged) are the most viable methods for obtaining accurate predictions for excited states. For practical reasons it is desirable to have MCSCF procedures which are sufficiently simple to be performed in the atomic orbital (or symmetry orbital) basis so that wave function optimization methods which require costly transformations into the molecular orbital basis are not necessary. By converging on a higher root of a small MCSCF, one can obtain good zeroth-order wave functions for excited states, even for relatively large molecular

systems. Of course, appropriate caution must be exercised if a manifold of states of the same symmetry occurs in a narrow energy range. A typical occurrence is the mixing of $(\pi\rightarrow\pi^*)^1$ valence states with nearby Rydberg states as exhibited in the formamide molecule.[1,9,10] However, even in these cases the $(\pi\rightarrow\pi^*)^1$ state may fall significantly below the Rydberg states in question once the $(\pi\rightarrow\pi^*)^1$ geometry is optimized. Therefore, it is reasonable to suspect that the prediction of optimum geometries, adiabatic excitation energies, and vibrational frequencies will in many cases be easier than the prediction of vertical excitation energies.

With regard to efficiency and reliability, the excited-state SCF method developed by Davidson and Stenkamp[11] over ten years ago has shown promise. This procedure is equivalent to converging on the second root of a three-configuration SCF[1] and is roughly comparable in expense to the conventional RHF SCF procedure for ground states. Preliminary results obtained with this method for the 2^1A_1 state of ketene were presented in Section 2.3.4. For the $2^1A'$ state of acrolein, Davidson and Nitzsche[3] computed a vertical excitation energy of 6.76 eV with the Davidson-Stenkamp method, and a CI performed with these orbitals gave a value of 7.52 eV. These acrolein values are in *much* better agreement with experiment despite the fact that the basis set employed was deficient in polarization and Rydberg functions and complications arise due to a nearby $(n\rightarrow 3p)^1$ Rydberg state.

Recently, the utility of the Davidson-Stenkamp method for open-shell singlet excited states of the same symmetry as the ground state was greatly enhanced when Fitzgerald and Schaefer[12] developed analytic first and second energy derivatives for the procedure. Specifically, Fitzgerald and Schaefer transformed the Davidson-Stenkamp wave function to a conventional two-configuration SCF (TCSCF) wave function and applied existing TCSCF analytic derivative methods to predict the optimum geometry and vibrational frequencies of the $(\pi\rightarrow\pi^*)$ 2^1A_1 state of formal-

dehyde. Another advance was made even more recently by Hamilton and Pulay,[13] who dealt with the Davidson-Stenkamp wave function in its three-configuration SCF form. The valuable contribution of Hamilton and Pulay consisted of the application of DIIS (Direct Inversion in the Iterative Subspace) techniques[14,15] to greatly facilitate the convergence of these MCSCF wave functions.

Dynamical electron correlation can be included in the description of an excited singlet state by writing the Davidson-Stenkamp wave function (hereafter called the SCFX wave function) in its TCSCF representation and subsequently converging on the second root in a two-reference CI calculation.[16] Correlation effects are sometimes very important for excited singlet states involving valence orbitals. Indeed, in the opinion of Davidson and McMurchie,[1] "No matter how the molecular orbitals are chosen, an accurate description of excitation energies and excited potential surfaces requires careful CI calculations." One well-known case is that of ethylene, for which SCF wave functions give the wrong order of the excited states and predict excessive Rydberg character for the $\pi \rightarrow \pi^*$ singlet state.[17–22] Thus, SCFX-CI (excited-state SCF configuration interaction) techniques are valuable tools for investigations of the potential energy surfaces of excited electronic states.

To facilitate the location of stationary points and the determination of vibrational frequencies, i.e., to effectively explore the potential energy surfaces of certain excited states, analytic energy first derivatives for SCFX-CI wave functions are a necessity. The purpose of this chapter is to describe the formulation and implementation of an efficient procedure for obtaining analytic SCFX-CI energy gradients. The mathematical formulation is outlined in the next two sections. Subsequently, the method is applied to the 2^1A_1 states of formaldehyde and ketene. In addition to brief reviews of previous studies of these states, geometrical structures, excitation energies, and harmonic vibrational frequencies are reported. Finally, a discussion is given concerning the pitfalls involved in predicting vibrational frequencies of excited states.

4.2 THEORY OF TCSCF-CI GRADIENTS

The formulation and implementation of analytic SCFX-CI gradients can be achieved through appropriate adaptation of analytic TCSCF-CI gradient methods. In this section an efficient procedure for the analytic evaluation of TCSCF-CI gradients is presented. This method avoids the transformation of derivative integrals and makes use of the Z-vector approach of Handy and Schaefer.[23,24] Thus the method represents a significant improvement in computational efficiency over previous MCSCF-CI gradient formalisms.[25–29] Consequently, the SCFX-CI gradient procedure described in Section 4.3 approaches optimal efficiency.

In the first two parts of this section (4.2.1 and 4.2.2), a presentation of relevant equations from previous theoretical work is given. The purpose of this presentation is not only to provide background material but also to introduce the notation and to recast certain equations into suitable forms. The discussion in 4.2.3 is intended to clarify the concept of redundant and non-redundant pairs of molecular orbitals in the various theoretical procedures and to define the procedure for the canonicalization of molecular orbitals. The last part of this section (4.2.4) deals explicitly with the new features of the current TCSCF-CI gradient formalism. Explicit equations are presented which allow TCSCF-CI gradients to be determined by solving only one set of CPTCSCF equations without storing or transforming any derivative integrals.

4.2.1 General CI Gradient Techniques

The theory for CI gradient techniques has been given several times,[30–33] and the notation used here follows most closely that of Rice, Amos, Handy, Lee, and Schaefer[33] (RAHLS). The letters i, j, k, l, r, and s refer to molecular orbitals. The atomic orbital basis is indicated by the indices μ, ν, ρ, and σ. Nuclear perturbation coordinates are denoted by the letter a. The first derivative of the CI energy with

respect to a nuclear degree of freedom as given by Brooks and co–workers[30] is

$$E^a_{CI} = \sum_{ij} Q_{ij}\, h^a_{ij} + \sum_{ijkl} G_{ijkl}\, (ij\,|\,kl)^a + 2\sum_{ij} X_{ji}\, U^a_{ij} \quad , \tag{1}$$

where h^a_{ij} and $(ij\,|\,kl)^a$ are the one- and two-electron derivative integrals transformed into the molecular orbital basis. Q_{ij} and G_{ijkl} are the reduced one- and two-particle density matrices, respectively, and X_{ji} is the CI Lagrangian defined by

$$X_{ji} = \sum_{r} Q_{jr}\, h_{ir} + 2\sum_{rkl} G_{jrkl}\, (ir\,|\,kl) \quad . \tag{2}$$

The density matrices are given by

$$Q_{ij} = \sum_{IJ} C_I\, C_J\, A^{IJ}_{ij} \tag{3}$$

and

$$G_{ijkl} = \sum_{IJ} C_I\, C_J\, B^{IJ}_{ijkl} \tag{4}$$

and are defined such that they have the full integral symmetry. The A^{IJ}_{ij} and B^{IJ}_{ijkl} are spin-adapted graphical unitary group coupling coefficients. Finally, the U^a_{ij} appearing in Eq. (1) are elements of the molecular orbital change matrices which, for an SCF reference function, are obtained by solving the coupled perturbed Hartree-Fock (CPHF) equations first introduced for nuclear perturbations by Gerratt and Mills.[34]

RAHLS recently demonstrated that the CPHF contribution to the SCF-CI gradient may be rewritten in a form in which the Z-vector method of Handy and Schaefer[23] can be utilized. Their expression for the CI gradient is general (i.e., correct for any kind of reference function) and is given by

$$E^a_{CI} = \sum_{ij} Q_{ij}\, h^a_{ij} + \sum_{ijkl} G_{ijkl}\, (ij\,|\,kl)^a + \sum_{i>j}^{cimr} (X_{ji} - X_{ij}) T^a_{ij} - \sum_{ij} X_{ij}\, S^a_{ij} \quad , \tag{5}$$

where the T^a_{ij} are defined by

$$T_{ij}^{a} = (U_{ij}^{a} - U_{ji}^{a}) \quad , \tag{6}$$

whence

$$U_{ij}^{a} = \frac{1}{2}(T_{ij}^{a} - S_{ij}^{a}) \quad . \tag{7}$$

The S_{ij}^{a} are the derivative overlap integrals transformed into the MO basis. The letters cinr in Eq. (5) refer to the CI non-redundant pairs of molecular orbitals. The SCF, or in our case TCSCF, non-redundant pairs are a subset of the CI non-redundant pairs, and the two spaces may be equivalent. This topic will be disscused in more detail later.

The set of equations which must be solved for T^{a} is determined by the type of reference wave function. The CPHF equations which determine the T_{ij}^{a} for an SCF reference wave function are

$$\mathbf{A}\, \mathbf{T}^{a} = \mathbf{B}^{a} \quad , \tag{8}$$

and RAHLS showed that by defining $\mathbf{Z}$ to be the solution to

$$\mathbf{A}^{T}\, \mathbf{Z} = \Delta \mathbf{X} \quad , \tag{9}$$

the CPHF contribution to Eq. (5) is given by[35]

$$\mathbf{Z}^{T}\, \mathbf{B}^{a} \quad . \tag{10}$$

The ΔX in Eq. (9) is defined by

$$\Delta X_{ij} = (X_{ij} - X_{ji}) \quad . \tag{11}$$

Thus, only one set of CPHF equations needs to be solved rather than N equations, where N is equal to three times the number of nuclei. Accordingly, a large saving in computational effort is achieved. One of the key purposes of this paper is to obtain a similar reduction in computational effort for TCSCF reference wave functions.

4.2.2 TCSCF Reference Wave Functions and the CPTCSCF Equations

When the reference wave function is determined via a TCSCF procedure, then instead of solving one set of CPHF equations it is necessary to solve one set of coupled-perturbed TCSCF (CPTCSCF) equations. Before explicitly writing out the CPTCSCF equations we shall introduce the notation we use (which follows that of Yamaguchi, Osamura, and Schaefer[22]) for TCSCF wave functions.

A TCSCF wave function may be defined in the following manner

$$\Psi_{TCSCF} = C_1\psi_1 + C_2\psi_2 \tag{12}$$

where

$$\psi_1 = A[1\bar{1}2\bar{2}\cdots M\bar{M}m\bar{m}] \tag{13}$$

and

$$\psi_2 = A[1\bar{1}2\bar{2}\cdots M\bar{M}n\bar{n}] \quad . \tag{14}$$

Note the relationship between the special orbital m and C_1 and also that of special orbital n and C_2. (A is the antisymmetrizer operator for the electrons, and M denotes the number of doubly occupied orbitals.) E_{TCSCF} (the electronic energy of the system) is then straightforwardly evaluated as

$$E_{TCSCF} = \sum_{IJ} C_I C_J H_{IJ} \quad , \tag{15}$$

where the Hamiltonian matrix elements are given by

$$\begin{aligned} H_{11} = {} & 2\sum_{i}^{do} h_{ii} + \sum_{ij}^{do} \left[2(ii|jj) - (ij|ij) \right] + 2h_{mm} \\ & + 2\sum_{i}^{do} \left[2(mm|ii) - (mi|mi) \right] + (mm|mm) \quad , \end{aligned} \tag{16}$$

$$H_{22} = 2\sum_{i}^{do} h_{ii} + \sum_{ij}^{do} \left[2(ii|jj) - (ij|ij) \right] + 2h_{nn}$$
$$+ 2\sum_{i}^{do} \left[2(nn|ii) - (ni|ni) \right] + (nn|nn) \quad , \tag{17}$$

and

$$H_{12} = (mn|mn) \quad . \tag{18}$$

Alternatively, the TCSCF energy may be written as

$$E_{TCSCF} = \sum_{i}^{occ} \left[f_i h_{ii} + \varepsilon_{ii} \right] \quad , \tag{19}$$

where ε_{ij} is defined by

$$\varepsilon_{ij} = f_i h_{ij} + \sum_{k}^{occ} \left[\alpha_{ik}(ij|kk) + \beta_{ik}(ik|jk) \right] \quad . \tag{20}$$

Thus, it is necessary to define the f, α, and β parameters for a singlet TCSCF wave function. For orbitals i and j doubly occupied (do) the f_i, α_{ij}, and β_{ij} are 1, 2, and -1, respectively. The changes for the variable occupancy space are

$$\begin{aligned} f_m &= \alpha_{mm} = C_1^2 \quad , \\ f_n &= \alpha_{nn} = C_2^2 \quad , \\ \alpha_{mn} &= \beta_{mm} = \beta_{nn} = \alpha_{nm} = 0 \, , \\ \beta_{mn} &= \beta_{nm} = C_1 C_2 \quad , \end{aligned} \tag{21}$$

and for i = do

$$\begin{aligned} \alpha_{im} &= \alpha_{mi} = 2C_1^2 \quad , \\ \beta_{im} &= \beta_{mi} = -C_1^2 \quad , \\ \alpha_{in} &= \alpha_{ni} = 2C_2^2 \quad , \\ \beta_{in} &= \beta_{ni} = -C_2^2 \quad . \end{aligned} \tag{22}$$

To derive the CPTCSCF equations, one differentiates the 2x2 CI eigenvalue equation and also the TCSCF variational condition, which is $\varepsilon_{ij} = \varepsilon_{ji}$. The form of

the CPTCSCF equations has been reported previously by Yamaguchi, Osamura, and Schaefer.[22] The CPTCSCF equations can be reformulated to suit our needs as

$$\begin{bmatrix} A^{11} & 2A^{21\dagger} \\ 2A^{21} & 4A^{22} \end{bmatrix} \begin{bmatrix} T^a \\ \dfrac{\partial C_I}{\partial a} \end{bmatrix} = \begin{bmatrix} B^{a1} \\ B^{a2} \end{bmatrix} \quad , \tag{23}$$

where the following definitions have been made:

$$A^{11}_{ij,kl} = 2(\alpha_{il} - \alpha_{jl} - \alpha_{ik} + \alpha_{jk})(ij\,|\,kl) + (\beta_{il} - \beta_{jl} - \beta_{ik} + \beta_{jk})\big[\,(ik\,|\,jl) + (il\,|\,jk)\,\big] + (\varepsilon_{jl} - \xi^j_{jl})\delta_{ik} + (\varepsilon_{ik} - \xi^j_{ik})\delta_{jl} - (\varepsilon_{il} - \xi^j_{il})\delta_{jk} - (\varepsilon_{jk} - \xi^j_{jk})\delta_{il} \quad , \tag{24}$$

$$A^{21}_{I,ij} = 2\sum_J C_J\,(\varepsilon^{IJ}_{ij} - \varepsilon^{IJ}_{ji}) = A^{12}_{ij,I} \quad , \tag{25}$$

$$A^{22}_{IJ} = -(1/2)\,\big[\,H_{IJ} - \delta_{IJ}E_{TCSCF} + C_IC_J\,\big] \quad , \tag{26}$$

$$B^{a1}_{ij} = 2\,\varepsilon^a_{ji} - 2\,\varepsilon^a_{ij} + \sum_{rs}^{all} S^a_{rs}\Big\{2(\alpha_{is} - \alpha_{js})(ij\,|\,rs) + (\beta_{is} - \beta_{js})\big[\,(ir\,|\,js) + (is\,|\,jr)\,\big] + (\varepsilon_{ir} - \xi^j_{ir})\delta_{js} - (\varepsilon_{jr} - \xi^i_{jr})\delta_{is}\Big\} \quad , \tag{27}$$

and

$$B^{a2}_I = 2\sum_J C_J\,\big[\,H^a_{IJ} - \sum_{ij}^{all} S^a_{ij}\,(\varepsilon^{IJ}_{ij} + \varepsilon^{IJ}_{ji})\,\big] - 2C_IE^a \quad . \tag{28}$$

The expressions in Eqs. (24) and (27) are identical to those given by RAHLS for the CPHF contribution to SCF-CI gradients. One difference between solving a set of CPTCSCF equations rather than one set of CPHF equations for an SCF-CI gradient is that although the derivatives of the configuration interaction coefficients appear in Eq. (23), according to Eq. (5) they give no direct contribution to the TCSCF-CI energy gradient. The ij pairs involved in Eq. (23) are the TCSCF non-redundant pairs (tcnr), which arise for

i = doubly occupied (do) and j = special 1 (m), special 2 (n), or unoccupied ;
i = special 1 (m) and j = special 2 (n) or unoccupied; and
i = special 2 (n) and j = unoccupied .

Special refers to the two molecular orbitals with variable occupation in a TCSCF. A more detailed discussion of independent (non-redundant) pairs is presented below.

Many of the terms appearing in Eqs. (24) through (28) have not yet been defined:[22]

$$\xi_{ij}^{k} = f_k h_{ij} + \sum_{l}^{occ} \left[\alpha_{kl}(ij\,|\,ll) + \beta_{kl}(il\,|\,jl) \right] \quad ; \tag{29}$$

$$\varepsilon_{ik}^{11} = h_{ik} + \sum_{j}^{do} \left[2(ik\,|\,jj) - (ij\,|\,kj) \right] + 2(ik\,|\,mm) - (im\,|\,km) \tag{30}$$

for k = all, i = doubly occupied (do) and special orbital m;

$$\varepsilon_{ik}^{22} = h_{ik} + \sum_{j}^{do} \left[2(ik\,|\,jj) - (ij\,|\,kj) \right] + 2(ik\,|\,nn) - (in\,|\,kn) \tag{31}$$

for k = all, i = do and special orbital n; and

$$\varepsilon_{mi}^{12} = \varepsilon_{mi}^{21} = (1/2)\ (in\,|\,mn) \quad , \tag{32}$$

and

$$\varepsilon_{ni}^{12} = \varepsilon_{ni}^{21} = (1/2)\ (im\,|\,nm) \tag{33}$$

for i = all. All ε^{IJ} matrix elements not explicitly defined in Eqs. (30) through (33) are zero. The H_{IJ}^{a} are defined similarly to the H_{IJ} except with derivative integrals transformed into the molecular orbital basis. Analogously, ε^{a} is defined just as ε but with MO derivative integrals. The E_{TCSCF} appearing in Eq. (26) is the TCSCF

energy less the nuclear contribution, and the E^a appearing in Eq. (28) is given by

$$E^a = 2\sum_{i}^{occ} f_i h_{ii}^a + \sum_{ij}^{occ} \left[\alpha_{ij}(ii|jj)^a + \beta_{ij}(ij|ij)^a \right] - 2\sum_{ij}^{occ} \varepsilon_{ij} S_{ij}^a \quad . \tag{34}$$

4.2.3 Additional CI Non-Redundant Pairs

Since the variational condition for a TCSCF wave function nontrivially affects only independent elements of the Fock matrix (the tcnr pairs), the CPTCSCF equations are only defined over this region. Therefore, among the CI non-redundant (cinr) pairs in Eq. (5) there are in general pairs for which the T_{ij}^a are not defined by the CPTCSCF equations. We refer to these pairs as additional CI non-redundant pairs (acnr=cinr-tcnr). In order to obtain equations for the acnr T_{ij}^a elements, a matrix ε' is constructed,[25] where

$$\varepsilon'_{ij} = h_{ij} + \sum_{k}^{occ} f_k \left[2(ij|kk) - (ik|jk) \right] \quad . \tag{35}$$

It should be realized that the definition of the ε' matrix is somewhat arbitrary and a few other workers[33] in the field use different definitions. The ε'_{ij} sub-blocks which arise when i and j belong to the same TCSCF shell are then diagonalized in order to obtain a convenient set of uniquely defined molecular orbitals within a given TCSCF shell. By taking derivatives of the diagonalization condition, equations for the remaining T_{ij}^a are obtained. All of the T_{ij}^a elements needed in Eq. (5) are then available.

The distinction between the CI non-redundant pairs (cinr) referred to in Eq. (5) and SCF non-redundant pairs was recently discussed in detail by RAHLS and is especially important for our purposes. Whether using a TCSCF or an SCF reference, the distinction between the different types of independent or non-redundant pairs is

really the same. For the reference wave function (i.e., the SCF or MCSCF wave function), an independent pair of molecular orbitals is defined to be one for which any mixing of the two orbitals would change the SCF, TCSCF, or MCSCF energy. In other words, the relationship between these orbitals either directly or indirectly is defined by the procedure, or more succinctly the variational condition of the system. In a general MCSCF virtually every pair of orbitals may be an independent pair, but in an SCF or certain types of MCSCFs it is really groups of orbitals which are related. Another way to visualize the non-redundant pairs of molecular orbitals is to realize which pairs are redundant, and the remaining pairs will be non-redundant. The redundant pairs of molecular orbitals are simply defined to be those for which unitary rotations between the two molecular orbitals will not affect the SCF or TCSCF energy. For example, in a closed-shell SCF calculation any unitary transformation between doubly occupied (unoccupied) orbitals will not change the SCF energy, and any pair of orbitals ij where i and j are both doubly occupied (both unoccupied) is a redundant pair. Thus, the independent pairs are any ij pair where i is doubly occupied and j is unoccupied.

The CI independent pairs of molecular orbitals in a TCSCF-CI are defined to be those for which any mixing of the two would result in a different TCSCF-CI energy. Clearly, the TCSCF non-redundant pairs are necessarily a subset of the TCSCF-CI non-redundant pairs, since the number of CI independent pairs will expand if orbitals in common shells in the TCSCF procedure are treated differently in the CI procedure. Probably the most common example of this situation is the use of frozen core and frozen virtual orbitals in the CI. Any unitary transformation of doubly occupied orbitals in a TCSCF will leave the TCSCF energy unaffected, but if frozen core orbitals are used to reduce the size of the CI expansion, then any mixing of a core orbital with any active doubly occupied orbital will necessarily change the TCSCF-CI

energy. Another often used method which increases the number of CI independent pairs is the multi-reference CI procedure with SCF orbitals, or alternatively, an MCSCF-CI procedure in which only some of the MCSCF configurations are used as references.

4.2.4 An Efficient TCSCF-CI Gradient Formulation

In order to use Eq. (5) directly in the determination of a TCSCF-CI gradient, the T_{ij}^{a} elements are explicitly required for all N nuclear perturbations (N equals three times the number of nuclei). Hence Eq. (23) must be solved N times. Moreover, in order to form the necessary B^{a} vectors in Eqs. (27) and (28), N distinct ε^{a} matrices and $H^{a}C$ products are required. Referring to Eqs. (16)-(18), and (20), one sees that this necessitates the transformation and storage of N sets of derivative integrals.

The latter point requires further clarification, since it is possible to construct the ε^{a} matrices in the AO basis as the derivative integrals are formed and then transform them to the MO basis.[36] However, such an explicit formation of these matrices is expensive; e.g., with a TZ2P basis set (94 functions), the derivative integral time required for a TCSCF-CI gradient of C_2H_4 in D_{2h} symmetry increases from 225 to 1085 IBM 3090 CPU seconds if the ε^{a} matrices are constructed explicitly. Furthermore, for a general MCSCF reference wave function the only viable means of forming the $H^{a}C$ products is to explicitly transform the derivative integrals into the MO basis. In this section we show how to dispense with the explicit formation of the N different T^{a} matrices and the transformation and storage of any derivative integrals in the evaluation of TCSCF-CI gradients. The crux of the method is in the reduction of the number of CPTCSCF equations which must be solved from N to 1. For the general MCSCF case (where the dimension of these equations will be much larger), this type of reduction itself will be of much greater significance than the removal of

derivative integral transformations from the procedure. Also, since the one set of equations to be solved is perturbation independent, then the MCSCF configuration space need not be expanded to include other symmetry types in the evaluation of the MCSCF-CI gradient.[37]

The contribution to the TCSCF-CI gradient due to the CI non-redundant pairs can be included in a fashion similar to that described by RAHLS for SCF-CI gradients. This approach avoids the numerical problems of past formalisms. The cinr contribution takes the form [cf. Eq. (5)]

$$\sum_{i>j}^{cinr}(X_{ji} - X_{ij})T_{ij}^{a} = \sum_{i>j}^{tcnr}\Delta X_{ji}T_{ij}^{a} + \sum_{i>j}^{acnr}\Delta X_{ji}T_{ij}^{a} \tag{36}$$

$$= \sum_{i>j}^{tcnr}\Delta X_{ji}T_{ij}^{a} + \sum_{i>j}^{acnr}\frac{(X_{ji} - X_{ij})}{\epsilon'_{ii} - \epsilon'_{jj}}\Big\{B'^{a}_{ij} - \sum_{r>l}^{tcnr}A'_{ij,rl}\,T^{a}_{rl}$$
$$- 4C_1\left[2(ij\,|\,mm) - (im\,|\,jm)\right]\frac{\partial C_1}{\partial a} - 4C_2\left[2(ij\,|\,nn) - (in\,|\,jn)\right]\frac{\partial C_2}{\partial a}\Big\} \tag{37}$$

where the following definitions have been made:

$$B'^{a}_{ij} = -2(\epsilon'_{ij})^{a} + \sum_{rl}^{all}S^{a}_{rl}\left\{f_l\left[4(ij\,|\,rl) - (ir\,|\,jl) - (il\,|\,jr)\right] + \delta_{ij}\epsilon'_{jr} + \delta_{jl}\epsilon'_{ir}\right\} \tag{38}$$

and

$$A'_{ij,rl} = (f_l - f_r)\left[4(ij\,|\,rl) - (ir\,|\,jl) - (il\,|\,jr)\right] + \delta_{il}\epsilon'_{jr} + \delta_{jl}\epsilon'_{ir} - \delta_{ir}\epsilon'_{jl} - \delta_{jr}\epsilon'_{il} \quad . \tag{39}$$

Note that $(\epsilon'_{ij})^{a}$ is defined as ϵ'_{ij} is in Eq. (35) except with derivative integrals transformed into the MO basis. It should be emphasized that in Eqs. (36) through (39) the acnr pairs are TCSCF redundant pairs but CI non-redundant pairs.

RAHLS handled the acnr contribution by expanding the set of linear equations to be solved when obtaining the Z-vector, but it is not necessary to do so, and in fact it is preferable not to expand the set of linear equations. This can be accomplished by rewriting Eq. (37) as

$$\sum_{i>j}^{cimr} \Delta X_{ji} T^{a}_{ij} = \sum_{i>j}^{acmr} \frac{\Delta X_{ji} B'^{a}_{ij}}{\epsilon'_{ii} - \epsilon'_{jj}} - \sum_{r>l}^{tcmr} (\Delta X'_{rl} + \Delta X_{rl})\, T^{a}_{rl} - \eta_1 \frac{\partial C_1}{\partial a} - \eta_2 \frac{\partial C_2}{\partial a} \quad , \tag{40}$$

where

$$\Delta X'_{rl} = \sum_{i>j}^{acmr} \frac{\Delta X_{ji}\, A'_{ij,rl}}{\epsilon'_{ii} - \epsilon'_{jj}} \quad , \tag{41}$$

$$\eta_1 = 4C_1 \sum_{i>j}^{acmr} \Delta X_{ji} \frac{[2(ij\,|\,mm) - (im\,|\,jm)]}{\epsilon'_{ii} - \epsilon'_{jj}} \quad , \tag{42}$$

and

$$\eta_2 = 4C_2 \sum_{i>j}^{acmr} \Delta X_{ji} \frac{[2(ij\,|\,nn) - (in\,|\,jn)]}{\epsilon'_{ii} - \epsilon'_{jj}} \quad . \tag{43}$$

Note that now the derivatives of the (TCSCF) CI coefficients do give a direct contribution to the TCSCF-CI gradient precisely because the f_m and f_n parameters used in Eq. (35) to canonicalize the orbitals depend on C_1 and C_2. Thus, proceeding analogously to Eqs. (8)-(10), one obtains the following expression for the TCSCF-CI gradient (excluding nuclear repulsion terms):

$$E^{a}_{TCSCF-CI} = \sum_{ij} Q_{ij} h^{a}_{ij} + \sum_{ijkl} G_{ijkl} (ij\,|\,kl)^{a} + \sum_{i>j}^{acmr} \frac{\Delta X_{ji}\, B'^{a}_{ij}}{\epsilon'_{ii} - \epsilon'_{jj}} - \sum_{ij}^{all} X_{ij}\, S^{a}_{ij}$$
$$+ \sum_{i>j}^{tcmr} Z_{ij}\, B^{a1}_{ij} + \zeta_1 B_1^{a2} + \zeta_2 B_2^{a2} \quad , \tag{44}$$

where the one set of CPTCSCF equations to be solved has the form

$$\begin{bmatrix} A^{11} & 2A^{21^{T}} \\ 2A^{21} & 4A^{22} \end{bmatrix} \begin{bmatrix} Z \\ \zeta \end{bmatrix} = (-1) \begin{bmatrix} \Delta X' + \Delta X \\ \eta \end{bmatrix} . \tag{45}$$

Since the A matrix is symmetric we have not indicated the use of its transpose in the above equation which would otherwise be required as outlined by Handy and Schaefer.[23] In Eq. (45) it is tacitly assumed that the independent pairs ij are ordered such that i>j on both sides. Alternatively, the negative sign on the right-hand side of

Eq. (45) can be removed by defining the ΔX and $\Delta X'$ vectors with i<j and changing the signs in the η definitions. In this regard it is worth noting that $Z_{ij} = - Z_{ji}$.

By rearranging the summations in a few of the terms in Eq. (44), a final working equation for the TCSCF-CI energy gradient is obtained:

$$E^a_{TCSCF-CI} = \sum_{ij} Q'_{ij} h^a_{ij} + \sum_{ijkl} G'_{ijkl} (ij\,|\,kl)^a + \sum_{ij} P_{ij} S^a_{ij} \quad , \tag{46}$$

where the following definitions have been made.

$$Q'_{ij} = Q_{ij} + \frac{\upsilon_{ij}\Delta X_{ji}}{\varepsilon'_{jj} - \varepsilon'_{ii}} + \omega_{ij}(f_j - f_i)Z_{ij} + 4\delta_{ij}\sum_I \zeta_I C_I (f^I_i - f_i) \quad , \tag{47}$$

$$\begin{aligned} G'_{ijkl} = G_{ijkl} &+ \frac{2\upsilon_{ij}\Delta X_{ij} f_k \delta_{kl}}{\varepsilon'_{ii} - \varepsilon'_{jj}} - \frac{\upsilon_{ik}\Delta X_{ik} f_j \delta_{jl}}{\varepsilon'_{ii} - \varepsilon'_{kk}} \\ &+ 2\sum_I \zeta_I C_I \left[(\alpha^I_{ik} - \alpha_{ik})\delta_{ij}\delta_{kl} + (\beta^I_{ij} - \beta_{ij})\delta_{ik}\delta_{jl} \right] \\ &+ 2\delta_{im}\delta_{jn}\delta_{km}\delta_{ln}\sum_{I\neq J} \zeta_I C_J + \omega_{ij} Z_{ij}(\alpha_{jk} - \alpha_{ik})\delta_{kl} + \omega_{ik} Z_{ik}(\beta_{kj} - \beta_{ij})\delta_{jl} \quad , \end{aligned} \tag{48}$$

and

$$\begin{aligned} P_{ij} = - X_{ij} &+ \sum_{r>l}^{acnr} \frac{\Delta X_{lr}}{\varepsilon'_{rr} - \varepsilon'_{ll}} \left\{ f_j \left[4(ij\,|\,rl) - (ir\,|\,jl) - (il\,|\,jr) \right] + \delta_{rj}\varepsilon'_{li} + \delta_{lj}\varepsilon'_{ri} \right\} \\ &+ \sum_{r>l}^{tcnr} Z_{rl} \left\{ 2(\alpha_{rj} - \alpha_{lj})(ij\,|\,rl) + (\beta_{rj} - \beta_{lj}) \left[(ir\,|\,jl) + (il\,|\,jr) \right] \right. \\ &\left. + (\varepsilon_{ri} - \xi^l_{ri})\delta_{lj} - (\varepsilon_{li} - \xi^r_{li})\delta_{rj} \right\} + 4\theta_{ij}\varepsilon_{ij}\sum_I \zeta_I C_I - 2\sum_{IJ} \zeta_I C_J (\varepsilon^{IJ}_{ij} + \varepsilon^{IJ}_{ji}) \quad , \end{aligned} \tag{49}$$

with

$$\theta_{ij} = \begin{cases} 1 & \text{for i and j occupied} \\ 0 & \text{otherwise} \quad , \end{cases} \tag{50}$$

$$\upsilon_{ij} = \begin{cases} 1 & \text{for i and j acnr} \\ 0 & \text{otherwise} \quad , \end{cases} \tag{51}$$

$$\omega_{ij} = \begin{cases} 1 & \text{for i and j tcnr} \\ 0 & \text{otherwise} \quad , \end{cases} \tag{52}$$

and

$$f_i^I,\ \alpha_{ij}^I,\ \text{and}\ \beta_{ij}^I = \text{the values of } f_i,\ \alpha_{ij},\ \text{and}\ \beta_{ij} \text{ in configuration I.} \qquad (53)$$

Note that the values of f_i^I, α_{ij}^I, and β_{ij}^I are simply the values of the standard single-determinant canonicalization parameters. For example, $f_m^1 = f_n^2 = 1$, and $f_m^2 = f_n^1 = 0$. Also note that the definitions in Eqs. (48) and (49) are for unsymmetrized $\mathbf{G}'$ and $\mathbf{P}$ matrices. However, since the derivative integrals have the same symmetry as the normal zeroth-order integrals, then $\mathbf{G}'$ and $\mathbf{P}$ may be forced to have this symmetry also. To wit, Eq. (46) still holds if G'_{ijkl} and P_{ij} are replaced by $\tilde{G}'_{ijkl} = (G'_{ijkl}+G'_{jikl}+G'_{ijlk}+G'_{jilk}+G'_{klij}+G'_{klji}+G'_{lkij}+G'_{lkji})/8$ and $\tilde{P}_{ij} = (P_{ij}+P_{ji})/2$, respectively. Finally then we have,

$$E^a_{TCSCF-CI} = \sum_{\mu\nu} Q'_{\mu\nu} h^a_{\mu\nu} + \sum_{\mu\nu\rho\sigma} \tilde{G}'_{\mu\nu\rho\sigma} (\mu\nu \mid \rho\sigma)^a + \sum_{\mu\nu} \tilde{P}_{\mu\nu} S^a_{\mu\nu} \quad . \qquad (54)$$

Back transforming $\mathbf{Q}'$, $\tilde{\mathbf{G}}'$, and $\tilde{\mathbf{P}}$ into the atomic orbital basis allows the entire TCSCF-CI gradient to be evaluated as the derivative integrals are determined. This procedure avoids writing out to disk or transforming any derivative integrals and also avoids the costly formation of the $\boldsymbol{\varepsilon}^a$ matrix. Furthermore, this procedure is easily generalized to the MCSCF-CI gradient.

In terms of the summary of the MCSCF-CI computational procedure given previously on p. 388 of Osamura, Yamaguchi, and Schaefer,[25] steps 6-12 are modified in the new procedure as follows: (6) The density matrices Q_{ij} and G_{ijkl} and the Lagrangian X_{ij} are obtained in the MO basis from the CI wave function. (7) The blocks of the A matrix in Eqs. (24)-(26) are formed. (8) The ΔX, $\Delta X'$, and η vectors in Eqs. (11), (41), (42), and (43) are evaluated. (9) The one set of CPTCSCF equations [Eq. (45)] is solved iteratively (or perhaps directly for small cases). (10) The symmetrized Q'_{ij}, $\tilde{G}'_{ijkl}$, and $\tilde{P}_{ij}$ matrices are formed and stored in the MO basis

according to Eqs. (47)-(49). (11) The Q'_{ij}, $\tilde{G}'_{ijkl}$, and $\tilde{P}_{ij}$ matrices are back transformed into the AO basis. (12) The TCSCF-CI gradient is evaluated according to Eq. (54) by contracting the $h^a_{\mu\nu}$, $(\mu\nu|\rho\sigma)^a$, and $S^a_{\mu\nu}$ derivative integrals as they are computed with the $Q'_{\mu\nu}$, $\tilde{G}'_{\mu\nu\rho\sigma}$, and $\tilde{P}_{\mu\nu}$ matrices.

It is important to note that it is computationally more efficient to form Q', $\tilde{G}'$, and $\tilde{P}$ in the MO basis and then back transform to the atomic orbital basis rather than to back transform Q and G and then add in the remaining contributions due to Z, ζ, and ΔX (by separately back transforming these quantities). The latter procedure essentially incorporates two n^5 (n is the number of atomic or molecular orbitals) back transformation steps whereas the former procedure has only one n^5 step since forming the extra contribution to $\tilde{G}'$ in the MO basis is less than n^4 in cost. Finally, it is helpful to understand the significance of the (Z,ζ) vector.[33] If one were to use this vector to rotate the molecular orbitals, perform another CI, form a new (Z,ζ) vector, and so forth, then eventually a stationary set of molecular orbitals would be obtained. This set of MOs would correspond to the MCSCF orbitals of the TCSCF-CI configuration space. So, in other words, the first (Z,ζ) vector is the first-order correction of the TCSCF-CI wave function toward the corresponding MCSCF solution.

4.3 THEORY OF SCFX-CI GRADIENTS

The adaptation of the TCSCF-CI formalism of Section 4.2 to obtain SCFX-CI gradients is the first implementation of analytic CI gradients based on Davidson-Stenkamp reference wave functions. As a point of departure, it is worthwhile to reiterate the description of the excited-state SCF method presented by Fitzgerald and Schaefer[12] and more succinctly in Section 2.2. The SCFX wave function is written in the usual open-shell singlet form

$$\Psi = \frac{1}{\sqrt{2}} \left| (\text{core})(a\bar{b} - \bar{a}b) \right| \tag{55}$$

except that the two open-shell orbitals |a> and |b> are allowed to have nonzero overlap S, which is variationally determined. Thus, one minimizes $E = \langle\Psi|H|\Psi\rangle/(1+S^2)$ subject to the constraint that all pairs of orbitals except (a,b) are orthogonal. The resulting equations[12] are solved by the sequential orthogonalization method of Davidson[38] to obtain either closed-shell singlet ground-state solutions (with overlap S=1) or open-shell singlet excited-state solutions (with overlap S=0). By defining the orthonormal orbitals

$$|u\rangle = \frac{(|a\rangle + |b\rangle)}{\sqrt{2(1+S)}} \quad \text{and} \quad |v\rangle = \frac{(|a\rangle - |b\rangle)}{\sqrt{2(1-S)}} \tag{56}$$

the wave function in Eq. (55) can be written in the form

$$\begin{aligned} \Psi &= C_1 \left| (\text{core})u\bar{u} \right| + C_2 \left| (\text{core})v\bar{v} \right| \\ &= C_1\Psi_1 + C_2\Psi_2 \quad , \end{aligned} \tag{57}$$

where

$$C_1 = \frac{(S+1)}{\sqrt{2(1+S^2)}} \quad \text{and} \quad C_2 = \frac{(S-1)}{\sqrt{2(1+S^2)}} \quad . \tag{58}$$

Since both the orbitals and the overlap S are fully optimized, the wave function in Eq. (57) is in fact a TCSCF wave function. In general, excited-state solutions will have $C_1 \simeq 1/\sqrt{2}$ and $C_2 \simeq -1/\sqrt{2}$ although large deviations from these values are not uncommon. The configuration state function (CSF)

$$\psi_3 = \frac{1}{\sqrt{2}} \left| (\text{core})(u\bar{v} - \bar{u}v) \right| \tag{59}$$

does not appear in Eq. (57) by construction, but it is at times one of the dominant components of large-scale CI wave functions based on the two references in Eq. (57). The significance of ψ_3 is elucidated when one realizes that any three-configuration MCSCF wave function

$$\Psi = C_1' \left| (\text{core})\, x\bar{x} \right| + C_2' \left| (\text{core})\, y\bar{y} \right| + C_3' \left| (\text{core})(x\bar{y} - \bar{x}y) \right| / \sqrt{2} \tag{60}$$

can be written in the TCSCF form of Eq. (57) by performing the orbital rotation

$$|u\rangle = \cos\theta\,|x\rangle + \sin\theta\,|y\rangle \quad \text{and} \quad |v\rangle = \sin\theta\,|x\rangle - \cos\theta\,|y\rangle \ , \tag{61}$$

where

$$\tan 2\theta = \frac{\sqrt{2}C_3'}{C_1' - C_2'} \quad \text{and} \quad S = \pm \frac{(C_1' + C_2')}{\sqrt{(C_1' - C_2')^2 + 2C_3'^2}} \ . \tag{62}$$

Thus, the excited-state SCF procedure gives solutions identical to the roots of the two-electron-in-three-orbital CASSCF in Eq. (60). The open-shell singlet (S=0, $C_3' \simeq 1$) solutions typically appear as second roots of this MCSCF and thus are variational, giving energies which are upper bounds to the exact excited-state energies. Hamilton and Pulay[13] choose to maintain the excited-state wave function in the form of Eq. (60) throughout the course of the wave function optimization, and they have successfully applied DIIS techniques to improve the convergence.

In summary, the Davidson-Stenkamp wave function [Eq. (55)] can be written in either a two-configuration SCF form [Eq. (57)] or a three-configuration SCF form [Eq. (60)]. As a consequence, the TCSCF-CI formalism of Section 4.2 can be applied to two-reference CI wave functions based on Eq. (57) or *three-reference CI wave functions* in which the reference ψ_3 [Eq. (59)] is also included. This statement is valid for both the ground-state and excited-state solutions possible in Eq. (55).

The SCFX wave function in Eq. (57) is identical in form to the TCSCF wave function in Eq. (12) of Section 4.2, except that the two special orbitals are labeled u and v instead of m and n. Thus, it follows that

$$E_{SCFX} = 2\sum_{i}^{occ} f_i h_{ii} + \sum_{ik}^{occ}[\alpha_{ik}(ii\,|\,kk)+\beta_{ik}(ik\,|\,ik)] \quad , \tag{63}$$

where the f, α, and β parameters are those given in Section 4.2 [Eqs. (21) and (22) and the preceding sentence therein]. The final equations for SCFX-CI gradients then follow directly from Eqs. (44) and (54):

$$E^a_{SCFX-CI} = \sum_{ij} Q_{ij} h^a_{ij} + \sum_{ijkl} G_{ijkl}(ij\,|\,kl)^a + \sum_{i>j}^{actr} \frac{\Delta X_{ji} B'^a_{ij}}{\varepsilon'_{ii} - \varepsilon'_{jj}} - \sum_{ij}^{all} X_{ij} S^a_{ij}$$
$$+ \sum_{i>j}^{tctr} Z_{ij} B^{a1}_{ij} + \zeta_1 B_1^{a2} + \zeta_2 B_2^{a2} \quad , \tag{64}$$

or

$$E^a_{SCFX-CI} = \sum_{\mu\nu} Q'_{\mu\nu} h^a_{\mu\nu} + \sum_{\mu\nu\rho\sigma} \tilde{G}'_{\mu\nu\rho\sigma}(\mu\nu\,|\,\rho\sigma)^a + \sum_{\mu\nu} \tilde{P}_{\mu\nu} S^a_{\mu\nu} \quad . \tag{65}$$

In the latter equation, $Q'_{\mu\nu}$ and $\tilde{G}'_{\mu\nu\rho\sigma}$ are modified one- and two-particle density matrices transformed into the atomic orbital basis. The coupled-perturbed TCSCF contribution to $E^a_{SCFX-CI}$ has been incorporated into the $Q'_{\mu\nu}$, $\tilde{G}'_{\mu\nu\rho\sigma}$, and $\tilde{P}_{\mu\nu}$ matrices so as to avert the need to transform or store derivative integrals. Furthermore, to obtain an SCFX-CI gradient using Eq. (65) it is only necessary to solve one set of CPTCSCF equations rather than N sets, where N is three times the number of

nuclei. The reader is referred to Section 4.2 for explicit definitions of the various quantities in Eqs. (64) and (65). The only difference in Eqs. (64) and (65) as applied to excited states instead of ground states is that the Lagrangian X_{ij} and the one- and two-particle density matrices Q_{ij} and G_{ijkl} are formed from the CI coefficients of the *second* root rather than those of the *first* root of the CI secular equation [see Eqs. (2), (3), (4), (47), (48), and (49)]. Hence, little effort is required to implement the SCFX-CI gradient procedure once a TCSCF-CI gradient program exists. In practice SCFX-CI gradients are somewhat more expensive to compute. The additional expense arises in the CI procedure itself, which typically requires an increase in the number of iterations by a factor of 1.5 to 2.0 in order to converge on the higher root.

4.4 COMPUTATIONAL DETAILS

Two basis sets were employed in the formaldehyde and ketene applications. The first of these is a standard Huzinaga[39] and Dunning[40] double-zeta plus polarization (DZP) basis set, which can be designated C(9s5p1d/4s2p1d), O(9s5p1d/4s2p1d), and H(4s1p/2s1p). For the sets of six Cartesian d functions on the carbon and oxygen atoms, the Gaussian exponents $\alpha_d(C)=0.75$ and $\alpha_d(O)=0.85$ were selected. The hydrogen s-function exponents were scaled by the usual factor of $1.2^2=1.44$, and $\alpha_p(H)=0.75$ was chosen for the polarization function exponent. The DZP basis used here is identical to that used by Allen and Schaefer[6] in a recent study of the low-lying electronic states of ketene. It is only slightly different from the DZP basis set used for formaldehyde by Fitzgerald and Schaefer,[12] who employed $\alpha_d(O)=0.80$ in contrast to the $\alpha_d(O)=0.85$ used here. For formaldehyde and ketene our DZP basis consists of 42 and 58 contracted Gaussian functions (CGFs), respectively.

The second basis set used in this study was obtained by adding Rydberg functions to the DZP basis set, and it is denoted DZP+R (R=Rydberg). Two additional Gaussian functions of s and p type were added to each carbon and oxygen atom. The exponents were chosen to be consistent with those of Dykstra and Schaefer[5] and Allen and Schaefer,[6] viz., α_s(C)=0.0474, 0.0146; α_p(C)=0.0365, 0.0117; α_s(O)=0.0862, 0.0261; and α_p(O)=0.0637, 0.0190. Thus, for formaldehyde and ketene the DZP+R basis set is comprised of 58 and 82 CGFs, respectively.

Geometrical structures were fully optimized using analytic gradient techniques. At all stationary points the internal coordinates were converged to 10^{-6} Å or radians, and the largest components of the Cartesian energy gradients were less than 10^{-6} hartree/bohr. Harmonic vibrational frequencies and quadratic force constants were determined either with analytic second derivative techniques (SCF,[41] TCSCF,[22] or SCFX[12]) or by taking finite differences of analytic gradients (SCF-CI,[42] TCSCF-CI, or SCFX-CI). For further discussion of analytic derivative techniques the reader is referred to two recent reviews.[43,44] In the finite-difference procedures the quadratic force constants (F_{ij}) were obtained by displacing internal coordinates ±0.005 Å or ± 0.01 rad. In this manner all cubic contaminations were removed from the numerical F_{ij} constants, and additional techniques were utilized to remove the quartic contaminations from the F_{ii} values. The final harmonic frequencies obtained from these numerical force constants are expected to differ from the analytic values by no more than 0.1 cm^{-1}.

In all configuration interaction wave functions the carbon and oxygen 1s core and 1s virtual orbitals were frozen. Thus, two core and two virtual orbitals were frozen for formaldehyde while three orbitals of each type were frozen for ketene. Otherwise, all singly- and doubly-excited configurations with respect to one, two, or three references (1R, 2R, or 3R) were included in the CI wave functions. The 3R

CISD results for formaldehyde include *all* singly- and doubly-excited configurations, including the non-interacting ones. The largest CI wave functions determined in this study were the DZP+R (82 CGF) 2R CISD wave functions for the 2^1A_1 state of ketene. In C_{2v} symmetry 80500 CSFs (configuration state functions) were present, and in C_s symmetry (encountered in the finite-difference procedures) as many as 155255 CSFs were included. The size of the basis set and the configuration space in these calculations clearly indicates the viability of the SCFX-CI gradient procedure presented in the previous section.

4.5 APPLICATION TO 2^1A_1 FORMALDEHYDE

4.5.1 Review

A meticulous review of experimental and theoretical studies of the low-lying electronic states of formaldehyde would constitute a tome. Thus, we must be highly selective in our discussion here. In a 1975 review, Moule and Walsh[45] discuss much of the early work on the ultraviolet spectra and excited states of formaldehyde, and the 1982 review of Davidson and McMurchie[1] contains a succinct recount of *ab initio* studies of H_2CO excited states. Many theoretical studies have investigated vertical excitation energies,[16,46–52] and in several studies the potential energy surfaces of the $(n\rightarrow\pi^*)$ $\tilde{a}^3A''$, $(n\rightarrow\pi^*)$ $\tilde{A}^1A''$, $(\pi\rightarrow\pi^*)$ $\tilde{b}^3A'$, and $(n\rightarrow 3s)$ $\tilde{B}^1B_2$ states have been examined in greater detail.[12,53–61] The first three of these states have out-of-plane-bent equilibrium geometries[12,56,57,62–64] while the $^1B_2$ Rydberg state has a C_{2v} geometry[59] similar to that of the $^2B_2$ H_2CO^+ cation.[65,66] For our purposes it is sufficient to concentrate primarily on the $(\pi\rightarrow\pi^*)^1$ and $(n\rightarrow 3p_y)^1$ states, whose potential energy surfaces have received less attention in large part because of the difficulties in treating excited $^1A_1$ states described above.

The history of the $\pi\rightarrow\pi^*$, $n\rightarrow\sigma^*$, $n\rightarrow 3s$, and $n\rightarrow 3p$ singlet states of formaldehyde is not a paragon of rapid scientific advance but rather a narrative of arduous scientific progress fraught with cycles of confusion and elucidation. At one time it was generally thought that all of the small amides and aldehydes have a $(\pi\rightarrow\pi^*)$ ^1A state near 7-8 eV.[67] Early semiempirical theoretical investigations assumed the $(\pi\rightarrow\pi^*)^1$ state of formaldehyde to be valence in character, and several energies in the 7.4 – 9.8 eV range were obtained.[68–71] For example, Sidman[69] arrived at a transition energy of 8.1 eV, apparently in excellent agreement with an experimental band at 8.0 eV. Similarly, several workers ascribed an observed band at 7.1 eV to the $n\rightarrow\sigma^*$ excitation.[69,71] Associated predictions[45,70] were that most of the strength of the

$\tilde{X}^1A_1 \rightarrow \tilde{a}^3A_2$ transition results from spin-orbit mixing of the $(n\rightarrow\pi^*)\ ^3A_2$ and $(\pi\rightarrow\pi^*)\ ^1A_1$ states and that certain forbidden $\tilde{X}^1A_1 \rightarrow \tilde{A}^1A_2$ transitions arise from vibronic mixing of the $(n\rightarrow\pi^*)\ ^1A_2$ and $(n\rightarrow\sigma^*)\ ^1B_2$ states.[72] However, Allison and Walsh[45] interpreted the 7.1 eV band as an $n\rightarrow 3s$ ($\tilde{X}^1A_1\rightarrow{}^1B_2$) Rydberg transition, and analyzed the 8.0 eV system as an $n\rightarrow 3p_y$ ($\tilde{X}^1A_1\rightarrow{}^1A_1$) and $n\rightarrow 3p_z$ ($\tilde{X}^1A_1\rightarrow{}^1B_2$) Rydberg doublet. As explained by Moule and Walsh in 1975, "No experimental evidence for the $^1A_1$ $(\pi,\pi^*)\leftarrow\tilde{X}^1A_1$ transition can be found in either the absorption or the electron scattering spectra which is one of the central puzzles of the spectroscopy of this region."

Several *ab initio* theoretical studies in the 1970s resolved much of the confusion.[47–52] The basic assignments of Allison and Walsh were vindicated, although Harding and Goddard[52] switched the order of the states in the assignment of the 8.0 eV Rydberg doublet. Furthermore, the $(\pi\rightarrow\pi^*)\ ^1A_1$ state was predicted to lie much higher in energy, values of 10.77, 10.10, 11.31, 10.43, and 11.41 eV having been proposed.[52,49,46,50,47] Some contention arose concerning the amount of Rydberg character in the $(\pi\rightarrow\pi^*)^1$ state, but the final conclusion of Harding and Goddard[52] was that this state is ≈90% valence in character. In any event, at the ground-state geometry the $(\pi\rightarrow\pi^*)^1$ state apparently lies above (or at least near) the $n\rightarrow\infty$ ionization limit of 10.87 eV[73] and thus is embedded in a multitude of $^1A_1$ states.

In Table I reliable experimental and theoretical vertical excitation energies from the paper of Harding and Goddard[52] are listed for several states of formaldehyde. (The reader is referred to Refs. 1 and 52 for summaries of other theoretical work.) Note that the $(\pi\rightarrow\pi^*)^3$ state at 6.0 eV is the lowest one of $^3A_1$ symmetry, but the $(\pi\rightarrow\pi^*)^1$ state is at least 4 eV higher and has many $^1A_1$ states below it. Fitzgerald and Schaefer[12] have recently investigated the effect of geometry optimization on the $(\pi\rightarrow\pi^*)^1$ state. At the DZP SCFX level of theory, a C_{2v} minimum is predicted with

r_e(C-O)=1.537 Å, r_e(C-H)=1.078 Å, and θ_e(H-C-H)=120.3°. The DZP SCFX adiabatic excitation energy is 8.68 eV, which is 2.27 eV below the corresponding vertical excitation energy. Fitzgerald and Schaefer cautiously concluded that the $(\pi\rightarrow\pi^*)^1$ state might lie below the ionization continuum but that a direct transition from the ground state is unlikely due to poor Franck-Condon overlap. Several questions then remain, among which are (a) What are the effects of diffuse basis functions and electron correlation on the $(\pi\rightarrow\pi^*)^1$ geometry and vibrational frequencies? (b) Is the SCFX method valid for the $(\pi\rightarrow\pi^*)^1$ state since the $(n\rightarrow 3p_y)^1$ state (among others) appears to lie below it (cf. Table I)? In other words, is variational collapse a problem? (c) Does the $(\pi\rightarrow\pi^*)^1$ state mix strongly with Rydberg states as its geometry is optimized and its energy is lowered? Answers to these questions are sought here through application of the new SCFX-CI gradient technique in conjunction with DZP and DZP+R basis sets. In particular, the $(n\rightarrow 3p_y)$ and $(\pi\rightarrow\pi^*)$ $^1A_1$ states are investigated in detail while keeping track of their position relative to several other electronic states.

4.5.2 Results and Discussion

4.5.2.1 The $\tilde{X}^1A_1$ State

In Table II theoretical results are given for the $\tilde{X}^1A_1$ and $(\pi\rightarrow\pi^*)$ 2^1A_1 states of H_2CO and the $(\pi\rightarrow\infty)$ $^2B_1$ state of H_2CO^+. It is prudent to concentrate first on the $\tilde{X}^1A_1$ H_2CO results since experimental data are available for comparison. The DZP SCF geometrical parameters and harmonic vibrational frequencies exhibit the type of agreement with experiment which is expected at this level of theory. The DZP SCF r_e(C-O) and r_e(C-H) values are 0.015 and 0.003 Å too short, respectively, and the harmonic frequencies range from 5.1 to 12.8% above the experimental *harmonic* frequencies. The 12.8% error occurs for $\omega_2(a_1)$, the C=O stretch, and indicates the importance of antibonding electronic configurations in the description of this multiple bond. Comparing the DZP and DZP+R SCF predictions in Table II, one finds the expected result that the Rydberg functions have essentially no effect on the ground state parameters. For example, with the inclusion of the Rydberg functions, r_e(C-O) decreases 0.0009 Å, θ_e(H-C-H) increases 0.12°, and all of the harmonic frequencies change less than 6 cm^{-1}.

The DZP CISD r_e(C-O), r_e(C-H), and θ_e(H-C-H) geometrical parameters are in error by only +0.008 Å, +0.005 Å, and -0.3°, respectively, and the DZP CISD harmonic frequencies range from 0.0 to +5.1% above experiment. The largest discrepancies still occur for r_e(C-O) and $\omega_2(a_1)$, but the CISD values represent substantial improvements over the SCF predictions. It is instructive to compare the DZP CISD values with the DZP MP2 results of Simandiras, Handy, and Amos[74] and the DZP CASSCF predictions of Dupuis, Lester, Lengsfield, and Liu[75] (Table II). The MP2 C=O bond length is 0.012 Å longer than the CISD distance, and the MP2 ω_2=1774 cm^{-1} result is 94 cm^{-1} lower than the analogous CISD frequency.

Furthermore, the r_e(C-O) and $\omega_2(a_1)$ MP2 results are very close to the CASSCF values of 1.224 Å and 1772 cm^{-1}. The CASSCF frequencies range in error from -3.9 to -0.1% and the corresponding MP2 range is -1.2 to +2.8%. Therefore, in general the MP2 and CASSCF frequencies are in better agreement with experiment than the CISD values while the MP2 and CASSCF C=O bond lengths are less accurate than the CISD distance. With a C(8s6p3d), O(8s6p3d), and H(6s2p) basis set, the MP2 r_e(C-O) distance is reduced to 1.2099 Å,[74] which is only 0.007 Å higher than experiment. One would expect the corresponding CISD C=O distance to be roughly 0.005 Å shorter than experiment. In summary, the data in Table II support the contention that in cases where a single configuration is strongly dominant, MP2 theory may give more accurate frequencies (and perhaps geometrical structures) than CISD theory because MP2 theory overestimates the effect of double excitations and thereby "includes" higher-order effects through cancellation of errors.

The $\tilde{X}^1A_1$ H_2CO predictions most pertinent to the investigation of the $(\pi\rightarrow\pi^*)$ 2^1A_1 state are the TCSCF, 2R CISD, and 3R CISD results in Table II. Consistent zeroth-order descriptions of the $\tilde{X}^1A_1$, $(\pi\rightarrow\pi^*)$ $^3A_1$, and $(\pi\rightarrow\pi^*)$ 2^1A_1 states can be achieved by treating the (π,π^*) pair correlation in an equivalent fashion for all three states. A single-configuration $\pi\pi^*$ SCF wave function suffices for the $^3A_1$ state, but for both the $\tilde{X}^1A_1$ and 2^1A_1 states, TCSCF wave functions involving the π^2 and π^{*2} configurations are required if a consistent treatment is to be achieved. Thus, in Table II the $\tilde{X}^1A_1$ results used for comparison with the 2^1A_1 state are TCSCF, 2R CISD, and 3R CISD values involving the π^2, π^{*2}, and $\pi\pi^*$ reference configurations [see Eqs. (3) and (5) and the accompanying discussion]. The 2R and 3R CISD geometrical structures and vibrational frequencies were obtained by implementing the new TCSCF-CI gradient method of Section 4.2.

The DZP TCSCF energy for the $\tilde{X}^1A_1$ state is 7751 cm^{-1} below the DZP SCF energy, and the TCSCF CI coefficient for the π^{*2} configuration is moderately large (C_2 = -0.206). Consequently, the DZP SCFX T_0 prediction for the 2^1A_1 state increases 0.96 eV if the TCSCF rather than the SCF energy is used for the ground state! Such an increase greatly improves the agreement between the DZP SCFX and 2R CISD T_0 results (see Table II and footnote b therein). Not surprisingly, r_e(C-O) is increased 0.0198 Å and $\omega_2(a_1)$ is decreased 147 cm^{-1} upon inclusion of the second configuration, both changes improving the agreement with experiment. As the C=O bond is weakened, the C-H bonds are strengthened, whence r_e(C-H) is decreased to 1.0922 Å and $\omega_1(a_1)$ and $\omega_5(b_2)$ are increased to 3163 and 3252 cm^{-1}, respectively. An interesting secondary effect is the large decrease of the CH_2 out-of-plane wag (ω_4) to 1168 cm^{-1}, which is 23 cm^{-1} below experiment. The effect of the π^{*2} configuration on $\omega_4(b_1)$ is moderated in the DZP 2R CISD wave functions, and the ω_4 = 1193 cm^{-1} 2R CISD prediction is 42 cm^{-1} below the 1R CISD result but within 2 cm^{-1} of experiment. For the C=O stretch the 2R CISD ω_2=1804 cm^{-1} frequency is 64 cm^{-1} below the 1R CISD frequency and only 26 cm^{-1} (1.5%) higher than experiment. For the other four modes (ω_1, ω_3, ω_5, and ω_6) the 2R CISD and 1R CISD values are in close agreement.

The DZP 3R CISD geometrical parameters and vibrational frequencies in Table II are essentially identical to the DZP 2R CISD values. For example, the C=O distance increases only 0.0004 Å upon addition of the third reference, and no frequency is altered more than 6 cm^{-1}. The DZP 3R CISD wave functions included 18940 CSFs in C_{2v} symmetry as compared to 10107 CSFs in the 2R CISD case. The fact that the extra 8833 CSFs have virtually no effect on the $\tilde{X}^1A_1$ structural parameters and vibrational frequencies is a reflection of the small contribution of the third reference to the final CI wave function. In particular, the open-shell singlet configuration

of Eq. (59) appears with the CI coefficient C_{172} = -0.0096, which means that there are 171 other configurations of more importance. One might have expected this lack of importance because the CSF ψ_3 of Eq. (59) does not appear at all in the reference wave function. Nevertheless, one must be cautious in general. As discussed below, ψ_3 is quite important for the 2^1A_1 state.

4.5.2.2 The ($\pi\rightarrow\pi^*$) 2^1A_1 State

The DZP SCFX geometrical structure and vibrational frequencies of the ($\pi\rightarrow\pi^*$) 2^1A_1 state which appear in Table II are practically identical to those reported by Fitzgerald and Schaefer.[12] Thus, the effects of changing α_d(O) from 0.80 to the 0.85 value used here are minuscule. Relative to the DZP TCSCF ground state parameters, r_e(C-H) is 0.014 Å smaller and θ_e(H-C-H) is 3.17° larger in the ($\pi\rightarrow\pi^*$) 2^1A_1 state. The key difference, however, is in the long C-O bond length (1.5366 Å) in the excited state, indicating a very weak single bond. For comparison, the C-O single bond length in the ground state of methanol is 1.425 Å.[78] Furthermore, the DZP SCF C-O length for the ($\pi\rightarrow\pi^*$) $^3A'$ state of H_2CO is 1.434 Å,[57] so there is an important qualitative difference in the electronic structures of the $^3A'$ and 2^1A_1 $\pi\rightarrow\pi^*$ states.

One indication of this difference is that the $^3A'$ state has a bent out-of-plane geometry whereas the 2^1A_1 state is planar.[12,57] Another point to consider is that the DZP SCFX method gives the TCSCF CI coefficients C_1=0.956 and C_2=-0.294 for the 2^1A_1 state, whence C'_1=C'_2=0.331 and C'_3=0.884 in Eq. (60). Referring to Eqs. (55)-(62), S=<a|b>=0 implies C'_1=0, C'_2=0, and C'_3=1, and the deviation of S from zero or C_1 and C_2 from $\pm 1/\sqrt{2}$ is a measure of the open-shell singlet character (or lack thereof) of the ($\pi\rightarrow\pi^*$) 2^1A_1 state. The C_1 and C_2 coefficients for this state deviate substantially from those expected for a "pure" open-shell singlet state with S=0. Hence, the designation of the 2^1A_1 state as an open-shell singlet is

questionable, and perhaps the zwitterionic structure

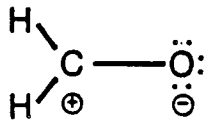

is more apt.[103] Evidence for this statement is abundant. First, the DZP SCFX dipole moment μ_z=-4.5 D is quite large. For comparison, the DZP TCSCF $\tilde{X}^1A_1$ μ_z value is -2.4 D, and μ_z=-7.4 D is the estimate one obtains by assuming that plus and minus charges are separated by r_e(C-O)=1.5366 Å in the 2^1A_1 state. Second, the u orbital in Eq. (57) has an occupation of 1.83 electrons in the DZP SCFX wave function and is predominantly centered on the oxygen atom. Finally, a DZP SCFX Mulliken population analysis yields the excess charges q(O)=-0.57 and q(C)=+0.28.

At this stage the questions listed above at the end of the formaldehyde review section can be addressed. The addition of Rydberg functions to the basis set lowers the SCFX T_0 value only 2102 cm^{-1} (Table II). The only significant SCFX geometrical change is the reduction of r_e(C-O) to 1.5173 Å, and among the vibrational frequencies only $\omega_4(b_1)$ changes more than 20 cm^{-1}. A small amount of additional electron density shifts to the oxygen atom as gauged by the DZP+R SCFX values μ_z=-4.7 D and q(O)=-0.62. In short, the ($\pi\rightarrow\pi^*$) 2^1A_1 state has little Rydberg character. This fact is dramatically illustrated by comparing the 2^1A_1 H_2CO and ($\pi\rightarrow\infty$) $^2B_1$ H_2CO^+ data in Table II. It is clear that the geometrical structure and vibrational frequencies of the 2^1A_1 state bear little resemblance to those of the $^2B_1$ H_2CO^+ state. This occurrence is quite consistent with the description of the 2^1A_1 state as a zwitterion rather than an open-shell singlet with a diffuse, singly-occupied π^* orbital.

The DZP 2R and 3R CISD results for the 2^1A_1 state exhibit several interesting features in Table II. The 2R CISD C-O length of 1.5383 Å is only 0.0017 Å longer than the SCFX value. Meanwhile, the differences in the r_e(C-H) and θ_e(H-C-H) predictions (+0.0125 Å and -1.41°) are more pronounced. Accordingly, the low

SCFX C-O stretching frequency of 847 cm^{-1} is only 12 cm^{-1} smaller at the 2R CISD level, but the C-H stretches ω_1 and ω_5 and the CH_2 scissor ω_3 are reduced 130, 139, and 50 cm^{-1}, respectively.

The most noteworthy occurrence in Table II is the large effect of the third reference on the 2^1A_1 predictions. The 3R CISD r_e(C-O)=1.5644 Å is 0.0261 Å longer than the 2R CISD distance, and the corresponding $\omega_2(a_1)$=737 cm^{-1} exhibits a 98 cm^{-1} reduction. Examining the CI coefficients in the 3R CISD 2^1A_1 wave function, one finds C_3=0.128 for the open-shell singlet configuration ψ_3, in sharp contrast to the $\tilde{X}^1A_1$ case. Equations (60)-(62) provide some insight into this phenomenon. In order to rotate the ψ_3 configuration out of the 3R CISD 2^1A_1 wave function, the angle θ in Eq. (61) must be 4.49°. (The analogous angle for the $\tilde{X}^1A_1$ state is a mere -0.35°.) In essence, *the orbitals which eliminate* ψ_3 *from the* 2^1A_1 *wave function are significantly different at the SCFX and CISD levels of theory. In such a case important configurations can be neglected if the third reference is not employed, and the effects of electron correlation can be predicted poorly.* Thus, in the case of the ($\pi\rightarrow\pi^*$) 2^1A_1 state of H_2CO, the expected increase in r_e(C-O) and decrease in $\omega_2(a_1)$ is not achieved unless a three-reference CISD wave function is employed.

The DZP 3R CISD adiabatic excitation energy for the ($\pi\rightarrow\pi^*$) 2^1A_1 state is 68564 cm^{-1} = 8.50 eV. The data in Table II suggest that this result would be reduced about 0.20 eV with the inclusion of Rydberg functions in the basis set. Thus, a final estimate of T_0=8.30 eV is obtained. In Table II the DZP+R CISD energy for the $\pi\rightarrow\infty$ ionization is 110125 cm^{-1} = 13.65 eV. Experimentally this ionization energy has been assigned as 14.4 eV.[52] Thus, it appears that 0.7 eV of correlation energy is missing in the $\tilde{X}^1A_1$ H_2CO energy relative to the $^2B_1$ H_2CO^+ value at the DZP+R CI level of theory. Since the 2^1A_1 state resembles a zwitterion rather than an open-shell singlet, the differential correlation energy effect on the 2^1A_1 T_0

value should be much less than +0.7 eV. In fact, the T_0=8.30 eV is probably a slight overestimate. (Note the SCFX vs. CISD T_0 values in Table II.)

In Table III the relative energies of several electronic states of H_2CO are given at the $(\pi\rightarrow\pi^*)$ 2^1A_1 optimum geometry. At the DZP+R TCSCF level of theory, the $\tilde{X}^1A_1$ energy lies 19592 cm^{-1} above the value at the $\tilde{X}^1A_1$ 2R CISD optimum geometry. The ground state is followed by the $(n_-\rightarrow\pi^*)$ $^1A_2$ state at 32274 cm^{-1}, the $(n_+\rightarrow\pi^*)$ $^1B_1$ state at 66222 cm^{-1}, and the $(n_-\rightarrow 3s)$ $^1B_2$ state at 74071 cm^{-1}. (For clarity the oxygen lone pair a_1 and b_2 orbitals are denoted n_+ and n_- in Table III. Unless otherwise stated, n refers to the n_- orbital.) The $(\pi\rightarrow\pi^*)$ 2^1A_1 state occurs at 75772 cm^{-1} whereas the $(n_-\rightarrow 3p_y)$ $^1A_1$ state lies at 82261 cm^{-1}. The primary effect of electron correlation is to shift the 2^1A_1 state below the $(n_-\rightarrow 3s)$ $^1B_2$ state to a value close to that of the $(n_+\rightarrow\pi^*)$ $^1B_1$ state. (The DZP+R 2R CIDVD result of 64428 cm^{-1} for the 2^1A_1 state should not be taken too seriously because the importance of the third configuration ψ_3 in the 2R CISD wave function probably engenders a Davidson correction which is too large.) In any event it is abundantly clear in Table III that the $(\pi\rightarrow\pi^*)$ 2^1A_1 state lies below the $(n_-\rightarrow 3p_y)$ $^1A_1$ state at the 2^1A_1 optimum geometry. Therefore, the answers to the remaining queries (b and c) raised at the end of the formaldehyde review section are now evident. First, the SCFX method is valid for the $(\pi\rightarrow\pi^*)^1$ state near its optimum geometry. Even though the *vertical* excitation energy of the $(n_-\rightarrow 3p_y)^1$ state is lower than that of the $(\pi\rightarrow\pi^*)^1$ state, an avoided crossing occurs as r(C-O) increases, and the 2^1A_1 state becomes $(\pi\rightarrow\pi^*)^1$ in character. This topic is discussed in more detail in the next section. Second, the $(\pi\rightarrow\pi^*)^1$ state is not mixed strongly with Rydberg states at its optimum geometry. This statement can be justified by noting in Table III the large ($\approx$15000 cm^{-1}) separation between the $(\pi\rightarrow\pi^*)^1$ state and the nearest $^1A_1$ Rydberg state $(n_-\rightarrow 3p_y)$ at the 2^1A_1 optimum geometry. In summary, the final T_0 = 8.30 eV

adiabatic excitation energy given above for the ($\pi \rightarrow \pi^*$) 2^1A_1 state should be reliable, and the existence of a C_{2v} minimum for this state well below the experimental $n_- \rightarrow \infty$ ionization limit of 10.87 eV is to be expected. Nevertheless, the spectroscopic accessibility of the ($\pi \rightarrow \pi^*$) 2^1A_1 state should be poor due to the large difference between the 2^1A_1 and $\tilde{X}^1A_1$ r_e(C-O) distances.

4.5.2.3 The $(n\rightarrow 3p_y)\ 2^1A_1$ State

Perusing the ordering of the $(\pi\rightarrow\pi^*)^1$ and $(n\rightarrow 3p_y)^1$ states in Tables I and III, it is apparent that the 2^1A_1 potential energy surface must have another region which is predominantly $(n\rightarrow 3p_y)^1$ in character. In Table IV DZP+R SCFX and 2R CISD geometrical structures and vibrational frequencies for this $(n\rightarrow 3p_y)\ 2^1A_1$ state are presented along with analogous results for $\tilde{X}^1A_1$ H_2CO and $(n\rightarrow\infty)$ $^2B_2$ H_2CO^+. For the same reasons that $\pi\rightarrow\pi^*$ TCSCF reference wave functions were used for $\tilde{X}^1A_1$ H_2CO in Tables II and III, $n\rightarrow 3p_y$ TCSCF reference wave functions were employed for $\tilde{X}^1A_1$ H_2CO in Tables IV and V. To our knowledge no other theoretical structures and vibrational frequencies have been reported for the $(n\rightarrow 3p_y)\ 2^1A_1$ state, but several studies have been performed on $^2B_2$ H_2CO^+.[65,66,78]

Note in Table IV that the SCFX C-O distance in the $(n\rightarrow 3p_y)\ 2^1A_1$ state is only 0.0306 Å longer than the $\tilde{X}^1A_1$ value and is within 0.0020 Å of the C-O distance in the $(n\rightarrow\infty)$ $^2B_2$ H_2CO^+ ion. The r_e(C-H) lengths in the three species do not vary much, but the θ_e(H-C-H) angle for $\tilde{X}^1A_1$ H_2CO is respectively, 10.49° and 8.55° smaller than the 2^1A_1 H_2CO and $^2B_2$ H_2CO^+ values. The effect of electron correlation on the 2^1A_1 geometry (at the DZP+R 2R CISD level) is to increase r_e(C-H) by 0.0159 Å with a concomitant decrease in r_e(C-O) by 0.0016 Å . In short, the $(n\rightarrow 3p_y)\ 2^1A_1$ geometry is very similar to that of the corresponding $n\rightarrow\infty$ cation, and the C-O distance is only slightly longer than that in the ground state. Similar characteristics are exhibited by the $(n\rightarrow 3s)$ $\tilde{B}^1B_2$ state,[59] in sharp contrast to those displayed by the $(\pi\rightarrow\pi^*)\ 2^1A_1$ state.

The dissimilarity between the $(n\rightarrow 3p_y)^1$ and $(\pi\rightarrow\pi^*)^1$ states is also evident in the wave functions themselves. In the $(n\rightarrow 3p_y)\ 2^1A_1$ case the DZP+R TCSCF CI coefficients are C_1=0.714 and C_2=-0.700, which arise for an overlap S=0.010. Con-

sequently, the $(n\rightarrow 3p_y)^1$ Rydberg state is truly open-shell singlet in character. The third reference ψ_3 is not important for this state either. In the DZP+R 2R CISD wave function, C_{55}=-0.0180 corresponds to ψ_3, and based on the 3R CISD results for the ground state it was not deemed necessary to include ψ_3 as a reference for the $(n\rightarrow 3p_y)^1$ state.

In Table V the relative energies of several electronic states of H_2CO are given at the $(n\rightarrow 3p_y)$ 2^1A_1 optimum geometry. The ordering of the states is concordant with the vertical excitation energies in Table I because the $(n\rightarrow 3p_y)$ 2^1A_1 and $\tilde{X}^1A_1$ geometries are similar. The most salient feature in Table V is the position of the $(n\rightarrow 3p_y)$ 2^1A_1 state at 64277 cm^{-1} (DZP+R 2R CISD) well below the $(\pi\rightarrow\pi^*)$ $^1A_1$ state at 86846 cm^{-1}. Thus, *the* $(n\rightarrow 3p_y)^1$ *and* $(\pi\rightarrow\pi^*)^1$ *"states" actually lie on the same potential energy surface.* Both states should be labeled 2^1A_1 at their respective optimum geometries, consistent with the notation already used throughout this paper. The qualitative nature of the 2^1A_1 surface is illustrated in Figure 1. The $(n\rightarrow 3p_y)^1$ and $(\pi\rightarrow\pi^*)^1$ regions are well separated, and the character of the 2^1A_1 state at the two C_{2v} minima is predominantly one configuration or the other. Spectroscopically the $(n\rightarrow 3p_y)^1$ region is far more accessible than the $(\pi\rightarrow\pi^*)^1$ region. In the region of the avoided crossing, the $(n\rightarrow 3p_y)^1$ and $(\pi\rightarrow\pi^*)^1$ descriptions are inadequate since the wave function there is strong mixture of these two components.

Finally, it is worthwhile to compare the data in Tables IV and V with the experimental results which are available for $(n\rightarrow 3p_y)$ 2^1A_1 H_2CO and $(n\rightarrow\infty)$ $^2B_2$ H_2CO^+. The difficulty here is that some question exists over the assignment of the 7.96 and 8.11 eV bands in the VUV spectrum of formaldehyde.[52,84] In January 1971 Peyerimhoff, Buenker, Kammer, and Hsu[47] (PBKH) reported small CI calculations which placed the $(n\rightarrow 3p_y)$ 2^1A_1 state at 8.11 eV and the $(n\rightarrow 3p_z)$ 2^1B_2 state at 8.39 eV. In December 1971 Mentall, Gentieu, Krauss, and Neumann[73] (MGKN) observed

complex sets of vibrational energy levels below 1000 cm^{-1} in the Rydberg states which were interpreted in terms of inversion splitting arising from the nonplanarity of the states. In agreement with PBKH, the 7.96 and 8.11 eV systems were assigned to $\tilde{X}^1A_1 \rightarrow 2^1A_1$ and $\tilde{X}^1A_1 \rightarrow 2^1B_2$ transitions, respectively. MGKN actually reported *ab initio* results based on one-electron energies of Rydberg orbitals which suggested this assignment be switched, but their interpretation of the experimental spectrum best fit the PBKH predictions. In a series of experimental studies culminating in 1977,[82–84] Lessard and Moule re-examined the VUV spectrum of formaldehyde and identified several new Rydberg series. Results were presented which "vitiated" the nonplanarity interpretation of the 7.96 and 8.11 eV bands given by MGKN. Instead, the potential function for the CH_2 rocking (not wagging) mode in the lower state was found to be very anharmonic with an abnormally low fundamental frequency ν_6. (This topic is discussed further in the final section of this paper.) Lessard and Moule[84] based their assignment of the 7.96 and 8.11 eV bands on the *ab initio* predictions of PBKH and stated that the available theoretical results "unequivocally" assigned the lower state as $(n\rightarrow 3p_y)\ 2^1A_1$ and the upper state as $(n\rightarrow 3p_z)\ 2^1B_2$. Finally, Harding and Goddard[52] switched this assignment in 1977, primarily on the basis of theoretical vs. experimental oscillator strengths. (The earlier oscillator strengths of Miller[86] suggest the same conclusion.)

As shown in Table IV, the DZP+R 2R CISD value for T_0 of the $(n\rightarrow 3p_y)\ 2^1A_1$ state is 7.93 eV. For comparison, the experimental first ionization potential for H_2CO is 10.87 eV,[83] and T_0=10.56 eV is obtained with the DZP+R CISD wave functions. Assuming the $(n\rightarrow 3s)^1$ and $(n\rightarrow 3p_y)^1$ states have similar geometries,[59] one surmises in Table V that T_0=7.03 eV is predicted for the $(n\rightarrow 3s)\ ^1B_2$ state at the DZP+R CISD level. (See footnote b of Table IV.) The experimental T_0 value is 7.09 eV.[84] Thus, one can argue that the 2^1A_1 T_0=7.93 eV is between 0.06 and 0.31 eV too

small, an error range which tends to support the conclusion that the $(n\rightarrow 3p_y)\ 2^1A_1$ state corresponds to the experimental band at 8.11 eV. In an attempt to be more definitive, five-reference CISD wave functions were obtained for the H_2CO states using $^2B_2$ H_2CO^+ orbitals. Diffuse d functions [$\alpha_d(C) = \alpha_d(O) = 0.015$][52] were added to the DZP+R basis set to account for possible interactions with higher-lying $(n\rightarrow 3d)^1$ Rydberg states. The five references involved the configurations $(n)^2$, $(n)(3p_y)$, $(3p_y)^2$, $(n)(3s)$, and $(n)(3p_z)$, and the $\tilde{X}^1A_1$, $(n\rightarrow 3p_y)\ 2^1A_1$, $(n\rightarrow 3s)\ ^1B_2$, and $(n\rightarrow 3p_z)\ 2^1B_2$ energies were all obtained from the same secular equation. (The $^1A_1$ block of the CI matrix consisted of 124857 CSFs while the $^1B_2$ block was comprised of 124380 CSFs.) Subsequently, $E(\tilde{X}^1A_1)=-114.168749$, $E(2^1A_1)=-113.911045$, $E(^1B_2)=-113.944099$, and $E(2^1B_2)=-113.911640$ were determined. Of course, the $\tilde{X}^1A_1$ energy is not accurate because the ground state is not described well by H_2CO^+ orbitals; however, the treatment should be consistent and unbiased in predicting the relative positions of the Rydberg states. Taking the experimental $T_0(n\rightarrow 3s)=7.09$ eV as a reference, the CI energies listed above give $T_0(n\rightarrow 3p_y)=7.99$ and $T_0(n\rightarrow 3p_z)=7.97$ eV. Obviously, these results are somewhat inconclusive about the ordering of the latter two states, the small 0.02 eV separation being comparable to previous theoretical values of 0.01 and 0.03 eV.[52,49] (See also Refs. 73, 85, and 86.) Upon comparing the quality of the PBKH results from 1971 and those presented in this paper, one finds that PBKH utilized a much smaller basis set, employed CI wave functions with far fewer configurations, and used $(n\rightarrow 3p_y)\ ^3A_1$ and $(n\rightarrow 3s)\ ^3B_2$ orbitals to obtain their 2^1A_1 and 2^1B_2 CI energies (which probably biased the energies in favor of the 2^1A_1 state). Therefore, the PBKH predictions should be less reliable. In summary, the current results are somewhat inconclusive but tend to support the conclusions of Harding and Goddard,[52] viz., that the 8.11 eV experimental band should be assigned as $(n\rightarrow 3p_y)$ and the 7.96 eV band as $(n\rightarrow 3p_z)$.[87] In any event the 1971

PBKH predictions certainly do not "unequivocally" assign the 8.11 and 7.96 eV experimental bands as Lessard and Moule assumed.

4.6 APPLICATION TO 2^1A_1 KETENE

4.6.1 Review

As mentioned previously, we recently revisited the low-lying electronic states of ketene in an *ab initio* theoretical study.[6] Therefore, a discussion of the electronic states of ketene below 50000 cm^{-1} will not be given here, and the reader is referred to the literature reviews in Refs. 5 and 6 for further information. The primary concern of the present article is the 2^1A_1 state, which was found in Ref. 6 to be Rydberg in character with a DZP+R CISD vertical excitation energy of 56051 cm^{-1}.[88] In terms of molecular orbitals, the 2^1A_1 state arises from the promotion of an electron from the $2b_1$ orbital (the HOMO) to the $3b_1$ orbital, which is the second lowest unoccupied MO. The necessity of the SCFX and the SCFX-CI procedures for this state became very apparent in our previous study,[6] and the problem of variational collapse for the 2^1A_1 state was mentioned in the introduction to this paper. With the aid of analytic SCFX-CI gradients, answers to several remaining questions are sought here. For example, if the 2^1A_1 state is Rydberg in character, then where is the $(\pi\rightarrow\pi^*)^1$ valence state, whose counterparts in ethylene[17–20] and formaldehyde have nonplussed many investigators? Is the 2^1A_1 state dissociative as is the lower-lying $^1B_1$ state? If not, what geometrical structure and vibrational frequencies result? Does the character of the 2^1A_1 state change as its geometry is optimized? Before wrestling with these issues, a review of available VUV spectral data for ketene is appropriate.

In 1951, Price, Teegan, and Walsh[89] reported the absorption spectrum of ketene in the far ultraviolet. Beginning at 46900 cm^{-1}, four diffuse bands spaced 1050 cm^{-1} apart were observed, which are attributable to $2b_2\rightarrow 3s$ ($\tilde{X}^1A_1\rightarrow{}^1B_1$) excitations. Theoretical studies have revealed that the upper ($^1B_1$) state dissociates directly to $\tilde{b}^1B_1$ CH_2 + $\tilde{X}^1\Sigma^+$ CO.[5,90,91] The absorptions above 54500 cm^{-1} observed by Price et al. are listed in Tables VI and VII. Because water vapor apparently contaminated the

sample of Price and co-workers, Braun, Bass, and Pilling[92] re-examined the absorption spectrum of ketene in the 53500-63500 cm^{-1} region in 1970. The peak positions measured directly from Fig. 1 of Braun et al. are also given in Table VI.

Five of the six bands in Table VII above 64500 cm^{-1} fit nicely into a Rydberg series (n=4,5,6,7, and 8) with a quantum defect of 1.07 and an ionization limit of 77500 cm^{-1}. Consistent with the observed quantum defect, Price et al. labeled the series as $\pi \rightarrow ns$ ($\tilde{X}^1A_1 \rightarrow m^1B_1$) and assigned the 54700 cm^{-1} band as the n=3 member. However, other interpretations are more plausible. The theoretical results of Ref. 6 suggest that the 54700 cm^{-1} band corresponds to a $^1A_1$ upper state. Thus, Herzberg's interpretation[93] of the Rydberg series as ($\tilde{X}^1A_1 \rightarrow m^1A_1$) was favored in Ref. 6 over that of Price and co-workers.[89] However, yet another interpretation not discussed in Ref. 6 is ostensibly the best of all. Specifically, Robin[94] reassigned the n=3 member of the Rydberg series to the 46900 cm^{-1} band (48039 cm^{-1} fits the formula) while labeling the series as $\pi \rightarrow ns$ ($\tilde{X}^1A_1 \rightarrow m^1B_1$). This interpretation is consistent with both the theoretical results of Ref. 6 and the observed quantum defect. Obviously a theoretical study of the higher members of the Rydberg series is needed to completely resolve the matter, but such a study is outside the scope of the current investigation. What will be concentrated on hereafter is the 54700 cm^{-1} system with some consideration given to the 61300 and 67000 cm^{-1} bands. None of these three absorptions are members of the $\pi \rightarrow ns$ Rydberg series.

The ketene absorption spectrum in the 54500-60500 cm^{-1} region (Ref. 92 and Table VI) is a challenge to interpret. Relatively sharp absorptions reveal a vibrational progression starting at 54660 cm^{-1} whose first two intervals are 830 and 840 cm^{-1}. Another progression apparently begins at 55020 cm^{-1} with slightly smaller initial intervals (780 and 800 cm^{-1}). The vibrational structure extends to 60500 cm^{-1}, and underneath this structure a broad continuum is seen. This continuum is centered

near 56500 cm^{-1}, and one can infer an oscillator strength $f \approx 0.3$ for it.[94] Robin interprets the 54660 cm^{-1} band as the n=3 member of a $\pi \rightarrow np$ Rydberg series, and he states that the broad continuum is "most likely the allowed $\pi \rightarrow \pi^*$ excitation corresponding to that at 53900 cm^{-1} in allene and at 61700 cm^{-1} in ethylene."[94]

The bands observed at 61300 and 67000 cm^{-1} in the VUV spectrum of ketene exhibit vibrational structure similar to that present in the $\pi \rightarrow ns$ Rydberg series (Table VII). In particular, two progressions with intervals near 1020 cm^{-1} are offset by 500-650 cm^{-1}. The 61300 cm^{-1} system probably corresponds to the n=3 member of a $\pi \rightarrow nd$ Rydberg series with $\delta \approx 0.38$. The other possibility is simply that the $(2b_1,3p)$ manifold is split by the aspherical core of the molecule, a phenomenon found in the spectra of other cumulenes.[94] Of course, the degree of splitting of the $(2b_1,3p)$ manifold is a consideration in the interpretation of the 54500-60500 cm^{-1} region because vibrational structure can easily be confused with a sequence of core-split Rydberg electronic states. Nevertheless, the 67000 cm^{-1} system with δ=0.77 is most likely a $\pi \rightarrow 4p$ band, but its profile does not reveal the presence of core-split components.

4.6.2 Results and Discussion

In Table VIII theoretical structures and vibrational frequencies for the 2^1A_1 state of ketene are tabulated and compared to the DZP SCF results for the ground state from Ref. 6. With the DZP basis set the 2^1A_1 state is predicted to have an extremely long C-C bond length (SCFX: 1.7568 Å and 2R CISD: 1.6871 Å). The SCFX 2^1A_1 C-O distance is not appreciably longer than that in the ground state, but the C-H length is unusually short (1.0648 Å) and the H-C-H angle quite large (137.66°). At the DZP CISD level, the latter structural differences between the 2^1A_1 and $\tilde{X}^1A_1$ states are moderated to some extent: r_e(C-O)=1.1738 Å , r_e(C-H)=1.0725 Å , and

θ_e(H-C-H)=133.81° are found for the upper state as compared to the r_e(C-O)=1.167 Å , r_e(C-H)=1.077 Å , and θ_e(H-C-H)=122.2° ground state values of Tanaka and Yoshimine.[95]

Not surprisingly, the DZP 2^1A_1 vibrational frequencies in Table VIII are also very different from the $\tilde{X}^1A_1$ values. The DZP SCFX 2^1A_1 C-H stretches, $\omega_1(a_1)$=3404 cm^{-1} and $\omega_7(b_2)$=3639 cm^{-1}, are respectively 49 and 172 cm^{-1} above the $\tilde{X}^1A_1$ frequencies. Concomitantly, the C-C-O in-plane bend, $\omega_9(b_2)$=275 cm^{-1}, and the C-C stretch, $\omega_4(a_1)$=431 cm^{-1}, are respectively 211 and 814 cm^{-1} below their $\tilde{X}^1A_1$ analogues. The DZP 2R CISD 2^1A_1 frequencies are generally 2-7% lower than the SCFX predictions, the lone exception being the C-C stretch ω_4. In this case the 2R CISD result (ω_4=533 cm^{-1}) is 102 cm^{-1} above the SCFX value, in accord with the 0.07 Å contraction of the C-C distance observed upon inclusion of electron correlation.

The most prominent DZP SCFX 2^1A_1 vibrational frequency in Table VIII is the CH_2 wag $\omega_5(b_1)$, which is actually imaginary. Along this mode the 2^1A_1 state should be designated $3^1A'$ since the $(2b_1 \rightarrow 8a_1)$ $^1B_1$ state mentioned previously has a DZP SCF energy 10198 cm^{-1} below the 2^1A_1 value at the 2^1A_1 SCFX optimum geometry. This fact is important for several reasons. First, the SCFX method cannot be employed with confidence to follow the 2^1A_1 state into the C_s^I symmetry regions of Refs. 5 and 6. Nevertheless, the 2^1A_1 ω_5=1138 *i* cm^{-1} result should be meaningful because the 2^1A_1–$^1B_1$ separation is large, i.e., the ω_5 value is not likely to be an artifact of variational collapse. In fact, if constrained to be valence in character, the 2^1A_1 ($3^1A'$) state would be expected to have a C_s^I stationary point similar to that of its $(2b_1 \rightarrow 3b_1)$ $^3A_1$ counterpart except with a much longer C-C distance.[6] Accordingly, a $C_{2v} \rightarrow C_s^I$ energy lowering of roughly 2000 cm^{-1} is a reasonable expectation,[96] in which case T_e(SCFX) ≈ 65800 cm^{-1} and T_e(2R CISD) ≈ 60600 cm^{-1} would

result for the 2^1A_1 ($3^1A'$) state with the DZP basis set. Finally, the C_s^I stationary point for the $3^1A'$ state should in fact be a local minimum, precisely because the $^1B_1$ ($2^1A'$) state lies lower in energy. In contrast, the $^3A'$ C_s^I stationary point is only a transition state for the interconversion of two equivalent $^3A''$ C_s^{II} minima through rotation about the C-C axis.[6] On the singlet surface it is the $^1B_1$ ($2^1A'$) state which correlates two $^1A''$ C_s^{II} minima in this fashion.

As discussed below, the addition of Rydberg functions to the basis set radically alters the character of the 2^1A_1 state. However, this does not necessarily invalidate the DZP predictions given in Table VIII. In interpreting the VUV absorption spectrum, the question of the existence of a $(\pi\rightarrow\pi^*)^1$ valence region of the 2^1A_1 surface arises, and thus it is worthwhile to investigate the peculiar properties of the 2^1A_1 state which result when it is constrained to be valence in character.

The extremely long C-C bond length in the "valence" 2^1A_1 state suggests a comparison with pertinent dissociation products. In Table IX DZP SCF theoretical data for fragments pertaining to 2^1A_1 ketene are given. Along C_{2v} dissociation paths, the C-C σ bonding electron pair in 2^1A_1 CH_2CO becomes a σ lone pair in the CO fragment while the C-C (π,π^*) system is cleaved homolytically *at the DZP SCFX level of theory*. Thus, at this level 2^1A_1 ketene correlates to $^2\Pi$ CH_2^+ + $^2\Pi$ CO^- in C_{2v} symmetry, and these products lie 121294 cm^{-1} above the $\tilde{X}^1A_1$ state.[98] (In reality, the correlation is probably to a Rydberg state of CH_2 (2^1A_1) + $^1\Sigma^+$ CO.) Obviously then, the 2^1A_1 minimum with T_e (DZP SCFX)=67794 cm^{-1} should not be described as a loosely associated complex. For example, the DZP SCFX 2^1A_1 structure and vibrational frequencies in Table VIII are quite different from the $^2\Pi$ CH_2^+ + $^2\Pi$ CO^- results in Table IX. In particular there are large disparities among the r_e(C-O), r_e(C-H), $\omega_1(a_1)$, $\omega_2(a_1)$, and $\omega_7(b_2)$ values in the two systems.

If 2^1A_1 ketene is displaced into C_s^I symmetry along the CH_2 wagging mode (see Table VIII), then the $2^1A_1(3^1A')$ state correlates to a different set of dissociation products. Experimentally, the $\tilde{X}^3B_1$ CH_2 + $\tilde{a}^3\Pi$ CO system is the prime candidate as opposed to $(2^1B_1, 2^1A_1)$ CH_2 + $^1\Sigma^+$ CO or $\tilde{a}^1A_1$ CH_2 + $\tilde{A}^1\Pi$ CO. The $\tilde{X}^3B_1$ CH_2 + $\tilde{a}^3\Pi$ CO system lies at 75848 cm^{-1} and the $\tilde{a}^1A_1$ CH_2 + $\tilde{A}^1\Pi$ CO system at 95215 cm^{-1} relative to $\tilde{X}^1A_1$ CH_2CO.[99] The point is that the 2^1A_1 CH_2CO state is not loosely bound even though the C-C bond length is quite long.

How then should the electronic structure of the "valence" 2^1A_1 state be explained? First of all, the "valence" 2^1A_1 state is hardly a "pure" open-shell singlet. The DZP SCFX CI coefficients for the 2^1A_1 state are C_1=0.916 and C_2=-0.402 at the 2R CISD geometry, and the |u> and |v> orbitals in Eq. (57) have occupations of 1.68 and 0.32 electrons, respectively, in the DZP SCFX wave functions. In terms of the atomic $2p_x$ orbitals χ and χ' on the heavy atoms,

$$|u\rangle = 0.14\,\chi(O) + 0.17\,\chi'(O) - 0.39\,\chi(C') - 0.31\,\chi'(C') + 0.62\,\chi(C) + 0.54\,\chi'(C) \quad , \tag{12}$$

where C′ is the central carbon and C is the methylene carbon. Thus, a significant amount of π electron density is shifted into a p_x-type orbital on the methylene carbon. Concurrently, σ electron density in the C-C′ bond is shifted toward the central C′ atom. A simple description is that the hybridization of the methylene carbon moves from sp^2 in the ground state *toward* sp in the 2^1A_1 state. In the limit, the C-H bonds in the upper state are formed from sp hybrids, the methylene-carbon p_x orbital is doubly occupied, and the associated p_z orbital is empty. A shift in hybridization toward this crude, idealized limit would explain both the small C-H distances and the large H-C-H angle in the 2^1A_1 state. Of course, this bonding description might change upon displacement of the molecule into C_s^I symmetry.

If the DZP basis set is augmented with Rydberg functions and a geometry optimization is begun at the DZP SCFX stationary point, the "valence" 2^1A_1 state collapses to a lower-energy Rydberg state, as the results in Table VIII show. The DZP+R SCFX C-C distance is 1.4046 Å, which is within 0.0074 Å of the DZP SCF distance in the $(2b_1 \rightarrow \infty)$ CH_2CO^+ cation (Table IX). In fact, all of the geometrical parameters in 2^1A_1 CH_2CO are very close to the $^2B_1$ CH_2CO^+ values. For example, the DZP+R SCFX r_e(C-O)=1.1027 Å is only 0.0012 Å longer than the CH_2CO^+ distance but 0.0487 Å shorter than that obtained with the DZP basis set. In contrast to the unusually short DZP SCFX C-H distance, the 2^1A_1 DZP+R r_e(C-H)=1.0766 Å is comparable to the $\tilde{X}^1A_1$ length. Similarly the DZP+R H-C-H angle is 13.01° smaller than the DZP SCFX value, only 2.66° larger than the ground state angle, and within 0.10° of the angle in the CH_2CO^+ cation.

The key feature of the DZP+R SCFX vibrational frequencies in Table VIII is the lack of any imaginary values. Therefore, when the 2^1A_1 state of ketene is allowed to mix in Rydberg character, it assumes a local minimum in C_{2v} symmetry. The seven a_1 and b_2 vibrational frequencies of 2^1A_1 CH_2CO and $^2B_1$ CH_2CO^+ display a mean absolute percentage difference (DZP+R SCFX – DZP SCF) of only 0.38%. Thus, on the whole the 2^1A_1 ketene frequencies are very close to their CH_2CO^+ counterparts. However, the two b_1 vibrational frequencies (ω_5 and ω_6) exhibit percentage differences of 11.1 and 8.1%. These larger differences can be attributed to the interaction of the 2^1A_1 and $^1B_1$ states of CH_2CO along the b_1 normal modes.

The character of the 2^1A_1 state of ketene changes little at the DZP+R 2R CISD level of theory. The 2R CISD C-C distance is 1.4028 Å, which differs from the SCFX value by only 0.0018 Å. Moreover, only the expected increases in the C-O and C-H bond lengths are observed in Table VIII upon inclusion of electron correla-

tion. The a_1 and b_2 DZP+R 2R CISD vibrational frequencies range from 1.8 to 8.5% below the SCFX results, but once again different effects are seen in the b_1 frequencies. The CH_2 wagging frequency increases 38 cm^{-1} (5.2%) in going from DZP+R SCFX to 2R CISD while the C-C-O out-of-plane bend decreases 119 cm^{-1} (24.9%). For future analyses the quadratic force fields determined at the various levels of theory for $^2B_1$ CH_2CO^+ and 2^1A_1 CH_2CO are reported in Table X.

In Table XI are given the relative energies of several singlet electronic states of ketene at the DZP+R 2R CISD 2^1A_1 geometry. The ordering of the states is the same as the ordering at the DZP SCF $\tilde{X}^1A_1$ geometry,[6] viz., the ground state is followed by the $(2b_1 \rightarrow 3b_2)$ $^1A_2$ state, the $(2b_1 \rightarrow 8a_1)$ $^1B_1$ state, and the $(2b_1 \rightarrow 3b_1)$ 2^1A_1 state. The lowest $^1B_2$ state lies much higher in energy. As mentioned above, the location of the $^1B_1$ state below the 2^1A_1 state is an important point because it leads to qualitative differences between the $^3A_1$ and 2^1A_1 potential energy surfaces. The DZP+R SCFX, 2R CISD, and 2R CIDVD (Davidson-corrected CISD) relative energies (55111, 56083, and 55818 cm^{-1}, respectively) for the 2^1A_1 state are all consistent with the assignment of this state to the experimental band beginning at 54660 cm^{-1} (Table VI). Both the theoretical and experimental data indicate that the 2^1A_1 state is *predominantly* Rydberg in character, and thus it is appropriate to label it as the $(\pi \rightarrow 3p_x)^1$ state. Assuming an ionization energy of 77491 cm^{-1} (the limit of the $\pi \rightarrow ns$ series), a quantum defect of 0.808 is obtained for the $(\pi \rightarrow 3p_x)^1$ state, in good agreement with the $\pi \rightarrow 4p$ δ=0.768 value (Table VII).

Robin[94] has associated the $(\pi \rightarrow \pi^*)^1$ state with the underlying continuum centered near 56500 cm^{-1} in the experimental VUV absorption spectrum of ketene. The profile of the band suggests an antiresonance between the "state" responsible for the continuum and the Rydberg "state" responsible for the sharp peaks listed in Table VI. Having identified the Rydberg "state" as $(\pi \rightarrow 3p_x)$ 2^1A_1, then the underlying contin-

uum must be associated with another $^1A_1$ "state" for an antiresonance to be observed. The key question is whether the spectrum should be interpreted in terms of two distinct electronic states (or two distinct minima on the same surface) or simply one state (or one minimum) which is a mixture of Rydberg and valence components. The latter choice is proposed here. Nevertheless, caution must be exercised because Rydberg-valence mixing can be very difficult to treat theoretically. In ethylene the vertical $(\pi\rightarrow\pi^*)^1$ state is predicted to be Rydberg in character at the SCF level, but the spatial extent of the state is greatly diminished upon inclusion of enough electron correlation.[17-20] While the case of ethylene should be kept in mind, the analogy with 2^1A_1 ketene should not be pressed too far. In C_2H_4 the $(\pi\rightarrow\pi^*)^1$ state is more diffuse than its triplet counterpart but predominantly valence nonetheless. In CH_2CO the 2^1A_1 state is predominantly Rydberg in character, even though its spatial extent is likely to undergo modest contractions at higher levels of theory.

In support of the contention that there is no distinct $(\pi\rightarrow\pi^*)^1$ minimum near 56500 cm^{-1} is the fact that the C_{2v} stationary point on the 2^1A_1 surface corresponding to the $(\pi\rightarrow\pi^*)^1$ state vanishes upon addition of Rydberg functions to the DZP basis set. However, the DZP CISD and CIDVD T_e values (Table XII) for the valence 2^1A_1 state are 62604 and 59189 cm^{-1}, respectively, and further energy lowering would result from optimization in C_s^I symmetry. Therefore, the DZP CISD and CIDVD 2^1A_1 T_e values are indeed comparable to the experimental 56500 cm^{-1} excitation energy, and it would be imprudent at this stage to categorically rule out the possibility of a second $(\pi\rightarrow\pi^*)^1$ minimum on the 2^1A_1 surface. However, even if a $(\pi\rightarrow\pi^*)^1$ C_s^I minimum exists at a level of theory higher than DZP+R 2R CISD, the DZP SCFX and CISD results in Table VIII predict that the geometry of such a minimum would be so far removed from the $\tilde{X}^1A_1$ geometry that the $(\pi\rightarrow\pi^*)^1$ state would not be observed spectroscopically. In contrast, the $(\pi\rightarrow 3p_x)$ 2^1A_1 minimum *is*

Franck-Condon accessible. Mixing a moderate amount of $(\pi\rightarrow\pi^*)^1$ character into the $(\pi\rightarrow 3p_x)$ 2^1A_1 state could impart significant oscillator strength to the observed transition without greatly affecting the C-C distance. However, such mixing is not present in the DZP+R SCFX reference wave function, where C_1=0.738 and C_2=-0.675. These SCFX CI coefficients are characteristic of a true open-shell singlet state and are quite different from the C_1=0.916 and C_2=-0.402 values for the "valence" 2^1A_1 state. A resolution to this problem could perhaps be provided by converging on the second root in a CASSCF procedure involving two electrons in the three orbitals π, $3p_x$, and π^* ($2b_1$, $3b_1$, and $4b_1$). This approach might well allow one to ascertain in an unbiased manner the degree of $(\pi\rightarrow 3p_x)^1$ and $(\pi\rightarrow\pi^*)^1$ mixing in the 2^1A_1 state.

In Table XII DZP and DZP+R SCFX, 2R CISD, and 2R CIDVD energies are listed for the 2^1A_1 state at three different geometries: A=$\bar{X}^1A_1$ DZP CISD, B=2^1A_1 DZP+R 2R CISD, and C=2^1A_1 DZP 2R CISD. As depicted in Fig. 2, these data allow one to examine the DZP and DZP+R ("valence" and "Rydberg") 2^1A_1 energies as the C-C distance varies. At geometries A and B the DZP and DZP+R CISD relative energies are 14048 and 12603 cm^{-1} apart, respectively. At geometry C the separation is only 1447 cm^{-1}, and from Fig. 2 one finds a separation of 1 eV (8065 cm^{-1}) at r(C-C)=1.52 Å. These values give some indication of the region of the potential energy surface where the character of the 2^1A_1 state changes. One surmises that for r(C-C)>1.5 Å the surface could well be flattened by further Rydberg-valence mixing.

Additional results for the 2^1A_1 state were obtained with a basis set consisting of 107 CGFs which is of quadruple-zeta plus double-polarization (QZ2P) quality in the valence space. For oxygen and carbon this is a Huzinaga-Dunning[39,100] (10s6p2d/5s4p2d) basis with α_d(O)=1.35, 0.45 and α_d(C)=1.20, 0.40. For hydrogen the (6s2p/4s2p) basis used in Ref. 101 was employed with α_p(H)=1.00, 0.30. In

Table XII appear the $(2b_1)^2 \rightarrow (3b_1)^2$ TCSCF, 2R CISD, and 2R CIDVD $\tilde{X}^1A_1$ reference energies determined with the QZ2P basis. It is worthwhile to note that for $^2B_1$ CH_2CO^+, T_e(QZ2P SCF)=71423 cm^{-1}, T_e(QZ2P CISD)=75139 cm^{-1}, T_e(QZ2P CIDVD)=75822 cm^{-1} as compared to the corresponding DZP values of 71909, 74424, and 74823 cm^{-1}. The experimental first ionization energy of ketene is 77700 cm^{-1},[80,97] so the QZ2P CISD and CIDVD results do indeed represent improvements over the DZP predictions. The QZ2P CISD and CIDVD relative energies for 2^1A_1 CH_2CO are only 455 and 141 cm^{-1}, respectively, above the corresponding DZP values at geometry C (Table XII). The QZ2P CIDVD 59330 cm^{-1} prediction is also comparable to the DZP+R CIDVD 59082 cm^{-1} result at geometry C. In contrast, at geometries A and B the QZ2P 2^1A_1 relative energies are appreciably below the DZP values (by 1000-4000 cm^{-1}), but part of this energy lowering surely arises because the QZ2P basis contains functions which are more diffuse than those in the DZP basis, thus allowing some Rydberg character in the 2^1A_1 wave function. In summary, the use of a QZ2P basis does not significantly alter the DZP predictions for the 2^1A_1 state.

Further insight into the nature of the 2^1A_1 state of ketene can be achieved through an examination of the vibrational structure of the 54500-60500 cm^{-1} experimental band (Table VI) in light of the theoretical predictions in Table VIII. The first series of bands beginning at 54660 cm^{-1} surely corresponds to a vibrational progression in the C-C stretch $\nu_4(a_1)$. The 2^1A_1 DZP+R SCFX C-C stretch (ω_4=1030 cm^{-1}) is within 6 cm^{-1} of the $^2B_1$ CH_2CO^+ frequency (as expected for a Rydberg state), and the DZP+R 2R CISD frequency (ω_4=1006 cm^{-1}) is consistent with the SCFX value. However, the first two experimental intervals (830 and 840 cm^{-1}) indicate a 19.8-21.2% error in the DZP+R 2R CISD prediction. In fact, the DZP+R 2^1A_1 theoretical frequencies are in closer agreement with the first members (1010-1030

cm^{-1}) of the ν_4 progressions in the higher Rydberg states in Tables VI and VII. Moreover, the experimental photoelectron spectrum of ketene gives ν_4=1020 cm^{-1} for $^2B_1$ CH_2CO^+,[80] which is also in close agreement with the ν_4 values of the higher Rydberg states of ketene but again 21.4-22.9% higher than the initial intervals observed in the 2^1A_1 state. For comparison, the "valence" 2^1A_1 state is predicted in Table VIII to have ω_4=533 cm^{-1} at the DZP CISD level. Thus it appears that a moderate amount of valence character is present in the 2^1A_1 state which is not accounted for theoretically. Such an occurrence would indeed be consistent with the interpretation of the 54500-60500 cm^{-1} experimental band in terms of a single electronic state.

The second series of $\tilde{X}^1A_1 \rightarrow 2^1A_1$ CH_2CO bands can also be ascribed to a vibrational progression in the C-C stretch but with either one quantum in another a_1 mode or two quanta in a b_1 or b_2 mode. It is interesting that the photoelectron spectrum does not exhibit a second ν_4 progression but rather a progression in the C-O stretch (ν_2=2140 cm^{-1}).[80] The offset between the members of the two VUV $\nu_4(a_1)$ progressions varies significantly down the series, the first three separations being 360, 310, and 270 cm^{-1}. Herzberg[93] actually interprets all of the UV absorptions above 50000 cm^{-1} in ketene in terms of two active a_1 modes, ν_3 and ν_4. For example, the vibrational structure in the $\pi \rightarrow 4s$ 64760 cm^{-1} band (Table VII) is explained in terms of ν_3=1025 and ν_4=608 cm^{-1}. However, the $^2B_1$ CH_2CO^+ DZP SCF frequencies (ω_3=1496 and ω_4=1024 cm^{-1}) are much higher and thus invalidate such an interpretation. Similarly, the theoretical predictions for the 2^1A_1 state weigh against the activity of a second a_1 mode in the 54500-60500 cm^{-1} band. Unfortunately, other interpretations are not without difficulties. Perhaps the second active mode is the b_1 C-C-O bend or, alternatively, the b_1 CH_2 wag. The 2^1A_1 ω_6=358 cm^{-1} DZP+R 2R CISD result appears to be too large for $2\nu_6$ to correspond to the initial 360 cm^{-1}

offset in the ν_4 progressions, but recall that the "valence" 2^1A_1 state actually has an imaginary b_1 frequency so that Rydberg-valence mixing might account for the observed separation. Supporting this interpretation is the fact that the higher Rydberg states exhibit larger initial offsets (500-630 cm^{-1}).

4.7 PITFALLS IN THE PREDICTION OF VIBRATIONAL FREQUENCIES OF EXCITED STATES

In the presentation of the 2^1A_1 formaldehyde and ketene results, the discussion of one important topic was reserved for this final section, i.e., problems which arise in the prediction of vibrational frequencies for excited states but not for ground states. If a theoretical method yields energies which are upper bounds for an excited state, then by assumption variational collapse is not a problem in the prediction of the optimum geometry and totally symmetric vibrational frequencies of the state in question. However, this does not mean that the frequencies which are not totally symmetric will be correct in a variational sense. This point was raised in the introduction to this paper using the $^1A''$ state of ketene as an example. In each particular case an inquiry should be made to ascertain which vibrational frequencies are suspect. In order to do this, it is necessary to know the locations of other electronic states at the optimum geometry of the state in question. Hence, Tables III, V, and XI in this paper serve an important purpose.

The $(\pi\rightarrow\pi^*)^1$ state of H_2CO can be used to illustrate the concept. Note in Table III that the $(n_+\rightarrow\pi^*)$ $^1B_1$ state lies below the $(\pi\rightarrow\pi^*)$ 2^1A_1 state at the SCF and CISD levels of theory. Thus, along the b_1 normal mode corresponding to the CH_2 out-of-plane wag ω_4, the 2^1A_1 state becomes the $3^1A'$ state. Since the SCFX wave function cannot provide a variationally correct description of the $3^1A'$ state, the DZP and DZP+R SCFX 2^1A_1 ω_4 frequencies listed in Table II are suspect. The DZP 2R CISD and 3R CISD ω_4 values would also suffer from this potential deficiency, even if computed analytically. In fact, it was not possible to determine these ω_4 frequencies by finite-difference techniques because the SCFX procedure collapsed to give the $(n_+\rightarrow\pi^*)$ $2^1A'$ reference wave function at the displaced geometries. Consequently, the DZP 2R CISD and 3R CISD ω_4 values are not given in Table II.

In contrast to $\omega_4(b_1)$, the b_2 frequencies listed in Table II for the 2^1A_1 state are *not* suspect. Both the $(n_-\rightarrow\pi^*)$ $^1A_2$ and $(n_+\rightarrow\pi^*)$ $^1B_1$ states lie below the $(\pi\rightarrow\pi^*)$ 2^1A_1 state, but both become $^1A''$ states along the b_2 normal modes, whence the 2^1A_1 state becomes the $2^1A'$ and not the $3^1A'$ state. Therefore, the DZP SCFX, 2R CISD, and 3R CISD ω_5 and ω_6 frequencies are variationally correct. Table III suggests that the DZP+R SCFX b_2 frequencies might be suspect because of the presence of the $(n_-\rightarrow 3s)$ $^1B_2$ Rydberg state; however, the agreement between the DZP and DZP+R SCFX ω_5 and ω_6 values shows that this is not the case.

In determining vibrational frequencies using finite-difference techniques, it is important to distinguish between wave function convergence problems and the problem of variational collapse. In principle one could determine the DZP 2R and 3R CISD ω_4 frequencies for the $(\pi\rightarrow\pi^*)$ 2^1A_1 state by employing more sophisticated techniques to converge on the reference wave functions at the displaced geometries. Neglecting numerical errors, the frequencies so obtained would be precisely equivalent to values computed analytically at the C_{2v} reference geometry. Nevertheless, these frequencies would still be suspect due to the problem of variational collapse. For example, by carefully converging the reference wave functions in C_s symmetry, it was possible to obtain both of the DZP+R 2R CISD b_2 frequencies for the $(n\rightarrow 3p_y)$ 2^1A_1 state of formaldehyde (Table IV). However, Table V reveals that variational collapse is a potential problem for these frequencies due to the presence of the lower-lying $(n_-\rightarrow 3s)$ $^1B_2$ state.

While it is paramount to understand which vibrational frequencies predicted for an excited state *might* suffer from variational collapse, one should not discount the validity of all such frequencies. In second-order perturbation theory, two electronic states will interact under a symmetry-breaking geometrical perturbation according to both the energy separation between the two states and the size of the corresponding

matrix element. In the $^1A''$ ketene example discussed in Ref. 6, a conventional analytic SCF second derivative calculation gave $\omega_8(a'')=599$ and $\omega_9(a'')=427$ cm^{-1}. In contrast, $\omega_8(a'')=1383$ and $\omega_9(a'')=483$ cm^{-1} were obtained using an SCFX wave function for the $^1A''$ state.[102] The disparity between the two results arises because the $\tilde{X}^1A'$ state is only 2861 cm^{-1} lower in energy at the DZP TCSCF level,[88] and there apparently is a large matrix element of the geometrical perturbation between the $\tilde{X}^1A'$ and $^1A''$ valence states. As mentioned in footnote 88 of Ref. 6, the two a'' frequencies of the $^1A''$ state of formaldehyde change much less (0 and 18 cm^{-1}) if SCFX wave functions are employed, and in this case the $\tilde{X}^1A'$ state indeed lies much lower (16403 cm^{-1}) in energy. Applying these concepts to the results in this paper, one might expect that $\omega_4(b_1)$ for the $(\pi\rightarrow\pi^*)$ 2^1A_1 state of H_2CO would be unreliable at the DZP or DZP+R 2R CISD level due to the close-lying $(n_+\rightarrow\pi^*)$ $^1B_1$ state (Table III). On the other hand, the DZP+R SCFX and 2R CISD b_1 frequencies (ω_5 and ω_6) listed in Table VIII for the 2^1A_1 state of ketene *should* be reliable, because the $(2b_1\rightarrow 8a_1)$ $^1B_1$ state lies almost 10000 cm^{-1} lower in energy (Table XI) and the interaction matrix elements between the 2^1A_1 and $^1B_1$ Rydberg states should be relatively small.

The problem of variational collapse in the prediction of excited-state vibrational frequencies can be considered to be an example of a more general problem, namely, the problem of maintaining the correct root structure in an approximate wave function at all geometries. For example, one can imagine trying to determine vibrational frequencies for a state A when a state B of different symmetry lies only a few thousand wavenumbers *higher* in energy. Along certain symmetry-breaking normal modes, the potential energy surface for state A could be severely flattened by interactions with state B. In other words, the inverse of the variational collapse problem could be encountered. The key question is whether the approximate wave function is

flexible enough to accurately describe the interactions between states A and B. One approach to this problem would be to use state-averaged MCSCF techniques to obtain molecular orbitals which adequately describe the state in question but maintain the correct root structure in a larger, state-specific CI procedure. Such approaches are largely untested but warrant attention. In addition to their potential for practical utility in the determination of vibrational frequencies, state-averaged MCSCF procedures followed by state-specific CI calculations may provide insight into the reliability of less satisfactory techniques such as the SCFX method.

In summary, the reliability of theoretical excited-state vibrational frequencies depends on the presence of other close-lying electronic states and the ability of the theoretical method to incorporate the correct root structure into the approximate wave function. However, the situation may in cases be even more complex, because the Born-Oppenheimer approximation may become invalid if two electronic states are close enough in energy. Thus, it may be necessary to consider dynamical non-Born-Oppenheimer effects (vibronic coupling) in addition to the static interaction of Born-Oppenheimer potential energy surfaces (the mixing of electronic configurations).

The interaction of the $(n\rightarrow 3p_z)$ $^1B_2$ and $(n\rightarrow 3p_y)$ 2^1A_1 Rydberg states of formaldehyde is noteworthy in this regard. In the 7.96 eV system in the VUV absorption spectrum of H_2CO, a weak progression of bands at +411, +683, and +1454 cm^{-1} from the origin band can be identified.[84] The +1454 cm^{-1} band overlaps and perturbs the origin of the 8.11 eV system. As discussed earlier, Lessard and Moule[84] assigned the 7.96 eV system as $(n\rightarrow 3p_y)$ 2^1A_1 and the 8.11 eV system as $(n\rightarrow 3p_z)$ $^1B_2$. Therefore, the active vibrational mode in the lower state must be ν_6, the b_2 CH_2 rock, and the three bands can be assigned to the 6_0^1, 6_0^2, and 6_0^3 transitions. Even if the assignment of the 7.96 and 8.11 eV systems should be switched, as Harding and Goddard suggested,[52] it would still be ν_6 which is active.

Lessard and Moule used the observed ν_6 levels in the lower state to derive a one-dimensional potential function $V(Q_6)$, which contained a double minimum. However, the barrier height in $V(Q_6)$ was only 26 cm^{-1}, which is well below the first vibrational level. Of course, the theoretical results in Table IV are not consistent with a double-well ν_6 potential, so vibronic coupling may be playing an important role in the observed spectrum. Nevertheless, it appears that static interactions of the $(n\rightarrow 3p_z)$ $^1B_2$ and $(n\rightarrow 3p_y)$ 2^1A_1 Born-Oppenheimer potential energy surfaces reduce the curvature of the ν_6 potential. Thus it is interesting that the DZP+R 2R CISD $\omega_6(b_2)$=630 cm^{-1} result given in Table IV for the $(n\rightarrow 3p_y)$ 2^1A_1 state is 417 cm^{-1} below the SCFX value. It is tempting to ascribe this reduction to interactions with a higher-lying $^1B_2$ state, in support of the analysis of Lessard and Moule. However, such an interpretation should not be made without further study. If the reduction in ω_6 is due to interactions between close-lying states, then it is necessary to ascertain whether the root structure is qualitatively correct at the DZP+R 2R CISD level and, in any event, what effect the root structure has on the predicted ν_6 value.

4.8 ACKNOWLEDGEMENTS

This research was supported by the Director, Office of Energy Research, Office of Basic Energy Sciences, Chemical Sciences Division of the U.S. Department of Energy under Contract Number DE-AC03-76SF00098. The vast majority of the computer programming effort required for the evaluation of analytic TCSCF-CI energy gradients was performed by Dr. Timothy J. Lee, and he is the primary author of a previous paper which describes our TCSCF-CI gradient procedure. The implementation of the SCFX-CI gradient procedure described here required only modest modifications of the existing TCSCF-CI computer codes. Therefore, we acknowledge Dr. Lee for his previous work on TCSCF-CI gradients and thank him for helpful discussions.

4.9 REFERENCES AND NOTES

1 E.R. Davidson and L.E. McMurchie, in *Excited States*, edited by E.C. Lim (Academic, New York, 1982), Vol. 5.

2 In general the lower-state wave functions referred to here are the exact wave functions. However, if the wave functions are obtained by diagonalizing the hamiltonian in a finite basis, then the *n*th excited-state wave function is merely orthogonal to the approximate lower-state wave functions, but it nevertheless provides an energy which is an upper bound for the state in question. See Refs. 7 and 8.

3 E.R. Davidson and L.E. Nitzsche, J. Am. Chem. Soc. **101**, 6524 (1979).

4 A.D. Walsh, Trans. Faraday Soc. **41**, 498 (1945); M.B. Robin, *Higher Excited States of Polyatomic Molecules*, Vol. 2, (Academic Press, New York, 1975).

5 C.E. Dykstra and H.F. Schaefer III, J. Am. Chem. Soc. **98**, 2689 (1976).

6 W.D. Allen and H.F. Schaefer III, J. Chem. Phys. **84**, 2212 (1986).
Chapter 2 of this dissertation is an updated version of Ref. 6.

7 E.A. Hylleraas and B. Undheim, Z. Physik **65**, 759 (1930).

8 J.K.L. MacDonald, Phys. Rev. **43**, 830 (1933).

9 L.Z. Stenkamp and E.R. Davidson, Theor. Chim. Acta **44**, 405 (1977).

10 L.E. Nitzsche and E.R. Davidson, J. Chem. Phys. **68**, 3103 (1978).

11 E.R. Davidson and L.Z. Stenkamp, Int. J. Quantum Chem. Symp. **10**, 21 (1976).

12 G. Fitzgerald and H.F. Schaefer III, J. Chem. Phys. **83**, 1162 (1985).

13 T.P. Hamilton and P. Pulay, J. Chem. Phys. **84**, 5728 (1986).

14 P. Pulay, Chem. Phys. Lett. **73**, 393 (1980).

15 P. Pulay, J. Comput. Chem. **3**, 556 (1982).

16 S.R. Langhoff, S.T. Elbert, C.F. Jackels, and E.R. Davidson, Chem. Phys. Lett. **29**, 247 (1974).

17 C.F. Bender, T.H. Dunning, Jr., H.F. Schaefer III, W.A. Goddard III, and W.J. Hunt, Chem. Phys. Lett. **15**, 171 (1972).

[18] L.E. McMurchie and E.R. Davidson, J. Chem. Phys. **66**, 2959 (1977); C.F. Bender, V. McKoy, and E.R. Davidson, J. Chem. Phys. **67**, 2178 (1977).

[19] B.R. Brooks and H.F. Schaefer III, J. Chem. Phys. **68**, 4839 (1978).

[20] R.J. Buenker, S.-K. Shih, and S.D. Peyerimhoff, Chem. Phys. **36**, 97 (1979).

[21] B.R. Brooks and H.F. Schaefer III, J. Am. Chem. Soc. **101**, 307 (1979).

[22] Y. Yamaguchi, Y. Osamura, and H.F. Schaefer III, J. Am. Chem. Soc. **105**, 7506 (1983).

[23] N.C. Handy and H.F. Schaefer, J. Chem. Phys. **81**, 5031 (1984).

[24] J.E. Rice and R.D. Amos, Chem. Phys. Lett. **122**, 585 (1985).

[25] Y. Osamura, Y. Yamaguchi, and H. F. Schaefer, J. Chem. Phys. **77**, 383 (1982).

[26] P. Jorgensen and J. Simons, J. Chem. Phys. **79**, 334 (1983).

[27] A. Banerjee, J.O. Jensen, J. Simons, and R. Shepard, Chem. Phys. **87**, 203 (1984).

[28] M. Page, P. Saxe, G.F. Adams, and B.H. Lengsfield, J. Chem. Phys. **81**, 434 (1984).

[29] R.S. Shepard, in *Geometrical Derivatives of Energy Surfaces and Molecular Properties*, eds. J. Simons and P. Jorgensen, (Reidel, Dordrecht, 1986).

[30] B.R. Brooks, W.D. Laidig, P. Saxe, J.D. Goddard, Y. Yamaguchi, and H.F. Schaefer, J. Chem. Phys. **72**, 4652 (1980).

[31] R. Krishnan, H.B. Schlegel, and J.A. Pople, J. Chem. Phys. **72**, 4654 (1980).

[32] Y. Osamura, Y. Yamaguchi, and H.F. Schaefer, J. Chem. Phys. **77**, 383 (1982).

[33] J.E. Rice, R.D. Amos, N.C. Handy, T.J. Lee, and H.F. Schaefer, J. Chem. Phys. **85**, 963 (1986).

[34] J. Gerratt and I.M. Mills, J. Chem. Phys. **49**, 1719 (1968).

[35] An inconsistency exists in the formalism of RAHLS in Ref. 33. The equations which were actually programmed are correct, but Eqs. 2.11-2.13 therein are not consistent with Eq. 2.10. With X_{pq} as defined in Eq. 2.10, the CPHF contribution $\sum_{p>q} (X_{pq}-X_{qp})\, T^{a}_{pq}$ is of the wrong sign. In other words, the CPHF contribution is actually $-\mathbf{Z}^{T}\mathbf{B}^{a}$ in their formalism.

[36] P. Saxe, Y. Yamaguchi, and H.F. Schaefer, J. Chem. Phys. **77**, 5647 (1982).

[37] T.J. Lee, Ph.D. thesis, University of California, Berkeley, 1986.

[38] E.R. Davidson, Chem. Phys. Lett. **21**, 565 (1973).

[39] S. Huzinaga, J. Chem. Phys. **42**, 1293 (1965).

[40] T.H. Dunning, Jr., J. Chem. Phys. **53**, 2823 (1970).

[41] Y. Osamura, Y. Yamaguchi, P. Saxe, M.A. Vincent, J.F. Gaw, and H.F. Schaefer III, Chem. Phys. **72**, 131 (1982).

[42] J.E. Rice, R.D. Amos, N.C. Handy, T.J. Lee, and H.F. Schaefer III, J. Chem. Phys. **85**, 963 (1986).

[43] J.F. Gaw and N.C. Handy, "Derivatives of the Potential Energy Hypersurface by Analytic Techniques", in *Annual Reports C, The Royal Society of Chemistry*, (London, 1984), pp. 291-323.

[44] H.F. Schaefer III and Y. Yamaguchi, J. Mol. Struct. (Theochem) **135**, 369 (1986).

[45] D.C. Moule and A.D. Walsh, Chem. Rev. **75**, 67 (1975).

[46] J.L. Whitten and M. Hackmeyer, J. Chem. Phys. **51**, 5584 (1969).

[47] S.D. Peyerimhoff, R.J. Buenker, W.E. Kammer, and H. Hsu, Chem. Phys. Lett. **8**, 129 (1971).

[48] J.L. Whitten, J. Chem. Phys. **56**, 5458 (1972).

[49] D.L. Yeager and V. McKoy, J. Chem. Phys. **60**, 2714 (1974).

[50] J.F. Gouyet and M.T. Prat, J. Chem. Phys. **64**, 946 (1976).

[51] R. Colle, R. Montagnani, P. Riani, and O. Salvetti, Theor. Chim. Acta **49**, 37 (1978).

[52] L.B. Harding and W.A. Goddard III, J. Am. Chem. Soc. **99**, 677 (1977).

[53] R.J. Buenker and S.D. Peyerimhoff, J. Chem. Phys. **53**, 1368 (1970).

[54] S. Bell, Mol. Phys. **73**, 255 (1979).

[55] K. Yamashita, A. Tachibana, T. Yamabe, and K. Fukui, Chem. Phys. Lett. **69**, 413 (1980).

[56] P. Saxe, Y. Yamaguchi, and H.F. Schaefer III, J. Chem. Phys. **77**, 5647 (1982).

[57] Y. Osamura, Y. Yamaguchi, P. Saxe, M.A. Vincent, J.F. Gaw, and H.F. Schaefer III, Chem. Phys. **72**, 131 (1982).

[58] M. Baba, U. Nagashima, and I. Hanazaki, Chem. Phys. **93**, 425 (1985).

[59] S. Bell and J.S. Crighton, J. Chem. Soc., Faraday Trans. 2 **81**, 1813 (1985).

[60] J.F. Gaw, Y. Yamaguchi, R.B. Remington, Y. Osamura, and H.F. Schaefer III, Chem. Phys. **109**, 237 (1986).

[61] P. Jensen and P.R. Bunker, J. Mol. Spectrosc. **94**, 114 (1982).

[62] G. Herzberg, *Electronic Spectra of Polyatomic Molecules* (Van Nostrand, New York, 1966) pp. 518-522, 612.

[63] V.A. Job, V. Sethuraman, and K.K. Innes, J. Mol. Spectrosc. **30**, 365 (1969); **33**, 189 (1970).

[64] V.T. Jones and J.B. Coon, J. Mol. Spectrosc. **31**, 137 (1969).

[65] Y. Osamura, J.D. Goddard, Henry F. Schaefer III, and K.S. Kim, J. Chem. Phys. **74**, 617 (1981).

[66] D. Feller and E.R. Davidson, Theor. Chim. Acta **68**, 57 (1985).

[67] A.J. Maria, D. Larson, M.E. McCarville, and S.P. McGlynn, Acc. Chem. Res. **3**, 368 (1970).

[68] T. Anno and A. Sadô, J. Chem. Phys. **26**, 1759 (1957).

[69] J.W. Sidman, J. Chem. Phys. **27**, 429 (1957).

[70] R.L. Ellis, R. Squire, and H.H. Jaffe, J. Chem. Phys. **55**, 3500 (1971).

[71] I. Absar, C.S. Lin, and K.L. McEwen, Can. J. Chem. **50**, 646 (1972).

[72] J.A. Pople and J.W. Sidman, J. Chem. Phys. **27**, 1270 (1957).

[73] J. E. Mentall, E.P. Gentieu, M. Krauss, and D. Neumann, J. Chem. Phys. **55**, 5471 (1971).

[74] E.D. Simandiras, N.C. Handy, and R.D. Amos, Chem. Phys. Lett. **133**, 324 (1987).

[75] M. Dupuis, W.A. Lester, Jr., B.H. Lengsfield III, and B. Liu, J. Chem. Phys. **79**, 6167 (1983).

[76] J.H. Callmon, E. Hirota, K. Kuchitsu, W.J. Lafferty, A.G. Maki, and C.S. Pote, in *Numerical Data and Functional Relationships in Science and Technology, New Series*, ed. by K.-H. Hellwege (Springer, Berlin, 1976), Vol. 7.

[77] D.E. Reisner, R.W. Field, J.L. Kinsey, and H.-L. Dai, J. Chem. Phys. **80**, 5968 (1984).

[78] D.J. DeFrees and A.D. McLean, J. Chem. Phys. **82**, 333 (1985).

[79] A.D. Baker, C. Baker, C.R. Brundle, and D.W. Turner, Intern. J. Mass Spectrom. Ion Phys. **1**, 285 (1968).

[80] D.W. Turner, C.Baker, A.D. Baker, and C.R. Brundle, *Molecular Photoelectron Spectroscopy* (Wiley-Interscience, New York, 1970) pp. 132-135, 139-140.

[81] R.M. Lees and J.G. Baker, J. Chem. Phys. **48**, 5299 (1968).

[82] C.R. Lessard, D.C. Moule, and S. Bell, Chem. Phys. Lett. **29**, 603 (1974).

[83] C.R. Drury-Lessard and D.C. Moule, Chem. Phys. Lett. **47**, 300 (1977).

[84] C.R. Lessard and D.C. Moule, J. Chem. Phys. **66**, 3908 (1977).

[85] T.C. Betts and V. McKoy, J. Chem. Phys. **60**, 2947 (1974).

[86] K.J. Miller, J. Chem. Phys. **62**, 1759 (1975).

[87] The quantum defect (and hence the term value) of a Rydberg state is integrally related to the penetration of the ion core by the Rydberg orbital in question. See, for example, M.B. Robin, *Higher Excited States of Polyatomic Molecules* (Academic, New York, 1974), Vol. 1. It is reasonable to expect that the $3p_z$ orbital in formaldehyde penetrates the core more than the $3p_y$ orbital, in which case the $(n\rightarrow 3p_z)$ transition should in fact be lower in energy.

[88] An error in the excited-state SCF computer program has been found which affected certain results in Ref. 6. All of the errors are quite small, and none of the qualitative conclusions in Ref. 6 need be altered. In Fig. 5 the 53084 and 12811 cm^{-1} entries should be changed to 53083 and 12328 cm^{-1}, and in note c of the caption C_1=0.981 and C_2=-0.196 should read C_1=0.978 and C_2=-0.206. In Fig. 6 the 56054 and 12957 cm^{-1} entries should be 56051 and 12883 cm^{-1}. Finally, the 2^1A_1 energies in the last column of Table XIV should be altered from 76657, 72693, 69600, 53084, 56054, and 56297 cm^{-1} to 76003, 71690, 68959, 53083, 56051, and 56294 cm^{-1}. The values in question in Table XIV and Figs. 5 and 6 also appear in the discussion on pages 2219 and 2222. No other changes are required. All necessary changes in Ref. 6 have been made in Chapter 2 of this dissertation.

[89] W.C. Price, J.M. Teegan, and A.D. Walsh, J. Chem. Soc. **1951**, 920.

[90] H. Basch, Theor. Chim. Acta **28**, 151 (1973).

[91] P. Pendergast and W.H. Fink, J. Am. Chem. Soc. **98**, 648 (1976).

[92] W. Braun, A.M. Bass, and M. Pilling, J. Chem. Phys. **52**, 5131 (1970).

[93] G. Herzberg, *Electronic Spectra of Polyatomic Molecules* (Van Nostrand, New York, 1966), pp. 530, 622.

[94] M.B. Robin, *Higher Excited States of Polyatomic Molecules* (Academic, New York, 1975), Vol. 2, pp. 202-204.

[95] K. Tanaka and M. Yoshimine, J. Am. Chem. Soc. **102**, 7655 (1980).

[96] This guess is primarily based on the magnitude of ω_5 and the data reported on p. 2221 of Ref. 6 concerning the potential energy surface of the $^3A'$ state as a function of the CH_2 wagging coordinate γ. The location of the $^1B_1$ state 10198 cm^{-1} below the 2^1A_1 state probably precludes a $C_{2v} \rightarrow C_s^I$ energy lowering larger than 5000 cm^{-1}.

[97] D. Hall, J.P. Maier, and P. Rosmus, Chem. Phys. **24**, 373 (1977).

[98] The CO^- anion is not stable experimentally. See R.D. Rempt, Phys. Rev. Lett. **22**, 1034 (1969). The purpose of discussing the $^2\Pi$ CH_2^+ + $^2\Pi$ CO^- system here is pedagogical in that a qualitative understanding of the 2^1A_1 ketene DZP SCFX wave function is sought rather than a prediction of the actual dissociation products.

[99] For the dissociation energies $\tilde{X}^1A_1$ $CH_2CO \rightarrow \tilde{X}^3B_1$ CH_2 + $^1\Sigma^+$ CO and $\tilde{X}^1A_1$ $CH_2CO \rightarrow \tilde{a}^1A_1$ CH_2 + $^1\Sigma^+$ CO see C.C. Hayden, D.M. Neumark, K. Shobatake, R.K. Sparks, and Y.T. Lee, J. Chem. Phys. **76**, 3607 (1982). For the excitation energies $\tilde{X}^1\Sigma^+$ CO $\rightarrow \tilde{a}^3\Pi$ CO and $\tilde{X}^1\Sigma^+$ CO $\rightarrow \tilde{A}^1\Pi$ CO see G. Herzberg, *Spectra of Diatomic Molecules*, 2nd edition (Van Nostrand, New York, 1950) pp. 521,522.

[100] T.H. Dunning, Jr., J. Chem. Phys. **55**, 716 (1971).

[101] W.D. Allen and H.F. Schaefer III, Chem. Phys. **108**, 243 (1986).

[102] As explained in Ref. 6, SCFX wave functions for $^1A''$ ketene are not entirely satisfactory either, but they do seem to provide qualitatively correct predictions.

[103] A comparison with the vertical $(\pi\rightarrow\pi^*)^1$ state of ethylene clarifies this point. Assuming a D_{2h} molecular framework, the π and π^* orbitals are of b_{3u} and b_{2g} symmetry, respectively. Consequently, the overlap $S=\langle\pi|\pi^*\rangle$ is zero, and according to this criterion the state is an open-shell singlet. One can transform the $(\pi\rightarrow\pi^*)^1$ wave function from the form of Eq. (55) to that of Eq. (57), in which case the orbitals u and v are localized and $C_1=-C_2=\frac{1}{\sqrt{2}}$. Formally the $(\pi\rightarrow\pi^*)^1$ state could then be considered a superposition of the ionic structures $H_2C^+—{}^-CH_2$ and $H_2C^-—{}^+CH_2$. The crux is that both structures contribute equally so that the open-shell singlet designation is still apt. In the $(\pi\rightarrow\pi^*)^1$ state of formaldehyde, the $H_2C^+–O^-$ structure with $C_1\approx0.96$ is far more important than the $H_2C^-–O^+$ structure with $C_2\approx-0.29$. Thus, if one interprets the wave function in terms of Eq. (57), the zwitterion designation is applicable. This language is consistent with the fact that $S=\langle\pi|\pi^*\rangle$ deviates greatly from zero in 2^1A_1 formaldehyde, thereby invalidating the open-shell singlet designation.

Table I.

Previous experimental and theoretical vertical excitation energies (eV) for formaldehyde[a]

		Expt.	GVB-CI
Singlet states			
$n\rightarrow\pi^*$	$^1A_2$	4.1	4.09
$n\rightarrow 3s$	$^1B_2$	7.09	7.16
$n\rightarrow 3p_z$	$^1B_2$	7.97[b]	8.08
$n\rightarrow 3p_y$	$^1A_1$	8.14[b]	8.09
$n\rightarrow 3p_x$	$^1A_2$	-	8.32
.	.	.	.
.	.	.	.
$n\rightarrow\infty$	$^2B_2$	10.87	10.55
$\pi\rightarrow\pi^*$	$^1A_1$	10.7	10.77
.	.	.	.
.	.	.	.
$\pi\rightarrow\infty$	$^2B_1$	14.4	14.14
Triplet states			
$n\rightarrow\pi^*$	$^3A_2$	3.5	3.68
$\pi\rightarrow\pi^*$	$^3A_1$	6.0	5.95
$n\rightarrow 3s$	$^3B_2$	7.09	7.08
$n\rightarrow 3p_z$	$^3B_2$	7.92	7.99
$n\rightarrow 3p_y$	$^3A_1$	8.11	8.05
$n\rightarrow 3p_x$	$^3A_2$	-	8.31

[a] Summarized from the paper of Harding and Goddard (Ref. 52).

[b] In Ref. 84 bands at 7.96 and 8.11 eV are assigned to the $(n\rightarrow 3p_y)^1A_1$ and $(n\rightarrow 3p_z)^1B_2$ states, respectively, i.e., the assignments are switched.

Table II.

Theoretical structures and vibrational frequencies[a] of the $\tilde{X}^1A_1$ and $(\pi\rightarrow\pi^*)$ 2^1A_1 states of H_2CO and the $(\pi\rightarrow\infty)$ $^2B_1$ state of H_2CO^+

	Energy	T_0[b]	r_e(C-O)	r_e(C-H)	θ_e(H-C-H)	$\omega_1(a_1)$	$\omega_2(a_1)$	$\omega_3(a_1)$	$\omega_4(b_1)$	$\omega_5(b_2)$	$\omega_6(b_2)$
$\tilde{X}^1A_1$ H_2CO											
DZP SCF	-113.894761	-	1.1885	1.0960	116.19	3136	2006	1652	1332	3214	1365
DZP TCSCF[c]	-113.930077	0	1.2083	1.0922	117.14	3163	1859	1635	1168	3252	1350
DZP CISD	-114.195583	-	1.2109	1.1038	116.19	3053	1868	1587	1235	3131	1299
DZP 2R CISD	-114.205272	0	1.2194	1.1029	116.51	3058	1804	1575	1193	3141	1290
DZP 3R CISD[d]	-114.206606	0	1.2198	1.1033	116.47	3053	1801	1574	1194	3135	1288
DZP+R SCF	-113.897307	-	1.1876	1.0960	116.31	3134	2003	1649	1330	3209	1359
DZP+R TCSCF	-113.932376	0	(1.2083)	(1.0922)	(117.14)	-	-	-	-	-	-
DZP+R CISD	-114.200625	-	(1.2109)	(1.1038)	(116.19)	-	-	-	-	-	-
DZP+R 2R CISD	-114.210351	0	(1.2194)	(1.1029)	(116.51)	-	-	-	-	-	-
DZP MP2[e]	-	-	1.2231	1.1021	116.24	3040	1774	1572	1217	3128	1284
DZP CASSCF (MC10)[f]	-114.04531	-	1.224	1.122	115.72	2861	1772	1528	1180	2921	1264
Expt.[g]	-	-	1.203	1.099	116.5	2978	1778	1529	1191	2997	1299
$(\pi\rightarrow\pi^*)$ 2^1A_1 H_2CO											
DZP SCFX	-113.575308	77123	1.5366	1.0782	120.31	3323	847	1568	721	3464	1025
DZP 2R CISD	-113.884399	69684	1.5383	1.0907	118.90	3193	835	1518	-	3325	969
DZP 3R CISD[d]	-113.890834	68564	1.5644	1.0904	119.41	3191	737	1495	-	3328	938
DZP+R SCFX	-113.587185	75021	1.5173	1.0782	120.83	3325	859	1569	918	3470	1045
DZP+R 2R CISD	-113.896652	68109	(1.5383)	(1.0907)	(118.90)	-	-	-	-	-	-
$(\pi\rightarrow\infty)$ $^2B_1$ H_2CO^+											
DZP+R SCF	-113.457406	104145	1.3320	1.0882	122.58	3250	1646	1354	1333	3397	1249
DZP+R CISD	-113.708132	110125	(1.3320)	(1.0882)	(122.58)	-	-	-	-	-	-

Table II (continued)

[a] Energy in hartrees, T_0 in cm^{-1}, r_e in Å, θ_e in degrees, and frequencies in cm^{-1}. Geometrical parameters in parentheses indicate single-point energies obtained at a geometry from another level of theory. The normal modes of the 2^1A_1 state have been labeled as for the $\tilde{X}^1A_1$ state. Thus, ω_1 and ω_5 are the symmetric and asymmetric C-H stretches, ω_2 is the C-O stretch, ω_3 is the CH_2 scissor, ω_4 is the CH_2 out-of-plane wag, and ω_6 is the CH_2 rock.

[b] The zeros listed for the $\tilde{X}^1A_1$ state indicate the energies selected to calculate the T_0 values. The $\tilde{X}^1A_1 \rightarrow 2^1A_1$ adiabatic excitation energies include a -740 cm^{-1} zero-point vibrational energy (ZPVE) correction as obtained from the DZP TCSCF and DZP SCFX harmonic frequencies (without scaling). The ZPVE correction utilized for the $\tilde{X}^1A_1 \rightarrow {}^2B_1$ excitation energies is -99 cm^{-1} (from the DZP TCSCF and DZP+R SCF frequencies).

[c] A CI coeffiecient of C_2 = -0.2063 was obtained for the second (π^{*2}) configuration.

[d] 18940 CSFs in C_{2v} symmetry, based on the three references π^2, π^{*2}, and $\pi\pi^*$. *All* configurations (included the non-interacting ones) resulting from single and double excitations out of these three references were included.

[e] Reference 74.

[f] Reference 75.

[g] The structural parameters are from Ref. 76, and the frequencies are empirical harmonic frequencies from Ref. 77.

Table III.

Relative energies of several electronic states of H_2CO at the $(\pi\rightarrow\pi^*)$ 2^1A_1 optimum geometry[a]

	$\tilde{X}^1A_1$	$^1A_2$ $(n_-\rightarrow\pi^*)$	$^1B_1$ $(n_+\rightarrow\pi^*)$	2^1A_1 $(\pi\rightarrow\pi^*)$	$^1B_2$ $(n_-\rightarrow 3s)$	$^1A_1$[d] $(n_-\rightarrow 3p_y)$
DZP+R SCF	19592	32274	66222	75772	74071	82261
DZP+R CISD	17529	33132	67566	68849	74508	83124
DZP+R CIDVD[b]	16369	32620	67149	64428[c]	72971	81553

[a] Energies at the DZP 2R CISD $(\pi\rightarrow\pi^*)$ 2^1A_1 optimum geometry are listed in cm^{-1} relative to the corresponding $\tilde{X}^1A_1$ values obtained at the DZP 2R CISD $\tilde{X}^1A_1$ optimum geometry: E(DZP+R TCSCF) = -113.931929, E(DZP+R 2R CISD) = -114.210351, and E(DZP+R 2R CIDVD) = -114.232661. The TCSCF result involves the π^2 and π^{*2} configurations. The $\tilde{X}^1A_1$, $(\pi\rightarrow\pi^*)$ 2^1A_1, and $(n_-\rightarrow 3p_y)$ $^1A_1$ values are TCSCF, 2R CISD, and 2R CIDVD energies while the $^1A_2$, $^1B_1$, and $^1B_2$ results are based on a single reference.

[b] CIDVD=Davidson-corrected CISD. The two-reference Davidson corrections were computed according to the formula $\Delta E=(1-C_1^2-C_2^2)(E_{CISD}-E_{TCSCF})$.

[c] As mentioned in the text, this result is of questionable validity.

[d] These results were obtained by occupying the n_- and $3p_y$ orbitals (of b_2 symmetry) in the SCFX procedure rather than the π and π^* orbitals (of b_1 symmetry). The *second* root of the corresponding CI matrix was then determined. Thus, the $(n_-\rightarrow 3p_y)$ $^1A_1$ results are nonvariational estimates of a higher root (>2) which is predominantly $(n_-\rightarrow 3p_y)$ in character. The intent is to show that the $(\pi\rightarrow\pi^*)^1$ state is indeed the 2^1A_1 state at its optimum geometry.

Table IV.

Theoretical structures and vibrational frequencies[a] of the $\tilde{X}^1A_1$ and $(n\rightarrow 3p_y)\ 2^1A_1$ states of H_2CO and the $(n\rightarrow\infty)\ ^2B_2$ state of H_2CO^+

	Energy	T_0[b]	r_e(C-O)	r_e(C-H)	θ_e(H-C-H)	$\omega_1(a_1)$	$\omega_2(a_1)$	$\omega_3(a_1)$	$\omega_4(b_1)$	$\omega_5(b_2)$	$\omega_6(b_2)$
$\tilde{X}^1A_1$ H_2CO											
DZP+R TCSCF[c]	-113.907726	0	1.1875	1.0974	115.99	3114	2001	1649	1333	3178	1352
DZP+R 2R CISD	-114.202347	0	(1.1875)	(1.0974)	(115.99)	-	-	-	-	-	-
$(n\rightarrow 3p_y)\ 2^1A_1$ H_2CO											
DZP+R SCFX	-113.637018	59136	1.2181	1.0907	126.48	3221	1759	1465	1316	3263	1047
DZP+R 2R CISD	-113.909481	63999	1.2165	1.1066	126.04	3029	1689	1373	1173	3064	630
$(n\rightarrow\infty)\ ^2B_2$ H_2CO^+ [d]											
DZP+R SCF	-113.543386	79711	1.2161	1.0908	124.54	3201	1761	1461	1285	3342	1074
DZP+R CISD	-113.813149	85167	(1.2161)	(1.0908)	(124.54)	-	-	-	-	-	-
DZ SCF[e]	-113.4789	-	1.246	1.083	123.2	3269	1647	1464	1309	3416	1110
6-31 G* MP2[f]	-	-	-	-	-	2947	1644	1340	1132	3096	906
TZP CASSCF[g]	-113.6706	-	1.208	1.123	119.1	-	-	-	-	-	-

Table IV (continued)

[a] See footnote a of Table II.

[b] The $\tilde{X}^1A_1 \rightarrow 2^1A_1$ adiabatic excitation energies include a -278 cm^{-1} zero-point vibrational energy (ZPVE) correction as obtained from the DZP+R TCSCF and DZP+R SCFX harmonic frequencies (without scaling). The ZPVE correction utilized for the $\tilde{X}^1A_1 \rightarrow {}^2B_2$ excitation energies is -252 cm^{-1} (from the DZP+R TCSCF and DZP+R SCF frequencies).

[c] The second configuration results from the $n \rightarrow 3p_y$ excitation (C_2 = -0.0730).

[d] From an analysis of the photoelectron spectrum of H_2CO, Turner et al.[79,80] ascertained ν_1=2560, ν_2=1590, and ν_3=1210 cm^{-1} for ${}^2B_2$ H_2CO^+.

[e] Reference 65.

[f] Reference 78.

[g] Reference 66.

Table V.

Relative energies of several electronic states of H_2CO at the $(n\rightarrow 3p_y)$ 2^1A_1 optimum geometry[a]

	$\tilde{X}^1A_1$	$^1A_2$ $(n_-\rightarrow \pi^*)$	$^1B_2$ $(n_-\rightarrow 3s)$	2^1A_1 $(n_-\rightarrow 3p_y)$	$^1B_1$ $(n_+\rightarrow \pi^*)$	$^1A_1$[c] $(\pi\rightarrow \pi^*)$
DZP+R SCF	1059	26884	52801	59489	68694	82622
DZP+R CISD	516	31439	57037	64277	73347	86846
DZP+R CIDVD[b]	319	31908	56921	64284	73879	84865

[a] Energies at the DZP+R 2R CISD $(n\rightarrow 3p_y)$ 2^1A_1 optimum geometry are listed in cm^{-1} relative to the corresponding $\tilde{X}^1A_1$ values obtained at the DZP+R TCSCF $\tilde{X}^1A_1$ optimum geometry: E(DZP+R TCSCF) = -113.907726, E(DZP+R 2R CISD) = -114.202347, and E(DZP+R 2R CIDVD) = -114.228233. The TCSCF result involves the $(n_-)^2$ and $(3p_y)^2$ configurations. The $\tilde{X}^1A_1$, $(n\rightarrow 3p_y)$ 2^1A_1, and $(\pi\rightarrow \pi^*)$ 3^1A_1 values are TCSCF, 2R CISD, and 2R CIDVD energies while the $^1A_2$, $^1B_1$, and $^1B_2$ results are based on a single reference.

[b] CIDVD=Davidson-corrected CISD. See footnote b of Table III.

[c] The statements in footnote d of Table III hold here with the roles of the (π, π^*) and $(n_-, 3p_y)$ pairs reversed. See also the caption to Fig. 1.

Table VI.

Bands in the 54500-64500 cm^{-1} region of the VUV absorption spectrum of ketene[a]

Braun, Bass, and Pilling[b]				Price, Teegan, and Walsh[c]			
	54660				54680		
830		55020	780	830		55060	750
	55490				55510		
840		55800	800	860		55810	830
	56330				56370		
790		56600	870	980		56640	
	57120				57350		
620		57470	700				
	57740						
850		58170	950				
	58590						
1110		59130	970				
	59700						
700		60100					
	60400						
	61340				61350[d]		
1030		61840	1050	1020		61840	1060
	62370				62370		
980		62890		990		62900	1010
	63350				63360		
				1000		63910	
					64360		

[a] The bands (in cm^{-1}) are tabulated as members of two vibrational progressions. The intervals between successive members are indicated outside the brackets.

[b] Extracted from Fig. 1 of Ref. 92.

[c] Reference 89.

[d] In Table II of Ref. 89 this band is listed as 61550 cm^{-1}, which is apparently a typographical error.

Table VII.

Bands observed by Price, Teegan, and Walsh above 64500 cm^{-1} in the VUV absorption spectrum of ketene[a]

$\pi \rightarrow 4s$ $\delta = 1.064$	64760 1025 [65368] 1027 65785 66395
$\pi \rightarrow 4p$ $\delta = 0.768$	66984 1025 [67611] 1138 68009 1085 [68749] 955 69094 69704
$\pi \rightarrow 5s$ $\delta = 1.074$	70371 1023 [70963] 1101 71394 1072 [72064 72466
$\pi \rightarrow 6s$ $\delta = 1.066$	72983 1010 [73594] 1010 73993 74604
$\pi \rightarrow 7s$ $\delta = 1.073$	74367
$\pi \rightarrow 8s$ $\delta = 1.111$	75179

[a] Reference 89. See footnote a of Table VI. To the left of the tabulated bands the assignments are given along with the quantum defects. The $\pi \rightarrow ns$ Rydberg series converges to 77491 cm^{-1}. The first ionization energy observed directly by photoelectron spectroscopy is 77700 cm^{-1}.[80,97]

Table VIII.

Theoretical structures and vibrational frequencies of the 2^1A_1 state of ketene[a]

	$\tilde{X}^1A_1$	2^1A_1			
	DZP SCF[b]	DZP SCFX	DZP 2R CISD[c,e]	DZP+R SCFX	DZP+R 2R CISD[d,e]
Energy	-151.756673	-151.466957	-151.875875	-151.528858	-151.910919
T_e[f]	-	67794	62604	54695	56083
r_e(C-O)	1.1466	1.1514	1.1738	1.1027	1.1286
r_e(C-C)	1.3101	1.7568	1.6871	1.4046	1.4028
r_e(C-H)	1.0735	1.0648	1.0725	1.0766	1.0834
θ_e(H-C-H)	121.99	137.66	133.81	124.65	124.20
$\omega_1(a_1)$ C-H stretch	3355	3404	3340	3318	3258
$\omega_2(a_1)$ C-O stretch	2360	2341	2172	2576	2395
$\omega_3(a_1)$ CH_2 scissor	1537	1397	1366	1498	1444
$\omega_4(a_1)$ C-C stretch	1245	431	533	1030	1006
$\omega_5(b_1)$ CH_2 wag	702	1138 *i*	-	726	764
$\omega_6(b_1)$ C-C-O bend	618	668	-	477	358
$\omega_7(b_2)$ C-H stretch	3467	3639	3547	3467	3405
$\omega_8(b_2)$ CH_2 rock	1094	1062	1014	1126	1066
$\omega_9(b_2)$ C-C-O bend	486	275	258	449	411

Table VIII (continued)

[a] Energy in hartrees, T_e in cm^{-1}, r_e in Å, θ_e in degrees, and frequencies in cm^{-1}.

[b] Reference 6.

[c] 33364 CSFs in C_{2v} symmetry.

[d] 80500 CSFs in C_{2v} symmetry.

[e] The CSF ψ_3 of Eq. (59) was not found to be important in the 2R CISD wave functions, and thus three-reference CISD calculations were not performed.

[f] Based on the following $\tilde{X}^1A_1$ energies at the $\tilde{X}^1A_1$ DZP CISD geometry of Ref. 95: E(DZP TCSCF) = -151.775848, E(DZP 2R CISD) = -152.161119, E(DZP+R TCSCF) = -151.778066, and E(DZP+R 2R CISD) = -152.166452. The TCSCF and 2R CISD results involve the $(2b_1)^2$ and $(3b_1)^2$ reference configurations. According to the $\tilde{X}^1A_1$ DZP SCF and 2^1A_1 DZP+R SCFX harmonic frequencies, $T_0 = T_e - 98$ cm^{-1} for the 2^1A_1 state.

Table IX.

DZP SCF theoretical data for fragments pertaining to 2^1A_1 ketene[a]

	$^2B_1$ CH_2CO^+	$\tilde{a}^1A_1$ CH_2 + $\tilde{A}^1\Pi$ CO	$\tilde{X}^3B_1$ CH_2 + $\tilde{a}^3\Pi$ CO	$^2\Pi$ CH_2^+ + $^2\Pi$ CO^- [b]
Total Energy	-151.448206	-151.333839	-151.488199	-151.223190
Relative Energy[c]	71909 (77700)	97010 (95215)	63132 (75848)	121294
r_e(C-O)	1.1015	1.2000	1.1836	1.2146
r_e(C-C)	1.4120	-	-	-
r_e(C-H)	1.0780	1.1005	1.0756	1.0828
θ_e(H-C-H)	124.75	103.74	129.36	180.00
$\omega_1(a_1)$ C-H stretch	3305	3120	3287	3205
$\omega_2(a_1)$ C-O stretch	2597	1632	2023	1825
$\omega_3(a_1)$ CH_2 scissor	1496	1490	1300	1296, 1062*i*
$\omega_4(a_1)$ C-C stretch	1024	-	-	-
$\omega_5(b_1)$ CH_2 wag	650	-	-	-
$\omega_6(b_1)$ C-C-O bend	517	-	-	-
$\omega_7(b_2)$ C-H stretch	3456	3193	3494	3514
$\omega_8(b_2)$ CH_2 rock	1126	-	-	-
$\omega_9(b_2)$ C-C-O bend	447	-	-	-

[a] Total energy in hartrees, relative energy in cm^{-1}, r_e in Å, θ_e in degrees, and frequencies in cm^{-1}.

[b] The $^2\Pi$ CH_2^+ species is a Renner-Teller molecule, and thus the two ω_3 frequencies are indicative of the curvature of the potential energy surface rather than the true rovibronic energy levels.

[c] As compared to E(DZP TCSCF)=−151.775848 for the $\tilde{X}^1A_1$ state. See footnote f of Table VIII. Experimental values are given in parentheses.

Table X.

Quadratic force constants for $^2B_1$ CH_2CO^+ and 2^1A_1 CH_2CO [a]

	$^2B_1$ CH_2CO^+	2^1A_1 CH_2CO			
	DZP SCF	DZP SCFX	DZP 2R CISD	DZP+R SCFX	DZP+R 2R CISD
F_{11}	25.9727	21.1037	18.3167	25.3399	21.3045
F_{12}	0.8191	-0.4678	-0.0931	0.7159	0.4203
F_{13}	-0.1449	-0.0052	0.0180	-0.1546	-0.1195
F_{14}	0.0126	0.2191	0.1925	-0.0002	-0.0246
F_{22}	6.0770	1.3693	1.7891	6.2049	6.0721
F_{23}	0.1665	0.0414	0.0300	0.1766	0.1553
F_{24}	0.6011	0.6666	0.5648	0.5822	0.5346
F_{33}	6.2640	6.7430	6.4655	6.3128	6.0839
F_{34}	-0.0464	-0.1045	-0.0944	-0.0422	-0.0474
F_{44}	1.4300	1.2425	1.1976	1.4252	1.3361
F_{55}	0.0969	-0.1881	-	0.1216	0.1293
F_{56}	0.0424	-0.0897	-	0.0422	-0.0037
F_{66}	0.5534	1.0314	-	0.4664	0.2801
F_{77}	6.2741	6.8542	6.5460	6.3203	6.0987
F_{78}	0.0964	0.0341	0.0724	0.1121	0.1136
F_{79}	0.0256	0.0250	0.0234	0.0273	0.0258
F_{88}	0.5465	0.5794	0.5188	0.5404	0.4959
F_{89}	-0.1575	-0.1349	-0.1282	-0.1604	-0.1383
F_{99}	0.5881	0.2516	0.2278	0.5976	0.5048

[a] Relative to the C_{2v} symmetrized internal coordinates defined in Table IV of Ref. 6. Units: mdyn/Å, mdyn/rad, and mdyn·Å/rad^2.

Table XI.

Relative energies of several electronic states of ketene at the 2^1A_1 optimum geometry[a]

	$\tilde{X}^1A_1$	$^1A_2$ $(2b_1\rightarrow 3b_2)$	$^1B_1$ $(2b_1\rightarrow 8a_1)$	2^1A_1 $(2b_1\rightarrow 3b_1)$	$^1B_2$ $(2b_2\rightarrow 8a_1)$
DZP+R SCF	1602	30574	46205	55111	97420
DZP+R CISD	1885	31439	46416	56083	95652
DZP+R CIDVD	1917	31458	46053	55818	94161

[a] Energies at the DZP+R 2R CISD 2^1A_1 optimum geometry are listed in cm^{-1} relative to the corresponding $\tilde{X}^1A_1$ values obtained at the DZP CISD $\tilde{X}^1A_1$ optimum geometry of Ref. 95: E(DZP+R TCSCF)= -151.778066, E(DZP+R 2R CISD)= -152.166452, and E(DZP+R 2R CIDVD)= -152.208732. The TCSCF result involves the $(2b_1)^2$ and $(3b_1)^2$ configurations. The $\tilde{X}^1A_1$ and 2^1A_1 values are TCSCF, 2R CISD, and 2R CIDVD energies while the $^1A_2$, $^1B_1$, and $^1B_2$ results are based on a single reference.

[b] CIDVD=Davidson-corrected CISD. See footnote b of Table III.

Table XII.

Relative energies of 2^1A_1 ketene at various geometries[a]

Geometry r(C-C) (Å)	A 1.3190	B 1.4028	C 1.6871	$\tilde{X}^1A_1$ reference, Total energy[c]
DZP SCFX	79310	74430	68249	-151.775848
DZP 2R CISD	72020	68686	62604	-152.161119
DZP 2R CIDVD[b]	68541	65733	59189	-152.202912
DZP+R SCFX	58055	55111	63459	-151.778066
DZP+R 2R CISD	57972	56083	61157	-152.166452
DZP+R 2R CIDVD[b]	57435	55818	59082	-152.208732
QZ2P SCFX	75338	70909	67854	-151.803717
QZ2P 2R CISD	69886	66515	63059	-152.250136
QZ2P 2R CIDVD[b]	66998	64042	59330	-152.299946

[a] Relative energies in cm^{-1} and total energies in hartrees. Definition of geometries: A=$\tilde{X}^1A_1$ DZP CISD, B=2^1A_1 DZP+R 2R CISD, and C=2^1A_1 DZP 2R CISD.

[b] See footnote b of Table III.

[c] At geometry A.

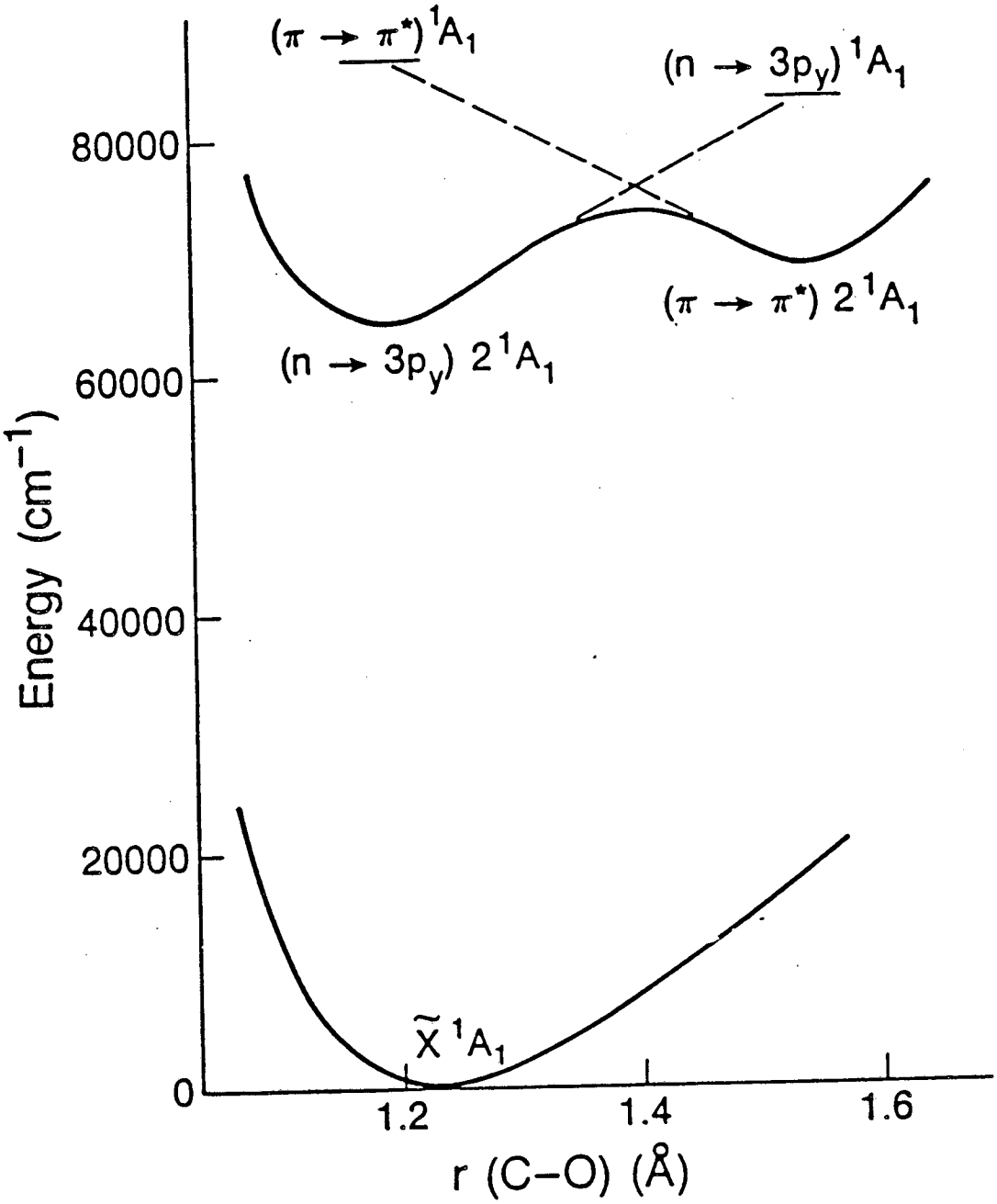

Figure 1. A one-dimensional representation of the 2^1A_1 and $\tilde{X}^1A_1$ potential energy surfaces of formaldehyde. The C-O bond length, r(C-O), varies within the constraint of C_{2v} molecular symmetry. The sketch should not be construed to predict the nature of the 3^1A_1 surface since several avoided crossings above 70000 cm^{-1} involving the $(\pi \rightarrow \pi^*)^1$ configuration are not depicted.

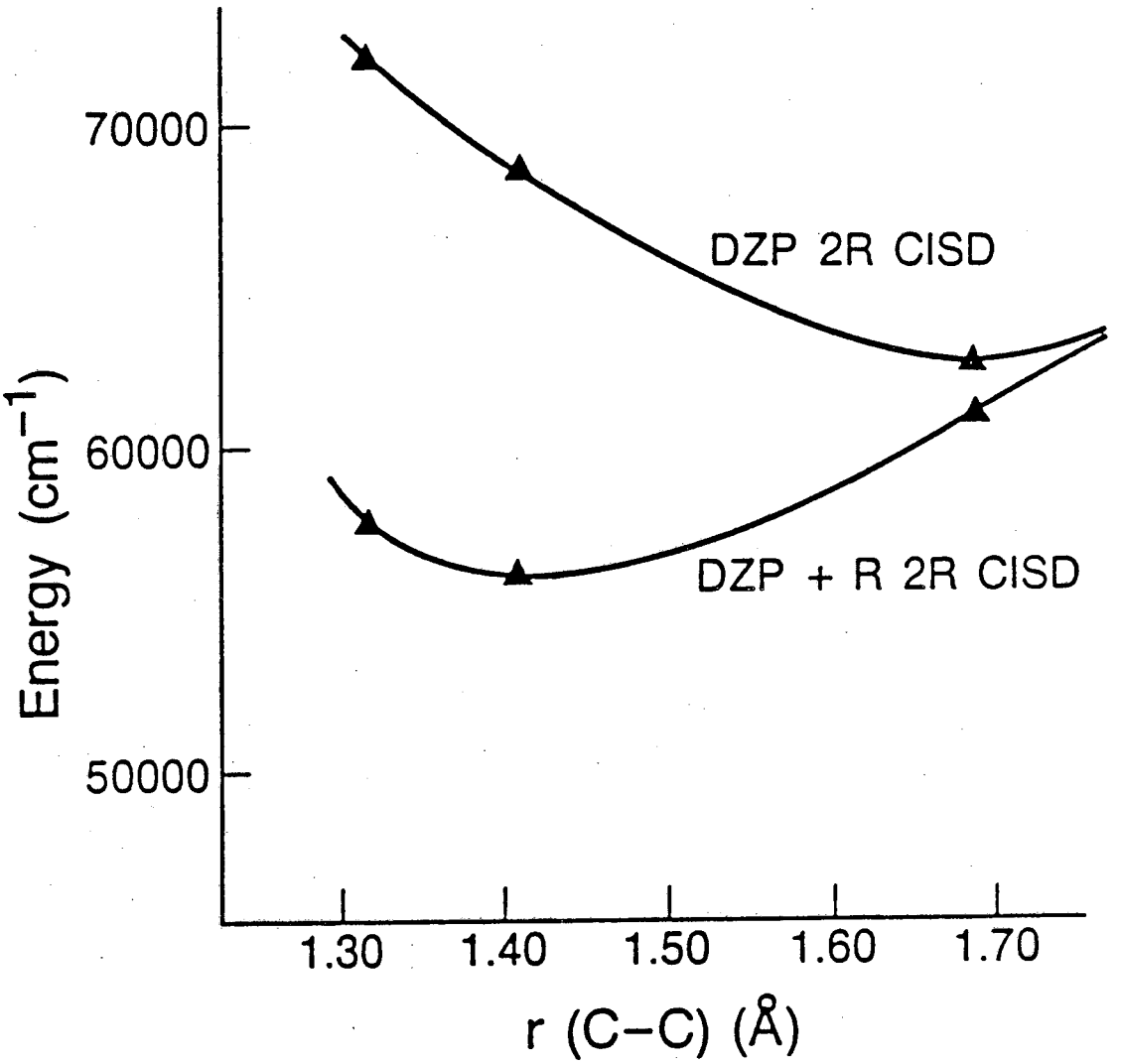

Figure 2. A sketch of the 2^1A_1 ketene DZP and DZP+R 2R CISD potential energy curves as a function of the C-C bond length. The three points on each curve correspond to the DZP CISD $\tilde{X}^1A_1$ geometry (r=1.3190 Å), the DZP+R 2R CISD 2^1A_1 geometry (r=1.4028 Å), and the DZP 2R CISD 2^1A_1 geometry (r=1.6871 Å).

Chapter 5 Summary

In summarizing the content of Chapters 2, 3, and 4, it is expedient to return to the theme of Chapter 1 and specifically to the five features mentioned therein which are exhibited in general by excited electronic states. Through retrospection it is then possible to elucidate the associated concepts with specific examples which are encountered in our paradigm, the ketene molecule.

(1) **The correlation of excited states to fragments.** In both C_{2v} and C_s^{II} symmetry $\tilde{X}^1A_1$ $CH_2CO \rightarrow \tilde{a}^1A_1$ CH_2 + $\tilde{X}^1\Sigma^+$ CO is forbidden, but along bent out-of-plane C_s^I paths this dissociation proceeds with no barrier. $\tilde{a}^3A''$ and $\tilde{A}^1A''$ ketene dissociate to $\tilde{X}^3B_1$ and $\tilde{b}^1B_1$ CH_2 (plus $\tilde{X}^1\Sigma^+$ CO) along bent in-plane C_s^{II} paths. Both of these fragmentation processes are allowed by conservation of orbital symmetry, but at least the $^3A''$ state has a small barrier (<4 kcal/mol) due to subtle electron reorganization effects. In C_s^I symmetry it is the $^3A_1$ state which becomes $^3A'$ and correlates to $\tilde{X}^3B_1$ CH_2 + $\tilde{X}^1\Sigma^+$ CO. A barrier is found in the exit channel, but the corresponding C_s^I transition state is really only a super transition state for the interconversion of the two equivalent $^3A''$ C_s^{II} transition states through rotation about the C-C axis. It is fascinating that the singlet counterpart of the $^3A_1$ state, the 2^1A_1 state, does *not* correlate to $\tilde{b}^1B_1$ CH_2 + $\tilde{X}^1\Sigma^+$ CO. Instead it is the $^1B_1$ Rydberg state of ketene which correlates to these products along both C_{2v} and C_s^I paths.

(2) **Gross qualitative differences between singlet and triplet states with the same orbital occupancies.** The $(2b_1 \rightarrow 3b_1)$ $^3A_1$ state of ketene is valence in character and displays a propensity toward a bent out-of-plane C_s^I structure. However, due to a curve crossing the $^3A_1$ state achieves a C_s^I minimum at a conical intersection and thus has no valid minimum in a Born-Oppenheimer sense. In contrast, the corresponding $(2b_1 \rightarrow 3b_1)$ 2^1A_1 state is predominantly Rydberg in character and

possesses a true minimum at a C_{2v} geometry similar to that of the $(2b_1 \rightarrow \infty)$ CH_2CO^+ cation. The $^3A''$ and $^1A''$ states of ketene do not exhibit the large structural and energetic differences found in the ($^3A_1$, 2^1A_1) pair, but the a'' vibrational frequencies of the $^1A''$ state are radically different from their $^3A''$ counterparts because of the close proximity of the $\tilde{X}^1A'$ state at the $^1A''$ geometry.

(3) **Conical intersections of potential energy surfaces.** Conical intersections of the two lowest triplet surfaces of ketene (Ch. 2, Fig. 4) lead to some peculiar phenomena as alluded to above in Point (2). Not only does the $^3A_1$ state not have a valid minimum but the $^3A'$ stationary point on the lowest triplet surface to which it correlates in C_s^I symmetry is actually only a transition state for the interconversion of two equivalent $^3A''$ C_s^{II} minima through rotation about the C-C axis. The rotational barrier for this process is approximately 8.0 kcal/mol, including ZPVE corrections. As mentioned in Point (1), an analogous situation obtains for the $^3A'$ C_s^I and $^3A''$ C_s^{II} transition states for dissociation, but the rotational barrier in this case is much less (1 kcal/mol).

(4) **Variational collapse of trial wave functions.** Conventional SCF methods predict that both the $^3A_1$ and 2^1A_1 states are valence in character with a $^3A_1 - 2^1A_1$ (vertical) energy separation of approximately 1700 cm^{-1}. However, predictions obtained with such methods for the 2^1A_1 state are unreliable due to variational collapse, and the variationally correct SCFX method gives an enormous $^3A_1 - 2^1A_1$ splitting of 34300 cm^{-1} if a valence (DZP) basis set is employed. If diffuse functions are subsequently added to the basis set, the 2^1A_1 state becomes Rydberg in character, and the final $^3A_1 - 2^1A_1$ vertical splitting (including electron correlation) is 11400 cm^{-1}. Comparison with experiment reveals that the DZP+R SCFX and 2R CISD predictions are accurate, and thus these methods are a viable means of overcoming the problem of variational collapse.

(5) **Rydberg-valence mixing.** The DZP 2R CISD optimum C_{2v} geometry for the $(\pi\rightarrow\pi^*)$ 2^1A_1 state of ketene has an extremely long C-C bond length of 1.687 Å and an adiabatic excitation energy of 62604 cm^{-1}. If diffuse functions are added to the basis set, the valence minimum collapses, and a C_{2v} minimum with r_e(C-C) = 1.403 Å and T_e = 56083 cm^{-1} is obtained. This latter structure is characteristic of a $(\pi\rightarrow 3p_x)$ 2^1A_1 state, but a comparison of the DZP+R 2R CISD prediction for $\omega_4(a_1)$, the C-C stretch, with an experimentally observed vibrational progression in the VUV spectrum suggests a moderate amount of mixing of the $(\pi\rightarrow 3p_x)^1$ and $(\pi\rightarrow\pi^*)^1$ states. A distinct $(\pi\rightarrow\pi^*)^1$ minimum is not apparent from the theoretical and experimental data but is not to be excluded unequivocally.

It is stated forthright in Chapter 1 that the goal of this dissertation is to provide an essentially complete theoretical description of all of the low-lying electronic states of ketene. Of course the degree to which this goal has been achieved depends on one's definition of "essentially complete"; nevertheless, a strong argument can be made that this goal has been accomplished in large part. It is hoped that these studies of the ketene molecule are a portent of successful campaigns, not merely forays, into the realm of the excited electronic states of other polyatomic molecules.

LAWRENCE BERKELEY LABORATORY
TECHNICAL INFORMATION DEPARTMENT
UNIVERSITY OF CALIFORNIA
BERKELEY, CALIFORNIA 94720